January 2015

A Heat Transfer Study Of SiO2 Colloid Flow In The Thermal Entry Region Of Mini Circular And Square Tubes

Sarbottam Pant

Follow this and additional works at: https://commons.und.edu/theses

A HEAT TRANSFER STUDY OF SiO$_2$ COLLOID FLOW IN THE THERMAL
ENTRY REGION OF MINI CIRCULAR AND SQUARE TUBES

by

Sarbottam Pant

Bachelor of Engineering, Tribhuvan University, 2010

A Thesis

Submitted to the Graduate Faculty

of the

University of North Dakota

in partial fulfillment of the requirements

for the degree of

Master of Science

Grand Forks, North Dakota

May

2015

This thesis, submitted by Sarbottam Pant in partial fulfillment of the requirements for the Degree of Master of Science from the University of North Dakota, has been read by the Faculty Advisory Committee under whom the work has been done and is hereby approved.

_____
Dr. Clement Tang, Chairperson
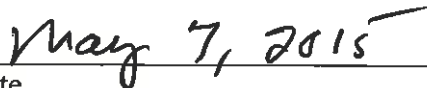
_____
Dr. Nanak Grewal, Committee Member

_____
Dr. Gautham Krishnamoorthy, Committee Member

This thesis is being submitted by the appointed advisory committee as having met all of the requirements of the School of Graduate Studies at the University of North Dakota and is hereby approved.

_____
Wayne Swisher
Dean of the School of Graduate Studies

_____
Date   May 7, 2015

iii

PERMISSION

Title	A heat transfer study of SiO_2 colloid flow in the thermal entry region of mini circular and square tubes
Department	Mechanical Engineering
Degree	Master of Science

In presenting this thesis in partial fulfillment of the requirements for a graduate degree from the University of North Dakota, I agree that the library of this University shall make it freely available for inspection. I further agree that permission for extensive copying for scholarly purposes may be granted by the professor who supervised my thesis work or, in her absence, by the Chairperson of the department or the dean of the School of Graduate Studies. It is understood that any copying or publication or other use of this thesis or part thereof for financial gain shall not be allowed without my written permission. It is also understood that due recognition shall be given to me and to the University of North Dakota in any scholarly use which may be made of any material in my thesis.

<div align="right">
Sarbottam Pant
April 15, 2015
</div>

TABLE OF CONTENTS

LIST OF FIGURES

LIST OF TABLES

ACKNOWLEDGMENTS

ABSTRACT

Flow and heat transfer behavior of silicon dioxide (SiO_2) nanofluid (9.58% by volume)
was studied in three sizes of hydraulic diameters and two cross-sectional shapes. Altogether
six test sections were used. The outer dimensions of these test sections were 1/8", 3/32",
and 1/16"; and shapes were circular and square with respective hydraulic diameters of
0.097", 0.066", and 0.035" (2.46 mm, 1.67 mm and 0.88 mm). Rheological study of the
fluid showed the SiO_2 nanofluid to be a dilatant non-Newtonian fluid. The friction factor
of SiO_2 nanofluid was compared with the friction factor of water over a range of Reynolds
number. In laminar regime the friction factor for both fluids was similar, and in post
laminar regime SiO_2 nanofluid had lower friction factor. There was no observed effect of
hydraulic diameter on the friction. For the same hydraulic diameters, flow in channels with
square cross-section had less friction factor than circular at same Reynolds number. The
Nusselt number at the same Reynolds number for SiO_2 nanofluid was higher than that for
water. Further, the difference between the Nusselt number of SiO_2 and water increased
with Reynolds number. Also the local heat transfer behavior of the two fluids was
compared along the length and this comparison revealed that improvement in heat transfer
was higher in earlier parts of the entrance region. Thus better enhancement in heat transfer
can be obtained in the turbulent regime and in the earlier parts of the entrance region. Heat
transfer behavior of SiO_2 nanofluid and water was also compared at the same pumping
power. This comparison evinced that at the same pumping power, water is a better heat
transfer medium than SiO_2 nanofluid. There was no observed effect of the hydraulic

diameter on the heat transfer, and for the same hydraulic diameters circular channels had better heat transfer behavior.

NOMENCLATURE

English letter symbols

1/16c   circular test section with outside diameter of 1/16"

1/16sq square test section with outside width of 1/16"

1/8c   circular test section with outside diameter of 1/8"

1/8sq   square test section with outside width of 1/8"

3/32c   circular test section with outside diameter of 3/32"

3/32sq square test section with outside width of 3/32"

A   surface area [m^2]

c_p specific heat capacity at constant pressure [J/kg-K]

D_h hydraulic diameter

f   friction factor

Gz   Graetz number

h   heat transfer coefficient [$W/m^{2\text{-}}K$]

I   current

ID   inner diameter

K   fluid consistency index in Equation (2.1.23)

k   thermal conductivity [W/m-K]

K'   fluid consistency index in Equation (2.1.24)

LPM liters per minute

$\dot{m}$ mass flow rate [kg/s] [g/s]

m'   empirical constant in Equation (3.3.4)

n   flow behavior index (dimensionless) in Equation (2.1.23)

n'   flow behavior index (dimensionless) in Equation (2.1.24)

nf   nanofluid

nm   nanometer [10^{-9} m]

Nu   Nusselt number

OD   outer diameter

P   power [W]

p   pressure [N/m^2]

Pa   Pascal

PP   pumping power

psi   pound per square inch

q   amount of heat per unit time per unit area [W/m^2]

Q   amount of heat that flows through a body in unit time [W]

q_g heat generated per unit volume [W/m^3]

r   radius [m]

Re   Reynolds number

Re_n Reynolds number for non-Newtonian fluid

rpm   revolutions per minute

T   temperature [K] or [$^{\circ}$C]

t   time [s] [min] [hr]

u   velocity of the fluid [m/s]

V   voltage in Equation (3.3.5)

$\dot{V}$ volume rate [m³/s]

w   water

x   length along x direction [m]

y   length along y direction [m]

z   length along z direction [m]

Greek letter symbols

Δ designates a difference when used as a prefix

$\in$ roughness factor

μ viscosity [kg/m-s] [N-s/m²]

α thermal diffusivity [m²/s]

$\dot{\gamma}$ rate of shear strain [1/s]

ρ density [kg/m³]

τ shear stress [N/m²]

ν kinematic viscosity [m-s]

$\varnothing$ particle volume fraction

Subscripts

b   bulk fluid

bf   basefluid

in   inlet

iw   inside wall

ow   outside wall

nf   nanofluid

out   outlet

w   water

CHAPTER 1

INTRODUCTION

1.1   General

In the recent times the designers are constantly trying to produce engines, computer-chips and machines that are smaller and more efficient than ever before. The challenge to designers is not in generating more power in engines and faster processing chips, but in dissipating heat generated from these devices that reduce the overall efficiency. To remove the heat, a cooling fluid (air, water or liquid coolant) is used. The ability of the fluid to remove heat from such devices is affected by its thermal conductivity. The most common fluids used for cooling are water and air, and they have thermal conductivities of 0.024 W/m-K and 0.58 W/m-K at 298 K, respectively, which can be inadequate for high performance devices. When nanoparticles of metal or metal oxides are dispersed in the cooling fluid (liquid) to form a colloid, the thermal conductivity of the fluid can be increased. Such a colloid has potential to improve the overall heat transfer coefficient due to its enhanced thermal conductivity, but this improvement comes along with increased viscosity. It is obvious that pumping fluid with increased viscosity through heat exchangers requires an increase in pumping energy, thus reducing the benefit from enhancement of thermal conductivity.

1.2   Research objectives

Until the present date, several researches have been carried out to characterize the flow and the heat transfer behavior of colloids. These researches had been carried out with a wide

1

variety of colloids with varying particles, particle sizes, particle concentrations and base fluid and consequently provided vast knowledge in this field and exposed colloids to many potential applications in heat transfer. Further each type of colloid has its own flow and heat transfer behavior and there are still not enough studies to establish the flow and the heat transfer characteristics of the colloids. Also most of the studies were carried out with particle concentrations of less than 2% (by volume) concentration. In this study the flow and heat transfer behavior of such a colloid, water based silicon dioxide (SiO_2) with comparatively higher volume concentration ($\sim 10\%$ by volume) is studied.

The main objective of this research is to study the flow behavior and the heat transfer characteristics of the colloid made up of silicon dioxide nanoparticles dispersed in water. The flow and the heat transfer behavior are studied in control volume with simple geometries i.e. straight tubes of circular and square cross-sections with varying hydraulic diameter.

1.3   Outline of the study

In this thesis the author first discusses the important terms and the general fluid properties of related to this research. This is then followed by studies that haven carried out in the field of nanofluid. Then the experimental setup and methodology is discussed which followed by results and discussion of the experiments. Finally the conclusions and the recommendations are presented.

CHAPTER 2

LITERATURE REVIEW

This chapter has two sections. In the first section, key terms related to the research are discussed. One of the terms is nanofluid which is used to describe the colloid consisting of nanoparticles and basefluid. And in the second section, studies carried out in the past that are related to this thesis are discussed.

2.1 Background

Products of technology that surrounds us today needs energy to vitalize them and if there is use of any form of energy, there is dissipation of heat. With ever improving technology, these equipment are getting smaller and, at the same time delivering higher output; computers are using faster and smaller processors, automotive industries are installing larger horsepower engines in vehicles and other manufacturing industries are using higher output industrial processes. Energy requirements may or may not have increased but either way the heat flux dissipating from them is increasing. This heat has to be removed from the equipment for better performance and reliability, and the unnecessary heat is removed from some form of heat exchanger surface. The amount of heat that can be removed from a heat exchanger depends on the overall heat transfer coefficient (h). The heat transfer coefficient depends on the temperature difference between the surface and the cooling fluid (heat transfer fluid), dimensions of the heat exchanging surface, and the thermophysical properties of the heat transfer fluid. With larger heat exchanging surface more heat can be removed but in expense of bigger overall dimension of the system which contradicts the

current trend of smaller equipment. Next option is to increase the temperature difference

which requires an extra cooling system. The other option is to change the properties of heat

transfer fluid. The property of a fluid related to removing heat from a surface is thermal

conductivity (k). Higher the value of thermal conductivity of a fluid greater the amount of

heat it can remove from a heat exchanging surface. One way to increase the thermal

conductivity of a heat transfer fluid is to disperse solid particle in it. The particle should be

such that its thermal conductivity is significantly higher than that of the fluid. Also the

particles should be able to remain suspended in the fluid. Thus forming a colloid whose

effective thermal conductivity is higher than that of the base fluid. At the same time

dispersion of such particles also affects the viscosity. Viscosity if the property which

controls the flow rate of the fluid. A fluid with a high viscosity has a high resistance to

flow. Dispersing particles in a fluid increases its viscosity. And therefore the colloid has

higher resistance to flow over a heat exchanging surface. In the subsequent part of this

section terms related to flow and heat transfer properties of a fluid are discussed.

2.1.1   Viscosity and its measurement

For a fluid flowing over a surface the shear stress on a layer of the fluid is directly

proportional to the rate of shear strain or the rate of deformation. The relation between

shear stress (τ) and rate of shear strain ($\dot{\gamma}$) is given by Equation (2.1.1)

$$\tau = \mu\dot{\gamma} \tag{2.1.1}$$

where μ is the viscosity of the fluid. Viscosity (also called absolute or dynamic viscosity)

is the property of a fluid which offers resistance to the movement of one layer of the fluid

over another adjacent layer of the fluid. In other words, viscosity is the property of a fluid

which controls the rate of flow and is referred to as fluid friction. For flow in a circular pipe Equation (2.1.1) can be written as

$$\tau = \mu \frac{du}{dr} \tag{2.1.2}$$

where u is the velocity of the pipe along the direction of the flow and r is the radius of the pipe.

Rotational viscometers are one of the types of viscometers used to measure the viscosity of nanofluids. This is a kind of viscometer in which the principal of operation is to drive a spindle, which is immersed in the fluid under study, through a calibrated spring. Torque applied on cylinder rotating in the sample is used to calculate the viscosity. The viscous resistance of the fluid against the cylinder is measured by a calibrated spring deflection and the spring deflection is measured with a rotary transducer. This kind of viscometers consists of two concentric cylinders, namely a bob (spindle) and a crucible (cylinder). The measurement range of a rotary cylinder viscometers is determined by the spindle rotational speed, size and shape of the rotating spindle, container in which spindle is rotating in, and the full-scale torque of the calibrated spring. In a constant rotational speed the viscosity of fluid can be obtained using Equation (2.1.3)

$$\mu = \left(\frac{1}{r_1^2} - \frac{1}{r_0^2} \right) \frac{M}{8\pi^2 nh} \tag{2.1.3}$$

where M is the torque, n is the number of revolutions per second, r_1 is the radius of spindle, r_0 is the radius of spindle and h is the height of spindle [1].

2.1.2 Pumping power

Pumping power required to overcome the pressure loss due to the fluid friction when a fluid flows through a tube with a volume flowrate of $\dot{V}$ is given by

$$P_{pump} = \dot{V}\Delta p \qquad\qquad (2.1.4)$$

where Δp is the pressure drop across the length of the tube.

2.1.3 Newtonian and non-Newtonian fluid

A fluid which obeys Equation (2.1.1) is called a Newtonian fluid. For a Newtonian fluid when shear stress is plotted against rate of shear strain, a straight line is obtained whose slope is equal to the viscosity. A fluid which does not follow Equation (2.1.1) is called the non-Newtonian fluid. For this type fluid the slope of shear stress to shear rate is not constant, i.e. the viscosity of the fluid changes with the rate of deformation or shear strain. Non-Newtonian fluids can be of two types, pseudo-plastic and dilatant. For a pseudo plastic non-Newtonian fluid the viscosity decreases with the increases in shear rate. And for a dilatant non-Newtonian fluid the viscosity increases with the increase in shear rate. Thus, a pseud-plastic non-Newtonian fluid has a shear-thinning behavior and a dilatant non-Newtonian fluid has a shear thickening behavior.
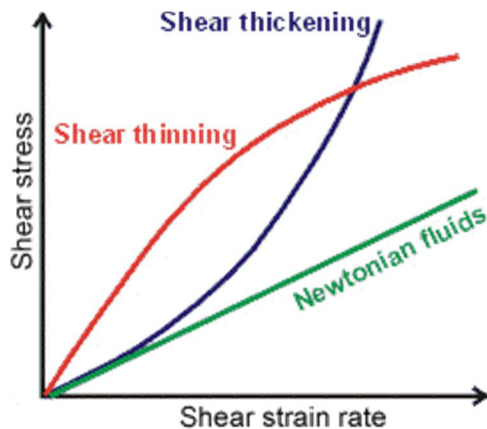
Figure 1. Shear stress-strain plot for Newtonian and non-Newtonian fluids

2.1.4 Friction factor

For flow inside tubes and channels, the fluid friction causes a pressure drop (Δp) which depends on the dynamic pressure term ($1/2\rho u^2$), length (L) of the tube and the hydraulic

diameter (D). This relation for the pressure drop and the factors affecting it is given in Equation (2.1.5).

$$\Delta p = f\frac{L}{D}\left(\frac{1}{2}\rho u^2\right) \tag{2.1.5}$$

where f is a non-dimensional quantity called the friction factor, ρ is the density of the fluid and u is the mean velocity of the fluid. For a Newtonian fluid flowing in a circular tubes, relations for friction factor, in terms of dimensionless Reynolds number, can be found in [2]. Equation (2.1.6) gives the friction factor flow in laminar regime (Re $\leq$2300). Equation (2.1.7) is for flow in turbulent regime.

For Re $\leq$2300

$$f = \frac{64}{Re} \tag{2.1.6}$$

Blasius friction factor for $4000 \leq Re \leq 10^5$

$$f = 0.316Re^{-0.25} \tag{2.1.7}$$

Chruchill friction factor [3], can be used for both laminar and turbulent regime.

$$f = 8\left[\left(\frac{8}{Re}\right)^{12} + \frac{1}{(A+B)^{1.5}}\right]^{\frac{1}{12}} \tag{2.1.8}$$

$$A = \left\{2.457 \ln\left[\frac{1}{\left(\frac{7}{Re}\right)^{0.9} + \left(0.27\frac{\epsilon}{D}\right)}\right]\right\}^{16}$$

$$B = \left(\frac{37530}{Re}\right)^{16}$$

Colebrook equation described in [4] can also be used to calculate the friction factor from Equation (2.1.9).
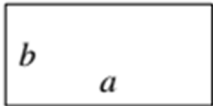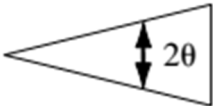
$$\frac{1}{\sqrt{f}} = -2 \log_{10} \left(\frac{2.51}{Re\sqrt{f}} + \frac{\epsilon}{3.71 D_h} \right) \qquad (2.1.9)$$

For non-circular channels the laminar friction factor can be estimated from Table 1.

For square tube, Equation (2.1.10) can be used to estimate the friction factor in laminar regime.

$$f = \frac{56.91}{Re} \qquad (2.1.10)$$

Table 1. Constants f*Re for rectangular and triangular ducts [2]

Rectangular		Isosceles triangle	

b/a	fRe_{D_h}	θ, deg	fRe_{D_h}
0.0	96.00	0	48.0
0.05	89.91	10	51.6
0.1	84.68	20	52.9
0.125	82.34	30	53.3
0.167	78.81	40	52.9
0.25	72.93	50	52.0
0.4	65.47	60	51.1
0.5	62.19	70	49.5
0.75	57.89	80	48.3
1.0	56.91	90	48.0

For the turbulent friction factor characteristic hydraulic diameter is calculated using Equation (2.1.11).

$$D_h = \frac{4 \times \text{cross section area}}{\text{wetted perimeter}} \qquad (2.1.11)$$

This hydraulic diameter is used to calculate the Reynolds number from Equation (2.1.17) which is then used in the turbulent friction factor correlations for the circular tubes to estimate the friction factor for the non-circular tubes.

2.1.5 Thermal conductivity and its measurement

Fourier law of heat conduction gives the relation between the amount of heat that flows through a body in a unit time and the thermal conductivity.

$$Q = kA \frac{dT}{dx} \qquad (2.1.12)$$

where

Q = amount of heat that flows through a body in unit time [W]

A = surface area of heat flow, taken right angles to the direction of heat flow [m^2]

dT = temperature difference on two faces of the body [K]

dx = thickness of the body through which the heat flows, taken along the direction of heat flow.

Thus, thermal conductivity of a material is defined as the quantity of heat that passes through a unit area and thickness in unit time when the temperature difference between two points at each end of the unit thickness is 1 degree Celsius/Kelvin. Thus, higher the value of thermal conductivity, higher is the amount of heat that can be removed by the heat transfer fluid from the heat exchanger surface. Thermal conductivity of some common materials and gases are listed in Table 2.

Table 2. Thermal conductivity of air and some common materials

Material and Gases	k @ 25°C (W/m-K)
Air, atmosphere (gas)	0.024
Alcohol	0.17
Aluminum	205
Aluminum Oxide	30
Brass	109
Copper	401
Carbon Steel	54
Engine Oil	0.15
Gasoline	0.15
Glyserol	0.28
Gold	310
Cast Iron	55
Kerosene	0.15
Lead Pb	35
Oil, machine lubricating SAE 50	0.15
Silver	429
Steel, Carbon 1%	43
Stainless Steel	16
Water	0.58
Silicon Dioxide	1.3 − 1.4

Most commonly used heat transfer fluids, air and water, have thermal conductivity of 0.024 and 0.58 [W/m-K] respectively, which is low when compared to thermal conductivities of metals. To improve the thermal conductivity of the heat transfer fluid, metallic particles were suspended in the fluid. As expected the thermal conductivity of the fluid improved. More than 100 years ago Maxwell presented the theoretical basis for predicting the effective conductivity of suspension in "Treatise on Electricity and Magnetism". Since then several studies have been carried out to enhance the thermal conductivity of the heat transfer fluid by suspending particles in it. Till few decades back these studies have been confined to millimeter and micrometer sized particle suspensions. This approach to improve the thermal conductivity had technical problems; the millimeter and micrometer

sized particles settled rapidly in the fluids; the conductivities of these suspensions were low at low concentrations; and did not work with miniaturized devices because they tend to clog the channels of such devices [5]. Then with the development of nanotechnology researchers were able to develop the suspension of nano-sized particles. This suspension overcame the earlier problems of settling of particles and had significant increase in thermal conductivity even at lower concentrations.

The most common method of thermal conductivity measurement is the transient hot-wire method. This is a fast and accurate method to measure the thermal conductivity. The mathematical model for this method is discussed by Das et al. [5].

An infinitely long line heat source is suspended vertically in liquid whose thermal conductivity is to be measured. The method is called transient because heat is supplied suddenly, so that eventually the wire gets heated. The working equation is based on a specific solution of Fourier's law for radial (one dimensional) transient heat conduction with a line heat source at the axis of the cylindrical domain. The 1-D differential equation of conduction of heat in cylindrical coordinates is

$$\frac{\partial^2 T}{\partial r^2} = \frac{1}{\alpha}\frac{\partial T}{\partial t} \tag{2.1.13}$$

From Equation (2.1.13) we can get the temperature distribution equation for a line heat source by integrating it over the entire length (z-direction) of the line (i.e., from $-\infty$ to $+\infty$ in cylindrical coordinates.

$$T = \frac{q}{4\pi k}\ln\frac{4kt}{r^2\rho c_p} - \frac{q}{4\pi k} \tag{2.1.14}$$

where, q is the heat liberated per unit time per unit length of the line source in W/m and k is the conductivity of the liquid in W/m-K. If temperatures of the heat source at time t_1 and

t_2 are T_1 and T_2, respectively, then putting these conditions in Equation (2.1.14) gives the conductivity relation of the liquid.

$$k = \frac{q}{4\pi(T_2 - T_1)} \ln\frac{t_2}{t_1} \tag{2.1.15}$$

Decagon Devices KD2 Pro thermal analyzer is one of the devices that uses the principle of Transient hot-wire method to measure the thermal conductivity of a fluid. To measure thermal conductivity, a pulse of heat rate is applied to the needle probe, and the temperature response to the heat pulse is monitored by a sensor with in the probe.

2.1.6   Heat transfer coefficient

The heat transfer that occurs between a fluid layer and a surface due to the motion of the fluid relative to the surface is called the convective heat transfer. (Other modes of heat transfer are conduction heat transfer and radiation heat transfer). Amount of heat transfer per unit time per unit area (q) by convection between the tube inner wall and the fluid flowing through it is given by is given by

$$q = h(T_{iw} - T_b) \tag{2.1.16}$$

where h is called the heat transfer coefficient which is the proportionality constant between the heat flux (q) and the temperature difference the surface and the fluid.

2.1.7   Important dimensionless numbers

A good summary of dimensionless numbers can be found in [6].

2.1.7.1   Reynolds number (Re)

Reynolds number is defined as the ratio of the inertia force to the viscous force.

$$Re = \frac{\text{inertia froce}}{\text{viscous froce}} = \frac{\rho u D_h}{\mu} = \frac{\dot{m} D_h}{A\mu} \tag{2.1.17}$$

12

It signifies the relative predominance of the inertia to the viscous forces occurring in the flow. Higher the value of the Reynolds numbe ($\geq$ 5000, flow in tubes) greater will be the contribution of the inertia effect. Such a flow is referred to as a turbulent flow. Smaller the value of Re ($\leq$2300) greater will be the relative magnitude of relative stress. Such flow is referred to as laminar flow regime.

2.1.7.2 Prandtl number (Pr)

Prandtl number is the ratio of kinematic viscosity (ν) to thermal diffusivity (α).

$$\text{Pr} = \frac{\nu}{\alpha} = \frac{\mu c_p}{k} \tag{2.1.18}$$

Kinematic viscosity indicates the impulse transport through the molecular friction whereas, thermal diffusivity indicates the heat energy transport by conduction. Prandtl number provides a measure of the relative effectiveness of the momentum and energy transport by diffusion. It is a connecting link between the velocity field and temperature field and its value strongly influences relative growth between velocity and thermal boundary layers.

2.1.7.3 Graetz number (Gz)

Graetz number is a dimensionless number related to transient heat conduction. It is the ratio of time taken by heat to diffuse radially into the fluid by conduction (also referred to as relaxation time, D^2/k) to the time taken for the fluid to reach the distance x (x/u) [7].

$$\text{Gz} = \frac{D^2/k}{x/u} = \frac{uD^2}{kx}$$

For small values of Gz ($<$20) radial temperatuere profiles are fully developed but for large values, thermal boundary layer development has to be taken into account

Also

$$Gz = \frac{D}{x} RePr \qquad (2.1.19)$$

The value Gz^{-1} is often used as a dimensionless form of axial distance in the representation of entrance effect in laminar heat transfer.

2.1.7.4 Nusselt number (Nu)

Nusselt number is a convenient measure of the convective heat transfer coefficient. For a given value of Nusselt number, the connective heat transfer is directly proportional to thermal conductivity of the fluid and inversely proportional to the characteristic length. Nusselt number can be defined as the ratio of heat flow by convection process under a unit temperature gradient to the heat flow rate by conduction under a unit temperature gradient through a stationary thickness, (for flow in tubes, hydraulic diameter would be the thickness).

$$Nu = \frac{hD}{k} \qquad (2.1.20)$$

For a uniform surface heat flux boundary condition, correlations to predict the Nusselt number can be found in [8]. When the flow is in turbulent regime ($3000 \leq Re \leq 5 \times 10^6$) Nusselt number can be predicted with Gnielinski correlation, Equation (2.1.21).

$$Nu = \frac{(f/8)(Re - 1000)Pr}{1 + 12.7(f/8)^{0.5}(Pr^{2/3} - 1)} \qquad (2.1.21)$$

When the flow is in laminar regime with fully developed velocity profile and developing thermal profile Lienhard and Lienhard correlation, Equation (2.1.22) is used to estimate the Nusselt number.

$$Nu = 1.302Gz^{1/3} \text{ for } 2 \times 10^4 \leq Gz$$

$$\text{Nu} = 1.302Gz^{\frac{1}{3}} - 0.5 \text{ for } 667 \leq \text{Gz} \leq 2 \times 10^4 \qquad (2.1.22)$$

$$\text{Nu} = 4.364 + 0.263\text{Gz}^{0.506}\exp(-41/\text{Gz}) \text{ for } 0 \leq \text{Gz} \leq 667$$

2.1.8   Friction factor and Reynolds number for non-Newtonian fluids

For majority of non-Newtonian fluids, the relation between the shear stress and the shear rate can be represented by a two constant power function of the form in Equation (2.1.23) [9].

$$\tau = K\left(\frac{du}{dr}\right)^n \qquad (2.1.23)$$

where (-du/dr) is the shear rate for flow with in a circular duct, n is called the flow behavior index and is dimensionless, and K is the fluid consistency index. Inspection shows that Equation (2.1.2) is a special case of Equation (2.1.23) when n is unity and K is equal to Newtonian viscosity.

For a non-Newtonian fluid flowing in a tube the power law is given by

$$\tau = \frac{D\Delta p}{4L} = K'\left(\frac{8u}{D}\right)^{n'} \qquad (2.1.24)$$

According to Metzner [9] there exists a unique relation between the shear stress at the wall (DΔp/4L) and a characteristic flow quantity (8u/D) for any liquid flowing through a circular cross-section tube and in laminar regime. For such flow the shear rate is only a function of shear stress. Thus flow characteristics can completely be defined by the terms (DΔp/4L) and (8u/D). Based on this concept the relationship between laminar friction factor and non-Newtonian Reynolds number was established.

$$f = \frac{64}{\text{Re}_n} \qquad (2.1.25)$$

Reynolds number for non-Newtonian (Re$_n$) fluid flowing in a circular tube is given by

$$Re_n = \frac{D^{n'} u^{2-n'} \rho}{K' 8^{n'-1}} \tag{2.1.26}$$

The relationships between shear rate and shear stress in Equation (2.1.24), and non-Newtonian Reynolds number in Equation (2.1.26) defined for laminar flow are again used for turbulent flow conditions to predict the friction factor using Equation (2.1.27).

$$\frac{1}{\sqrt{f}} = \frac{4.0}{(n')^{0.75}} \log\left[Re_n(f)^{1-n'/2}\right] - \frac{0.4}{(n')^{1.2}} \tag{2.1.27}$$

2.1.9 Different flow regimes

The flow of any fluid in a channel can be divided in to three regimes viz. laminar, transition and turbulent according to their corresponding Reynolds number, which is the ratio of inertia force to viscous force. For laminar flow, the fluid flows in streamlines without lateral mixing. The layers of fluid slides on each other like cards. In this type of flow, the effect of inertia forces of the fluid is much less than the turbulent flow. For laminar flow in circular tubes, the Reynolds number is less than 2300. For Reynolds number greater than 5000, the inertia force is clearly dominant over viscous force and such flow is termed as turbulent flow. The turbulent flow consist of eddy motions and these motion are responsible for mixing of fluid layers. In heat transfer applications, this behavior is desirable as more heat can be transferred from a heat exchanging surface to the fluid. At the same time a large part of mechanical energy of the flow goes in the formation of eddies thus causing a substantial pressure drop across a control volume when a fluid pass through it with turbulent flow. For Reynolds number between 2300 and 5000 the flow regime is termed as transition flow regime. In such a flow the inertia force is strong enough to create eddies but not enough to sustain them. Thus transition flow is characterized by onset and retreat of eddies and/or disorder in flow. The type of flow regime is governed by the value

of Reynolds number. And the Reynolds number is a function of flow speed, characteristic dimension (hydraulic diameter), density, and viscosity of the fluid. Conditions that are favorable for turbulent flow are high flow speed, large hydraulic diameter, high density, and low viscosity. Further, the flow regime, always does not changes from laminar to transition at Reynolds number of approximately 2300 or from transition to turbulent at approximately 5000. The exact value depends on the surface roughness, heat transfer, vibration, noise or presence of some form disturbances.

2.1.10 Colloids

A colloidal system is a mixture in which particles ranging from 1 and 1000 nm are evenly dispersed in a continuous medium. The particle, which remain dispersed and do not settle are referred to as dispersed phase and the continuous medium is referred to as continuous phase. Some example of colloids are milk, smoke, silicon dioxide nanofluid. etc.

One of the colloidal systems that is of interest to heat transfer engineers is nanofluid. It consists of nanoparticles of average size below 100 nm uniformly dispersed in traditional heat transfer fluid such as water oil or ethylene glycol [5].

2.2 Studies related to nanofluid

Wide variety of nanoparticles is commercially available and can be used for preparation of nanofluids. Also different heat transfer fluids, which can be used as base fluid, are available for nanofluids. Thus, the combination of these two materials, at different phases, provides an opportunity to create a new material (nanofluid) with even wider variety. Nanoparticle, a solid phase material, has different properties (density, specific heat, and thermal conductivity) than that of the base fluid. Consequently the suspension of nanoparticle and the base fluid, a two phase system, has different set of properties than that of base fluid.

Some studies have considered nanofluid as a three-phase-system including the solid phase (nanoparticles), the liquid phase (fluid media), and the interfacial phase, which contributes significantly to the system properties because of its extremely high surface-to-volume ratio in nanofluid [10].

Properties of a nanofluid can be addressed in four relevant scales, the molecular scale, the micro scale, the macro scale and the system scale [11]. The molecular scale is defined by the mean free path between the molecular collisions. The micro scale constitutes of smallest scale at which continuum mechanics can be applied. The macro scale is designated by the smallest scale at which a set of average properties of concern can be defined and the system scale is characterized by the length scale corresponding to domain of interest (control volume). The studies and researches on nanofluids, summarized in this chapter, are aimed to enhance the properties at macro scale and system scale by manipulating the properties at micro scale. One of the micro scale properties is the thermal conductivity that characterizes the rate of heat transfer, macro scale property. The thermal conductivity of the heat transfer fluid can be manipulated (increased) by dispersing nanoparticles in it and with increase in thermal conductivity, overall heat transfer rate is expected to be enhanced. However, this increase in thermal conductivity comes with a price of increased viscosity which offsets the overall benefit gained from thermal conductivity enhancement.

2.2.1   Thermal conductivity of nanofluid

In 1995, Choi and Eastman [12] introduced the term 'nanofluid' to describe a suspension of metallic nanoparticle in a base fluid which had higher thermal conductivity than that of the base fluid. Their study presented the possibility of doubling the convection heat transfer coefficient using ultra-high conductivity nanofluid. For a copper water nanofluid, with the

particle sphericity of 0.3 and concentration of 20% (by vol.), the thermal conductivity could be increased by a factor of 3.5. Lee et al. [13] used the transient hot-wire (TWH) method to measure the thermal conductivity of nanofluid with oxide nanoparticles (Al_2O_3 in water, Al_2O_3 in ethylene glycol, CuO in water and CuO in ethylene glycol). Their experiment result showed that nanofluid (nf) containing small amount of nanoparticle (np), have substantially higher thermal conductivities and that of the base fluid (more than 20%). Also, in the low-volume fraction range tested (up to 0.05) thermal conductivity was shown to increase linearly with volume fraction and the thermal conductivity of nanofluid depended on thermal conductivity of the nanoparticles and the base fluid. Tang et al. [8] measured the conductivity of water-based nanofluid with Al_2O_3 particles for the temperature range between 6 and 55°C, and found 8 to 17% higher than that of water. Study of Eastman et al. [14] showed that the effective thermal conductivity of ethylene glycol increased by up to 40% for a nanofluid consisting of ethylene glycol containing approximately 0.3 vol % Cu nanoparticles of mean diameter, 10 nm. Choi et al. [15] measured the thermal conductivity of nanotube-in-oil suspension as a function of nanotube volume fraction at room temperature using THW method. Multi-Walled Nanotubes (MWNTs) was dispersed in synthetic poly-(alfa-olefin). Measured thermal conductivity for the nanofluid was anomalously higher than the thermal conductivity of the basefluid (up to 150% at approximately 1 vol%). Further the experiment results showed that thermal conductivity is nonlinear with nanotube loading. Similar result was reported by Xie et al. [16]. Hong et al. [17] carried out the study of Fe-ethylene glycol nanofluid and reported the nonlinear relationship between thermal conductivity and concentration. Murhed et al. [18] reported the nonlinear behavior for water based nanofluid containing spherical and

19

rod-shaped TiO$_2$ nanoparticles. Das et al. [19] studied the thermal conductivity of water based nanofluid with Al$_2$O$_3$ or CuO over a temperature range of 20 and 50°C. The experimental results showed that thermal conductivity of the nanofluid increased by two to fourfold within the temperature range. Chon et al. [20] reported correlations for the thermal conductivity of Al$_2$O$_3$ nanofluids as a function of nanoparticle size (ranging from 11 nm to 150 nm nominal diameters) over a temperature range of 21 to 71°C. This article supports the fact that the thermal conductivity increases with increase in temperature and decreased with nanoparticle size. Chopkar et al. [21] studied the effect of particle size on the thermal conductivity of ethylene glycol–based nanofluids containing Al$_{70}$Cu$_{30}$ nanoparticles and the results from this study also supports the fact that thermal conductivity of the nanofluid is strongly dependent of the particle size.

Keleinstreur [22] reviewed more than 50 studies which support the following facts about nanofluid thermal conductivity

- nanofluid have high thermal conductivity even at low particle concentration

- there is nonlinear relationship between thermal conductivity and particle concentration

- thermal conductivity is strongly dependent on temperature

- thermal conductivity is strongly dependent on particle size

Many correlations have also been proposed to predict the thermal conductivity of nanofluid. Some correlations were theoretically derived and are applicable for any size of particle dispersion while others were empirically derived from the data obtained from experiments with specific conditions and for nanofluid with certain nanoparticle and basefluid, particle concentrations and shapes and sizes. Ding et. al. [23] has catalogued

20

some correlations used to predict the effective thermal conductivity of nanofluid. Few other correlations can be found in [20], [24], and [25].

2.2.2 Viscosity of nanofluid

With high thermal conductivity nanofluid has potential for a wide range of application in heat transfer, microelectronics, industrial processes, engine cooling/vehicle thermal management, refrigerator, chiller, heat exchanger, nuclear reactor coolant, machining, in boiler flue gas temperature reduction and so on. All these applications are associated with flow of nanofluid over a heat exchanger surface. The property of the fluid related to flow is viscosity (μ). At this point it is worthwhile to mention again that, by addition of nanoparticles in the base-fluid the viscosity changes.

Earliest study on viscosity of suspension that could be found on the literature is Einstein theory [5] and [26] according to which the effective viscosity of dispersed fluid depends only on the concentration of the dispersed particles and is always greater than the viscosity of the carrier fluid. For nanofluid, even though increasing particle concentration increases the viscosity, it is not the only factor affecting the viscosity. And the viscosity of nanofluids is much higher than that predicted by the classical Einstein theory for viscosity [27]. Many studies have been carried out on effect of concentration on viscosity of nanofluid and showed that the viscosity of nanofluid increases with concentration of particles. Prasher at el. [27] includes synopsis of such studies which show that the relative viscosity of nanofluid is a strong function of the nanofluid volume fraction. Experimental data presented in [28], for SiC nanofluid, is in agreement with [27]. It is well established that with increase in temperature the viscosity of a fluid decreases. Different correlations for temperature and viscosity of liquids (single phase) are given in [29]. In a nanofluid the

21

viscosity generally decreases with temperature faster than is the case for the basefluid on its own. [30]. For alumina, nanoparticles dispersed in car engine coolant [31], viscosity of the nanofluid decreased exponentially with increase in temperature of the nanofluid and authors assumed it to be due to the weakening of inter-particle and inter-molecular adhesion forces. Lee et al. [32] observed that, for 3% SiC/deionized water nanofluid, the "relative viscosity" increased from 68% to 102%. Such dependence of nanofluid viscosity on temperature is presented in review [33]. Most of the studies conclude that viscosity decreases with increase in temperature expect for [27] which indicate that the viscosity of nanofluid is independent of temperature. Different studies of dependence of viscosity of nanofluid on particle size have been reported in [33]. Results reported on different studies contradict with each other. Some studies report viscosity to increase in particle size and other report viscosity to decrease in particle size. Prasher et al. [27] reports viscosity is independent of particle size. Thus for particle size and viscosity of nanofluid, till now, there is no universally accepted relation. Viscosity of nanoparticles has a strong dependence with nanoparticle shape [10]. Tiemofeeva et al. [34] reported that elongated particle, such as cylindrical particles, result in higher viscosity at the same volume faction and spherical particles or lower aspect ratio spheroids are more desirable for lower viscosities. To predict the viscosity of nanofluid several correlations have been proposed. As in case of correlations for thermal conductivity, some of these correlations are universally applicable while others are applicable for specific conditions and for nanofluid with certain nanoparticle and basefluid, particle concentrations and shapes and sizes. Correlations for nanofluid viscosity can be found in [35].

2.2.3   Heat transfer with nanofluid

When nanoparticles, with higher thermal conductivity is dispersed in a base fluid the resulting colloid or nanofluid is expected to have thermal connectivity higher than that of the basefluid. Studies of nanofluid thermal conductivity, reviewed in earlier section of the chapter, confirms the improvement in thermal conductivity. Consequently the heat transfer of the nanofluid is expected to increase.

Kakac et al. [36] makes a good discussion about heat transfer of nanofluid. Some information from this paper related to current study is discussed in this paragraph. Enhancement in heat transfer mostly depends upon factors such as particle volume concentrations, particle material, particle size, particle shape, base fluid material, temperature and additives. Experiments with Al_2O_3 nanoparticles in water under laminar and turbulent regime resulted in heat transfer enhancement of more than 40% while the thermal conductivity enhancement was only 15%. Heat transfer by forced convection is defined by the Nusselt number which is a function of Reynolds number and Prandtl number for common fluids.

$$Nu = f(Re, Pr) \tag{2.2.1}$$

Nusselt number for nanofluid (Nu_{nf}) is expected to be a function of Re, Pr, and few more parameters viz. thermal conductivity and heat capacity of the base fluid and nanoparticles; volume fraction of suspended particles, and the shape of the particles.

$$Nu_{nf} = f\left(Re, Pr, \frac{k_{nf}}{k_{bf}}, \emptyset, \text{particle shape}, \text{flow geometry}\right) \tag{2.2.2}$$

where $\emptyset$ is the particle volume fraction and subscripts nf and bf denote nanofluid and basefluid respectively. This paper also suggested that one of the reasons for the enhancement in heat transfer is due to Brownian motion. Random motion of ultra-fine

particles would create a slip velocity between solid particle and fluid medium. To account for Brownian motion small perturbations in velocity and temperature formulations was to be included.

Ding et al. [37] discusses about natural convection in nanofluid. For natural convection, heat transfer is observed to decrease with increase in particle concentration and this is partially attributed to increase in viscosity. Experiments of natural convection heat transfer with aqueous based TiO_2 nanofluids with 0.8, 1.5 and 2.4 wt % concentration were conducted. Results of the experiment showed that Nusselt number decreased with increase in concentration.

Experimental works on convection in nanofluid is included in chapter 5 of Das et al [5]. Experiments with 1.34% and 2.78% volume fraction of Al_2O_3 enhanced the heat transfer coefficient by 45% and 75%. This enhancement was seen when heat transfer coefficient was compared at equal Reynolds number. However, only 3-12% decrease was observed when comparison at constant velocity. Experiment with pure copper particles showed an increase in heat transfer coefficient up to 40% at same velocity. The volume fraction of copper particles were 0.3%, 0.5%, 0.8%, 1.0%, 1.2%, 1.5%, and 2.0%. Researchers in this experiment stated that not only volume fraction but also the particle dimensions and material properties were important and pointed out that with proper design of nanofluid, significant increase in heat transfer can be achieved.

Kim et al. [38] investigated the effect of nanofluid on heat transfer in circular straight tube with constant heat flux. Water based alumina and amorphous carbonic nanofluid were studied in laminar and turbulent regime. This study concluded that improvement of heat transfer was higher, the improvement in thermal conductivity was obsereved and the

movement of nanoparticles enhanced the convective heat transfer at the entrance region. The results of the experiments carried out for this study showed that for 3% by volume of alumina nanofluid, thermal conductivity improved by 8% and convective heat transfer coefficient improved by 20%. For amorphous carbonic nanofluid (3.5% by vol.) there was no improvement in thermal conductivity and only 8% improvement in heat transfer coefficient. Comparison of heat transfer coefficients were made at equal Reynolds numbers (1460 and 6020) between deionized water and water based nanofluids.

Convective heat transfer performance and flow characteristics of TiO_2-water nanofluid was studied by Duangthongsuk et al. [39]. For this, experiments were carried out in turbulent regime in horizontal double tube counter-flow heat exchanger. From these experiments the authors concluded that at volume concentration of less than 1%, the heat transfer was significantly improved, up to 26% greater than that of pure water. But at particle concentrating of 2% by volume, the heat transfer coefficient lowered up to 14% than that of pure water. Here again the comparisons were made at same Reynolds number.

The effectiveness of Al_2O_3 nanoparticle (1% and 2 % by vol.) at enhancing single-phase and two-phase heat transfer in micro-channel heat sinks was studied by Lee and Mudawar [40]. This study showed that for single phase the overall improvement in heat transfer was insignificant. Greater heat transfer improvement was observed in thermal entrance region and in fully developed region lower heat transfer improvement was observed. Thus 'proving that nanoparticles have an appreciable effect on thermal boundary layer development'. For two-phase flow, deposition of nanoparticles at channel exit due localized evaporation was observed. In this is study the author has also pointed out some disadvantage of nanofluids, which is as follows

- Increased axial rise in wall temperature due to degraded specific heat

- Increased pumping power due to greater pressure drop

- Long-term fluid settling and potential clogging of flow passage

- Possible damage of flow loop parts by erosion

- Inability to sustain flow boiling

- High cost of nanoparticle suspensions

Steady state turbulent convective heat transfer and pressure drop characteristics of Al_2O_3 – water nanofluid inside a circular tube were investigated by Sahin et al. [41]. The experiments were carried out with 0.5%, 1%, 2% and 4% by volume particle concentration and Reynolds number range of 4000 to 20,000. Here the enhancement in heat transfer was observed only in experiments with particle concentrations less than 2% and maximum enhancement at 0.5% by volume particle concentration and Reynolds number of 8000. Selvakumar and Suresh [42] studied the effect of CuO/water nanofluid in a thin channeled copper heat sink under constant heat flux conditions. With volume fraction of 0.1% and 0.2% nanofluid the experiments were carried out at 0.79 LPM and 2.45 LPM. Maximum enhancement in heat transfer coefficient of 29.63% was observed for 0.2% volume fraction nanofluid. In this study it is also reported that the pumping power increased by 15.11%.

2.2.4 General properties of Nanofluid

Timofeeva at el. [10] related the nanofluid properties with engineering parameters in a decision matrix (Table 3). Each cell in the matrix represented the strength of the effect of a particular parameter to the nanofluids' property with symbols indicating - no, weak, medium, and strong dependence, respectively, that were scored as 0.0, 0.25, 0.5, and 1.0 correspondingly. The relative importance of each engineering parameter, contributing to

thermal transport, was estimated as the sum of the gained scored. The engineering parameter that contributed most was the nanoparticle concentration followed by base fluid, nanoparticle size, and so on. With exceptions of [27] , Table 3 can be used to summarize the effects of nanoparticle concentration, nanoparticle shape and size, temperature of nanofluid, and other parameters on nanofluid properties. Thermal conductivity of a nanofluid has medium dependence on nanoparticle material, and nanoparticle shape; and strong dependence on temperature and nanoparticle size. Viscosity of nanofluid has weak dependence on nanoparticle material; and strong dependence on nanoparticle concentration, nanoparticle shape, nanoparticle size, base fluid; and temperature. More importantly, the heat transfer coefficient of the nanofluid is strongly dependent on all the engineering parameters i.e. nanoparticle material, concentration, shape, size, base fluid and temperature. Also the pumping power has strong dependence on all the parameters except nanoparticle material.

Table 3. Nanofluid porperties and engineerin parmeters in decision matrix [10]

NANOFLUID PROPERTIES	ENGINEERING PARAMETERS	Nanoparticle material	Nanoparticle concentration	Nanoparticle shape	Nanoparticle size	Base fluid	Temperature
Stability	⇑	▲	▲	▲	■↓	○	?
Density	⇑	■	■↑	x	x	■	x
Specific Heat	⇑	■	■↓	x	x	■	▲
Thermal Conductivity	⇑	○	■↑	○	■↑	▲	○
Viscosity	⇓	▲	■↓	■	■↓	■↑	■
Heat Transfer Coefficient	⇑	■	■↑*	■	■↑	■	■
Pumping Power Penalty	⇓	x	■	■	■↑	■	■
Relative Importance		4.0	6.25	3.75	5.0	5.25	3.75

Symbols:

■- strong dependence; ○- medium dependence; ▲- weak dependence; x - no dependence;

? - unknown or varies from system to system; ⇑ - larger the better; ⇓ - smaller the better;

↑- increase with increase in parameter; ↓- decrease with increase in parameter; *-within the linear property increase.

Attempts had been made to generalize the dependence of naonofluid properties on different parameters. One of such studies was International Nanofluid Benchmark Exercise [43] and [44]. These studies included eight different nanofluids and involved 30 laboratories around the world. Buongiorno et al. [43] suggested that Maxwell equation can be used to predict the effective thermal conductivity of nanofluid and [44] agrees with above discussed dependence of viscosity of nanofluid on different parameters. This exercise is a state-of-art research, however, the results from INPBE are inadequate to make conclusion about nanofluid properties. This is due to the fact that these measurements of properties for this exercise were carried out without temperature control, in a narrow range of volume concentration of nanoparticles, with a wide range of nanoparticle and for different basefluids. Such exercise with wider scope would certainly advance the understanding of nanofluid properties, nonetheless no other papers have been published by INPBE.

2.2.5 Density and heat capacity of Nanofluid

Properties of density and the heat capacity of nanofluid are function of particle volume concentration. Correlations (2.2.3) and (2.2.4) are for nanofluid density and heat capacity.

$$\rho_{nf} = (1 - \emptyset)\rho_{bf} + \emptyset\rho_{np} \tag{2.2.3}$$

$$c_{p,nf} = (1 - \emptyset)c_{p.bf} + \emptyset c_{p,np} \tag{2.2.4}$$

2.2.6 SiO₂ nanofluid

Julia et al. [45] attempted to characterize the heat transfer and pressure drop of Al_2O_3 and SiO_2 water based nanofluid with particle size of 11 nm and 12 nm respectively. The experiment was carried out with volume concentrations of 1% and 5% and with flow rates corresponding to Reynolds number between 3×10^3 and 3×10^5. They reported a maximum heat transfer enhancement of 300% (compared at same Reynolds number) and pressure drop penalty of 1000% for SiO_2. Azmi et al [46] investigated heat transfer and friction factor of TiO_2 and SiO_2 water based nanofluid in a circular tube under turbulent flow and constant heat flux boundary conditions. Average particle size for TiO_2 and SiO_2 were 50 nm and 22 nm respectively and the range of Reynolds number was 5000 to 25000. For TiO_2, maximum enhancement in heat transfer was 26% with 1.0% concentration and for SiO_2, it was 33% with 3% volume concentration when compared with heat transfer of water at similar Reynolds number. They also observed that the pressure drop was directly proportional to the density of nanoparticles and the friction factor for TiO_2 and SiO_2 as 23.5% higher than that of water. Hussein at el. [47] studied the effect of nanofluid volume concentration on heat transfer and friction factor using numerical simulation. They measured the thermal properties of three types of nanoparticles ($Al2O_3$, TiO_2 and SiO_2) dispersed in water which was used as input parameters for forced convection heat transfer

inside a flat heated tube numerical simulation. From the simulation results, the authors concluded that friction factor and Nusselt number increased with volume concentration. They also reported enhancement of heat transfer of 6% and decrease of pressure drop by 4% when flat tube was compared with circular tube. The range of Reynolds number was from 5×10^3 to 50×10^3. In brief these studies on SiO_2 nanofluid were conducted with nanoparticle volume concentrations of 5% and less with flow in turbulent regime. They claim up 33% increase in heat transfer coefficient with SiO_2 nanofluid when compared to the basefluid.

CHAPTER 3

EXPERIMENTAL SETUP AND METHODOLOGY

This chapter discusses the setup and methodologies in two sections for various experiments carried out to accomplish the objectives of this study. Experiments were carried out to measure thermal conductivity, rheological property (shear stress-strain relationship), flow (pressure drop) and heat transfer (heat transfer coefficient). The results of these experiments are discussed in the subsequent chapters.

3.1 Experimental setup for thermal conductivity and rheological measurement

The experimental setup described in [48] was used to measure the thermal conductivity and the viscosity of the fluid under study. Decagon Devices KD2 Pro Thermal Properties Analyzer was used to measure the thermal conductivity. Brookfield temperature bath (model TC-550 MX) was used to control the temperature of the fluid. The schematic of thermal conductivity measurement using KD2 Pro is shown in Figure 2.
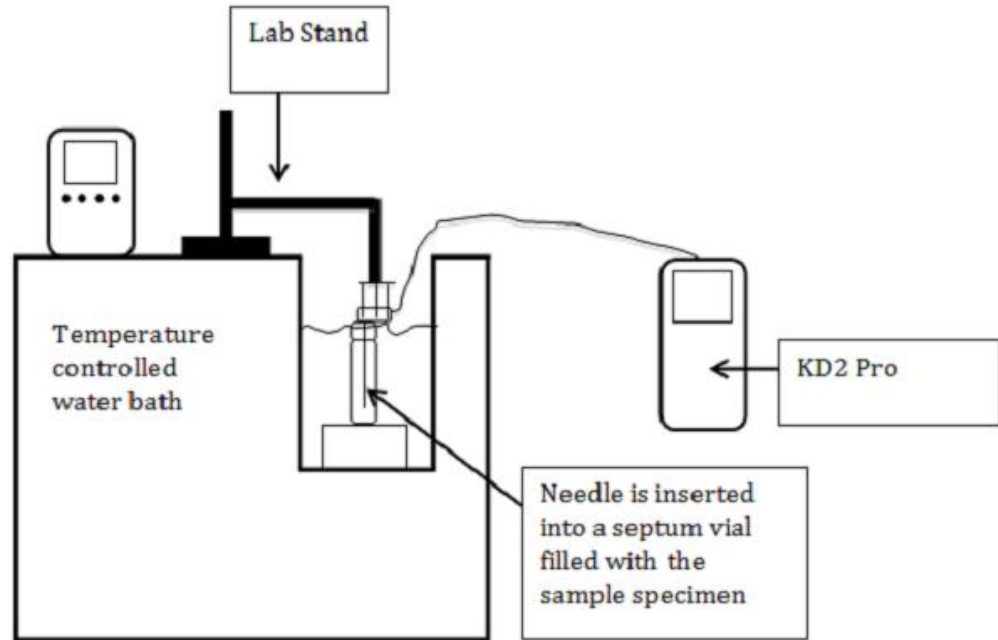
Figure 2. Schematic of thermal conductivity measurement [48]

To measure the viscosity of the fluid, Brookfield viscometer (model DV-II+ Pro Extra, ± 0.1% accuracy) was used. And to control the temperature of the fluid, water jacket connected to the temperature bath was used. A simplified schematic is presented in Figure 3. The viscometer was connected to a computer with Rehocalc V3.3 Build 49-1 software installed. This allowed the use of a computer to read, stored and analyze data of the shear stress and the viscosity from the viscometer. It also allowed to control the viscometer during experiment.
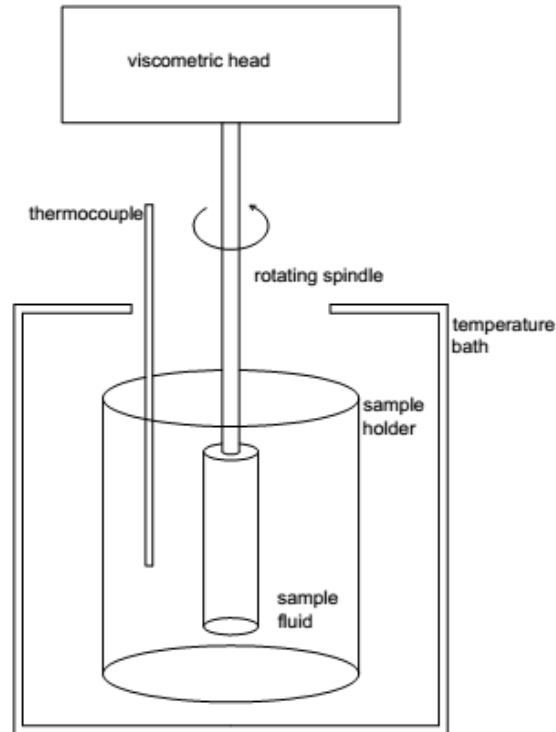
Figure 3. Rotational viscometer schematic

3.2 Experimental setup for flow and heat transfer measurement

The main objective of this research is to study the flow behavior and the heat transfer characteristics of colloid made up of silicon dioxide nanoparticles dispersed in water. To accomplish this objective, experimental flow loop described in [8] was used to measure the pressure drop across small tubes of various cross-sections and hydraulic diameters, and to measure the local heat transfer on the internal surface of the tube at different locations along its length. Figure 4 depicts the schematic of the experimental flow loop.

The experimental flow loop can be broken down into following components:

- Fluid storage tank

- Gear pump

- Shell and tube heat exchangers

- Mass flow meter

33

- Test sections and insulation

- Connecting tubes and valves

- Pressure transducers

- Temperature transducers

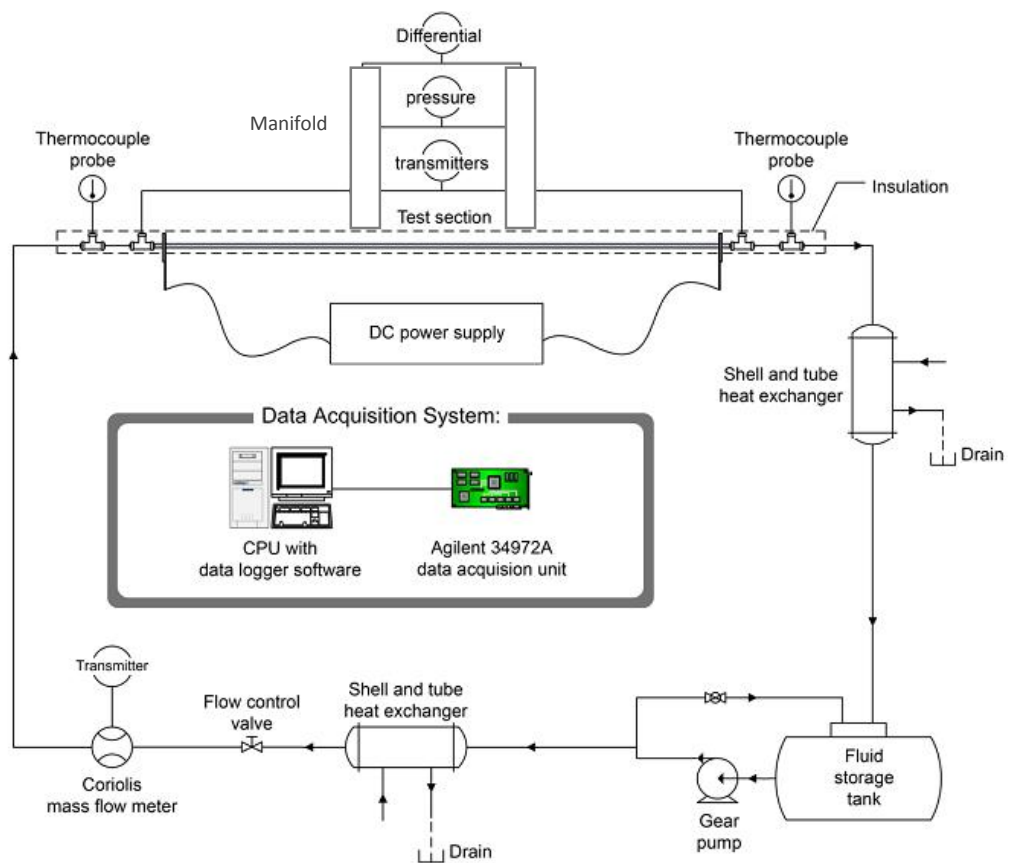- DC power supply unit

- Data acquisition unit

Figure 4. Schematic of the experimental flow loop [8]

3.2.1 Fluid storage tank

A three-gallon medium-density polyethylene tank was used as fluid storage tank. This tank had two inlet port at the top and an outlet port at the bottom. One of the inlet ports was connected to the by-pass valve with the flexible PVC tubing and the other was connected

to the outlet side of the heat exchanger which cooled the working fluid after flowing through the test section. The outlet port had an asphalt valve which was connected to the suction of the gear pump.

3.2.2 Gear pump

Liquiflow gear pump (Model 35F) was used to push the working fluid under study through the flow loop. This pump was driven by a motor which was controlled by a variable frequency drive, and the speed of the pump ranged from 0 to 1750 rpm. Maximum operating differential pressure for the pump was 100 psi. The discharge of the pump was connected to a T-connector. The T-connector then connected to the inlet of the heat exchanger, which was used to maintained temperature at the inlet of the test section, at one of the sides, and the other connected to the bypass valve which returned the fluid to the storage tank.

3.2.3 Shell and tube heat exchangers

Two counter-flow shell and tube heat exchangers were used in the flow loop. One of them was placed after the gear pump and its purpose was to maintain a constant temperature at the inlet of the test section. The other heat exchanger was placed after the test section and its function was to remove the heat added to the fluid under study flow through the test section.

3.2.4 Mass flow meter

From the first heat exchanger the working fluid flowed through a regulating valve and into a Micro Motion Coriolis mass flow meter (model CMFS010M). The accuracy of the mass flow meter was ±0.1% for a flow rate of 1-50 g/s. The working principle of the mass flow meter is Coriolis Effect. It consists of a vibrating U-shaped tube through which the fluid is

passed. The angular velocity and the inertia of the fluid causes the tube to twist which is sensed by an electromagnetic sensor in terms of phase change, and measured in terms of mass flow. The mass flow meter was connected to a digital transmitter (model 1700R) which conditioned the flow rate signal for data acquisition system.

3.2.5   Test sections and insulation

Six different brass test sections were studied. Each of them were 12 inches long and with wall thickness of 0.014". Three of them were circular with outer diameter of 1/16", 3/32" and 1/8" inches. The other three had square cross-section with external width of 1/16", 3/32" and 1/8" inches. For both shapes hydraulic diameters were 0.035", 0.066", and 0.097" (0.88 mm, 1.67 mm and 2.46 mm) Teflon collar of length 3/4 inch was fitted at the ends of these tubes with epoxy. Theses collars served the purpose of electrical insulation and connectors to the flow loop. The test sections were insulated using a wooden insulation box whose inner surface consisted of an inch thick glass-fiber (R-25).

3.2.6   Connecting tubes and valves

Stainless steel tubes of size 1/4 inch, stainless steel fittings and flexible PVC tubings were used to connect different components of the flow loop. The position of the valves are shown in Figure 4.

3.2.7   Pressure transducers

From the mass flow meter the working fluid was flowed into a T-connector which connected to a manifold and the test section. The manifold connected to the high pressure side of three Rosemount differential pressure transmitters. These pressure transducers corresponded to the differential pressure of 9, 36 and 300 psi (±0.65 accuracy) [62, 248 and 2070 kPa (±015% accuracy)]. Lower pressure side of these transducers were connected

a second manifold which was then connected to the outlet of the test section through a T-connector. Also a static pressure transducer was connected to each of the manifold which corresponded to 50 psi pressure. The accuracy of the pressure transducers were verified using Dwyer digital pressure gauges (model DPG-107, range 0-300 psi and model DPG-104, range 0-50 psi) and a pneumatic hand pump from Ametek (model.T-970, range 0-580 psi).

3.2.8 Temperature transducers

T-type thermocouples from Omega (model TMQSS-020U-6) were used to measure the bulk temperature of the fluid at the inlet and outlet. These thermocouples were inserted in the flow loop at upstream and downstream of the test section. To measure the wall temperature of the test section, T-type thermocouples, with wire diameters of 0.127 mm, were cemented on its outer surface along the length. These thermocouples were calibrated and at freezing and boiling temperature of water. The thermocouples were cemented at 10 different axial positions along the tube. The first and the last positons were 1.5 inches from the end of the tubes and the other 8 were positioned between them at an equal gap of 1 inch. The epoxy used to cement the thermocouple to the surface had thermal conductivity of 1.04 W/m-K and a high electrical resistivity of 1×10^{15} Ω-m.

3.2.9 DC power supply unit

To generate heat N5761A DC power supply from Agilent Technologies was used which created to create direct voltage drop across the tests sections. It had rated output of 6 V / 180 amps, 1080 W. Direct current was applied across the test section using 2 gauge wire and copper split screws and nuts. The flow of the current through tube generated uniform heat flux for the fluid flowing in it. A remote sense circuit was also connected to the copper

split screws and nuts DC power supply. This allowed the compensation of voltage drop due to resistance in wire.

3.2.10 Data Acquisition unit

The output direct current signals corresponding to mass flow rate, pressure, temperature, direct current and direct voltage from mass flow meter, pressure transducers, thermocouples and DC power supply respectively were logged using Agilent 34972A Data Acquisition unit connected to a computer. Relationship between direct current signal from thermocouples and temperature were pre-set in the data acquisition software. For mass flow rate and pressure, linear relations were developed for data logging.

3.3 Experimental methodology

3.3.1 Thermal conductivity measurement

Thermal conductivity of the fluids under study was measured using Decagon Devices KD2 Pro Thermal Properties Analyzer. The standard operating procedure for this equipment can be found in [3]. Initially the equipment was validated by measuring the thermal conductivity of the standard fluid (k=0.285 W/m-K at 20℃). About 50 ml of the fluid was taken in a vial whose temperature was controlled using temperature bath. Once the vial and the fluid had attained a uniform temperature the thermal conductivity was measured. The motivation behind the measurement of thermal conductivity was to observe its relationship with temperature. Thus thermal conductivity was measured between temperature range of 0 ℃ and 50℃. This range of temperature was governed by the freezing and boiling temperature of water as one the fluids whose thermal conductivity was of interest was water itself and the other was water based SiO_2 nanofluid. Once the temperature of bath was set

to desired value, the vial was allowed to attain uniform temperature distribution for 15 minutes.

3.3.2 Rheological measurement

Rheological properties of the fluids under study (water and SiO_2 nanofluid) was measured using Brookfield viscometer (model DV-II+ Pro Extra), a rotational type viscometer. The working principle of this viscometer is explained in Section 2.1.1. Standard operating procedure for this equipment can be found in [3]. Before the rheological properties of the fluids under study were measured, the viscometer was validated with the calibration fluid provided by the manufacturer (Brookfield) whose viscosity is known (493 cP at 25℃). The fluids were studied for a temperature range of 5℃ to 55℃. As in experiments to measure thermal conductivity, the temperature range was dictated by the freezing and boiling temperature of the water. The shear rate range, for which the rheological property was studied, was governed by the percentage of full scale torque of the calibrated spring in the viscometer (refer to working principle in section 2.1.1). Valid measurement readings are obtained between 10-90% of the full scale torque. First, the desired temperature of the fluid was maintained using the water jacket and the temperature bath. Then appropriate shear rate was applied to the fluid (by setting to the spindle rpm). Then shear stress developed at this shear rate was logged. Viscosity of the fluid can then be calculated for this shear rate using equation (2.1.1). This process was repeated for five to six steps of increasing (or decreasing) shear rate within 10-90% of the full scale torque range. Then this process was repeated for increasing (or decreasing) temperature steps of 5℃.

3.3.3 Friction factor and heat transfer measurement

3.3.3.1 Test section preparation

Each of the 6 test sections were 12 inches long whose surface was cleaned and ends made free form burrs. Teflon collar of 3/4 inch were fitted to each end of the test section Then half inch copper strips were soldered around the tube just at the inner end of the collar. To mark the positions of thermocouple on the tube a wooden board was used. On this board a straight line whose length was equal to the length of the tube was drawn and 10 points were marked accurately on this line at gap of 1 inch. The first and the last marks were 1.5 inches from the ends. Test sections were attached to this board and thermocouples were then cemented to the tube at the marks. Each thermocouples on each tubes were assigned with an identification number according to their location along the length of the tube, #1 being closest to the inlet. Summary of the thermocouple identification number is given in Table 4. On all the three circular tubes and 1/16sq, 10 thermocouples were cemented on them. On 1/8sq 19 thermocouples were cemented and on 3/32sq 20 thermocouples were cemented.

Table 4. Summary of thermocouple identification number

S.N.	Distance from inlet [in]	Thermocouple identification number					
		1/8 circular	3/32 circular	1/16 circular	1/8 square	3/32 square	1/16 square
1	1.5	1	1	1	1	1,2	1
2	2.5	2	2	2	2	3,4	2
3	3.5	3	3	3	3,4,5,6	5,6	3
4	4.5	4	4	4	7	7,8	4
5	5.5	5	5	5	8	9,10	5
6	6.5	6	6	6	9,10,11,12	11,12	6
7	7.5	7	7	7	13	13,14	7
8	8.5	8	8	8	14,15,16,17	15,16	8
9	9.5	9	9	9	18	17,18	9
10	10.5	10	10	10	19	19,20	10

3.3.3.2 Flow loop

Proper flow loop setup is crucial for overall success of the experiment. Proper flow loop setup would mean:

- the loop is free from leakage

- there is a steady supply of working fluid to test section

- there is proper thermal insulation of test section

- accurate measurement of pressure, temperature and mass flow rate

- un-interrupted supply of direct voltage across the test section

- there is proper electrical insulation of the test section

Components of the flow loop were assembled as explained in section 3.1. Once the flow loop was setup, only the test section had to be replaced as the experiment progressed. After the first test section was fitted to loop, it was check for leakage using a pneumatic hand pump from Ametek (model T-970). The pneumatic hand pump was connected to the T-connector at inlet of the test section. With the valves before the mass flow meter and after

41

the test section closed, pressure of about 6 psi was applied using the pneumatic hand pump. Then this pressure was observed for a minute. Loss of pressure would mean that there is leak in one or more connections. The leak was checked with soap bubble method. After the loop was made leak free, the working fluid was pumped through it and the air was purged. Then before supplying the direct voltage, electrical insulation was check between the test section and the fittings. Pressure readings, temperature reading, flow meter readings and direct voltage and current were logged for 2 minutes and made sure that there was no inconsistency in data logged.

3.3.3.3 Data logging

Once the flow loop was setup with appropriate test section temperature, pressure, current and voltage reading were logged for at least 23 different mass flow rates in computer using a data acquisition unit. The mass flow rates were chosen to include all the three flow regime i.e. laminar, transition and turbulent. However for smaller hydraulic diameter test sections the higher mass flow rate could not be attained due to the limitations of the experimental setup. For each mass flow rate, the system was allowed to attain a steady state condition of temperature and pressure. Before applying the direct current across the test-section, the working fluid was pumped through the flow loop at desired mass flow rate. It was then allowed to attain a steady state of pressure drop across the test section for that flow rate. To attain isothermal steady state it took about 3 to 4 minutes. Then 100 sets of data were logged. Then without disturbing the flow rate, DC power supply was turned on to heat the test section. The current supply was adjusted such that the temperature of the test section would not rise beyond 65°C. This was done to avoid local phase change (boiling) of the working fluid. Then again the system was allowed to attain steady state condition which

took about 10 to 12 minutes. The internal volume was then acting as a steady state control volume with constant heat flux. After that 350 data sets were logged of which last 100 sets were averaged and used for calculations of the friction factor, the heat transfer coefficient and eventually the Nusselt number. First distilled water was used to validate the experimental setup. Also these results were used as a basis to make comparisons. Then the experiment was continued with SiO_2 nanofluid. At the end of the experiment there were about 2.25 million data points.

3.3.3.4 Friction factor calculation

The friction factor was calculated using Equation (2.1.5) which gives the relationship between pressure drop across the length, dimensions of the control volume and dynamic pressure term $(1/2\rho u^2)$. Rearranging this equation we have

$$f = \Delta P \frac{D_h}{L} \frac{2}{\rho u^2} \qquad (3.3.1)$$

The average velocity (u) can be related to the mass flow rate as

$$u = \frac{\dot{m}}{A\rho} \qquad (3.3.2)$$

The Reynolds number for a Newtonian fluid can be related to the mass flow rate as

$$Re = \frac{\dot{m} D_h}{A\mu} \qquad (3.3.3)$$

The pressure drop and the mass flow rate used for the calculations were obtained by averaging the 100 data points logged after attaining steady state condition.

For a non-Newtonian fluid flowing in a circular tubes the relation for the Reynolds number is given by Equation (2.1.26)

$$Re_n = \frac{D_h^{n'} u^{2-n'} \rho}{K' 8^{n'-m'}} \qquad (3.3.4)$$

43

The value of K' and n' was obtained using Equation (2.1.24), m is equal to 1 for circular tubes and for other shapes (square in this case) is constant obtained empirically from experimental data. With simple algebra following relations can be derived.

$$\tau = \frac{D\Delta p}{4L} = K' \left(\frac{8u}{D}\right)^{n'}$$

$$\log\left(\frac{D\Delta p}{4L}\right) = \log K' + n' \log\left(\frac{8u}{D}\right)$$

Log (DΔP/4L) parameter was plotted against n'log(8u/D) to obtain a straight line whose slope was n' and intercept logK'. For this only mass flow rate were in laminar regime was used. And for turbulent regime for regime same values of K' and n' were used to obtain non-Newtonian turbulent Reynolds number.

3.3.3.5 Heat transfer coefficient and Nu calculations

The local heat transfer coefficient for each thermocouple position was calculated using Equation (2.1.16)

$$q = h(T_{iw} - T_b)$$

where q is the constant heat flux which can be obtained for the current and the voltage drop

$$q = \frac{IV}{\pi DL} \tag{3.3.5}$$

The bulk fluid temperature T_b was calculated from the inlet and the outlet temperature using Equation (3.3.6), assuming a linear relationship

$$T_b = T_{in} + \frac{x}{L}(T_{out} - T_{in}) \tag{3.3.6}$$

The inner wall temperature T_{iw} was calculated from the outer wall temperature T_{ow} measured by the thermocouples using the Equation (3.3.7).

$$T_{iw} = T_{ow} + \frac{q_g}{4k}\left[r_{ow}^2 \ln\frac{r_{iw}}{r_{ow}} + r_{ow}^2 - r_{iw}^2\right] \qquad (3.3.7)$$

Where q_g is the heat generated by direct current per unit volume of the tube

For circular tube

$$q_g = \frac{IV}{\pi(r_{ow}^2 - r_{iw}^2)L} \qquad (3.3.8)$$

Where r_{ow} and r_{iw} are the outer and inner radius of the tube.

For square tubes

$$q_g = \frac{IV}{(D_{ow}^2 - D_{iw}^2)L} \qquad (3.3.9)$$

where D_{ow} and D_{in} are the outer and inner width of the tube

The Local Nusselt number was then calculated using Equation (2.1.20). Also the overall heat transfer coefficient and the overall Nusselt number was calculated by integrating the local values over the length of the tube. For this, the local values at the inlet and the outlet were extrapolated from the four local values following or preceding it and trapezoidal method was used for integration.

$$h_{overall} = \frac{\sum_{i=1}^{11}(h_i + h_{i-1})(x_i - x_{i-1})}{L} \qquad (3.3.10)$$

$$Nu_{overall} = \frac{\sum_{i=1}^{11}(Nu_i + Nu_{i-1})(x_i - x_{i-1})}{L} \qquad (3.3.11)$$

3.3.3.6 SiO₂ nanofluid preparation

The fluid under study was water based SiO_2 nanofluid, with SiO_2 nanoparticle concentration of 9.58% by volume (20% by weight). Three and half gallons (13250 ml) of SiO_2 nf (9.58% by volume) was prepared by mixing 1.523 gallons (5762.5 ml) SiO_2 nanofluid of (40% by volume, 20 nm particle size) with 1.978 gallons (7487 ml) distilled water. The density of the SiO_2 nanofluid prepared was measured to be 1156 kg/m³.

3.4 Experimental Uncertainties

The measurement uncertainty in the Experiment was estimated using the Kline-McClintock Equation (3.4.1)

$$w_R = \sqrt{\left(w_1 \frac{\partial R}{\partial x_1}\right)^2 + \left(w_2 \frac{\partial R}{\partial x_2}\right)^2 + \cdots + \left(w_n \frac{\partial R}{\partial x_n}\right)^2} \qquad (3.4.1)$$

In this equation R is the calculated result which depends on measurements $x_1^{a_1}$, $x_2^{a_2}$,... and $x_n^{a_n}$ $\left(R = f(x_1^{a_1}, x_2^{a_2}, \dots x_n^{a_n})\right)$. The uncertainties related to these measurements are w_1, w_2, …. and w_n respectively [49]. Simplifying

$$\frac{W_R}{R} = \left[\sum \left(\frac{a_i w_i^2}{x_i}\right)\right]^{1/2}$$

For friction factor we have

$$f = f\left(\Delta p, D_h{}^5, \rho, L, \dot{m}^{-2}\right)$$

Since the friction factor is a function of the fifth power of hydraulic diameter, the uncertainty in fiction factor is highly sensitive to the uncertainty of diameter. Mere 3% uncertainty in hydraulic diameter can shoot the uncertainty of friction factor up to 25%. And for Nusselt number we have

$$Nu = f(I, V, D_h, \Delta T^{-1}, k^{-1})$$

Uncertainties in friction factor and heat transfer measurements are given in Tables 5 and 6.

Table 5. Uncertainty in friction factor measurement

Test section	Uncertainty in D_h %	Uncertainty in pressure drop %	Uncertainty in density %	Uncertainty in Length %	Uncertainty in flow rate %	Uncertainty in friction factor %
1/8c	0.62	0.65	1.03	0.52	0.05	3.37
3/32c	0.91					4.75
1/16c	1.74					8.80
1/8sq	0.62					3.37
3/32sq	0.91					4.75
1/16sq	1.74					8.80

Table 6. Uncertainty in Nusselt Number measurement

Test section	Uncertainty in D_h %	Uncertainty in ΔT %	Uncertainty in k %	Uncertainty in voltage %	Uncertainty in current %	Uncertainty in Nu %
1/8c	0.62	1.67	5.00	0.0001	0.0001	5.31
3/32c	0.91					5.35
1/16c	1.74					5.55
1/8sq	0.62					5.31
3/32sq	0.91					5.35
1/16sq	1.74					5.55

CHAPTER 4

RESULTS AND DISCUSSION

4.1   Thermal conductivity

Thermal conductivity for silicon dioxide nanofluid was measured between the temperature range of 0 °C and 50°C using a KD2-Pro Thermal Properties Analyzer. Then an empirical equation, Equation (4.1.1) for thermal conductivity of nanofluid and temperature in degree Celsius was established for this temperature range.

$$k = (-5e - 07)T^3 + (5e - 05)T^2 + 0.0002T + 0.5918 \qquad (4.1.1)$$

Figure 5 consists of a plot in which experimentally measured thermal conductivity of SiO_2 nanofluid, thermal conductivity derived from empirical relation and thermal conductivity of water are presented. From this figure it can be observed that the thermal conductivity of SiO_2 nanofluid is higher than that of the water.
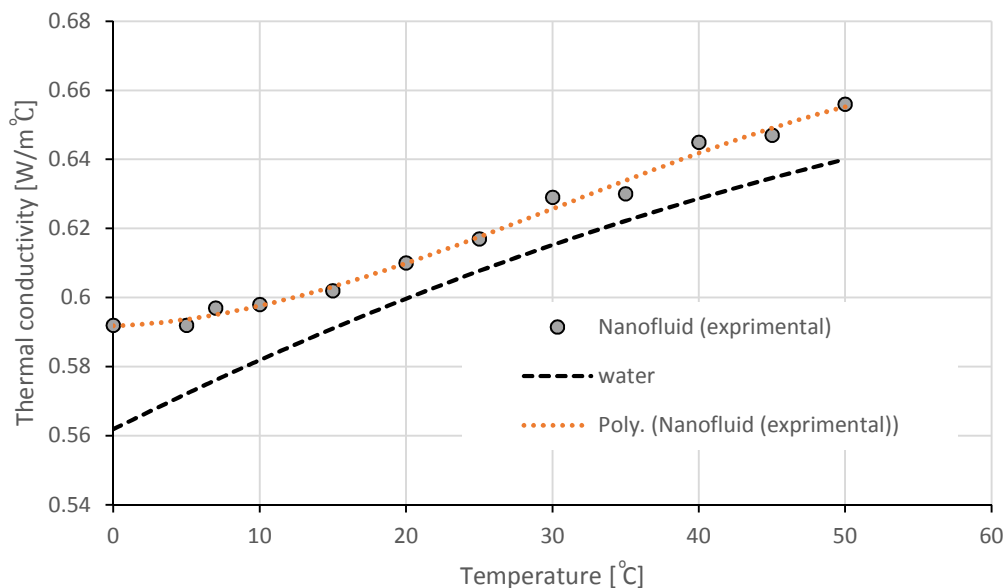
Figure 5. Thermal conductivity comparison for water and SiO_2 nanofluid

The ratio of the thermal conductivity of SiO$_2$ nanofluid to the thermal conductivity of water is plotted against their respective temperature in Figure 6. Using this plot, difference in thermal conductivities of SiO$_2$ nanofluid and water can be estimated. For instance, the ratio of the thermal conductivity of nanofluid to the thermal conductivity of water is 1.02 at 20 °C. This would mean that thermal conductivity of nanofluid is 1.02 time higher that of water. Or in other words the thermal conductivity of nanofluid is 2% higher than that of water. Thus using this figure it can be seen that the thermal conductivity of SiO$_2$ nanofluid is 1.5% to 4.25% higher than that of water for the temperature range of 0°C to 50°C.
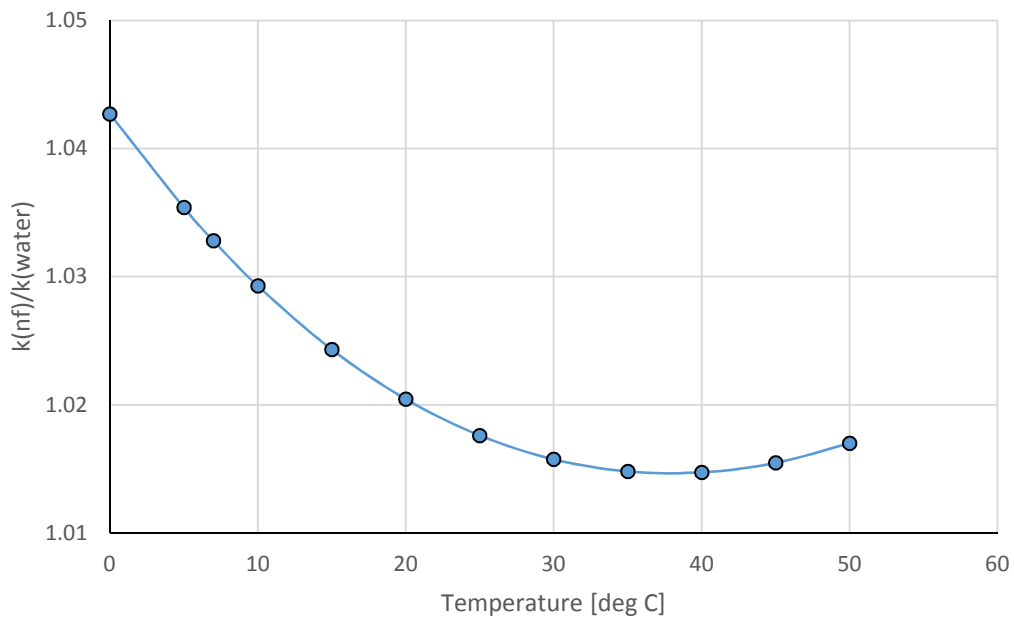
Figure 6. Ratio k(nf)/k(water) versus temperature [deg C]

4.2   Rheological behavior of SiO$_2$ nanofluid

Silicon dioxide nanofluid was subjected to shear rates ranging from 24 to 244 s^{-1}. The resulting shear stresses from these shear rates were measured for temperature range of 7 °C to 50°C. Figure 7 to Figure 10 shows the shear stress results at the temperatures 20 °C, 25

°C, 30 °C and 35 °C for varying shear rate. The markers on the plots represents the data points and the line is the trend line for linear curve fitting. It can be observed from the figure that the shear stress is not proportional to the shear rate. Thus silicon dioxide nanofluid does not behave as a Newtonian fluid within the measurement conditions. Compare following figures with Figure 1. A Newtonian fluid has a linear relationship between shear stress and shear rate and can be represented by a straight line on shear stress versus shear rate plot. This is not true for the plots in following figures. The trends lines representing the shear rate and the shear stress relationship have concave shape as that of shear thickening fluids.
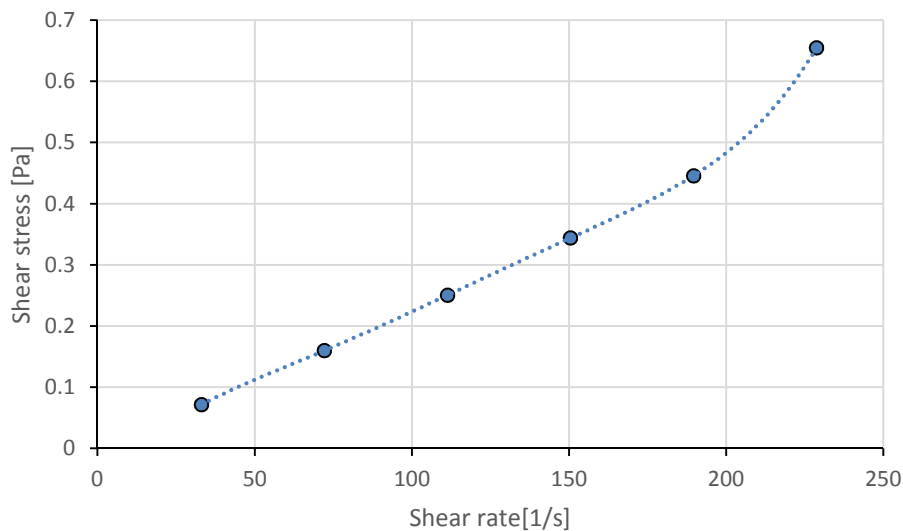
Figure 7. Results of shear stress for varying shear rate at 20 °C
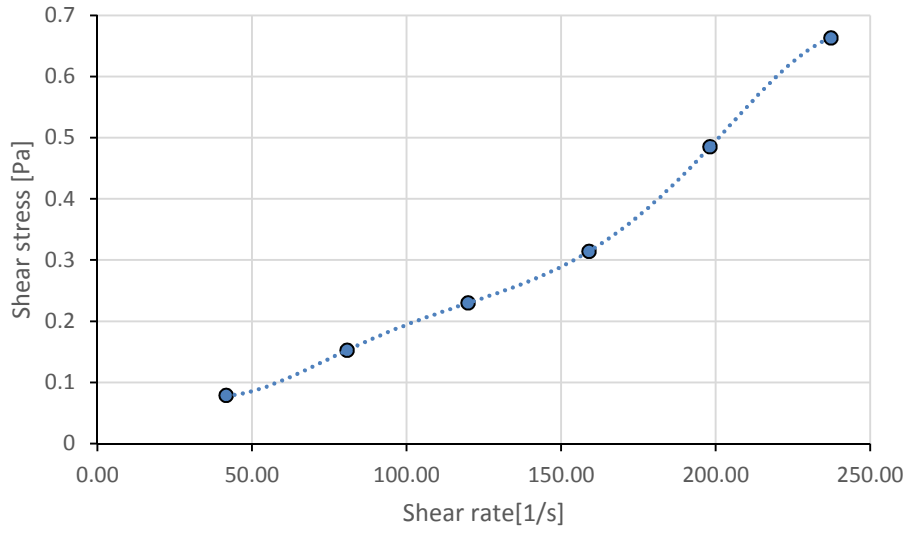
Figure 8. Results of shear stress for varying shear rate at 25 ℃
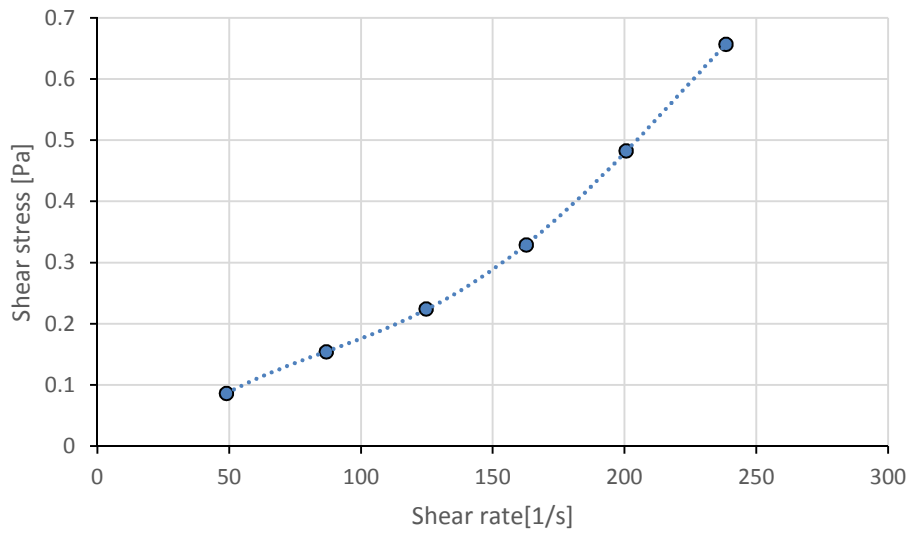
Figure 9. Results of shear stress for varying shear rate at 30 ℃
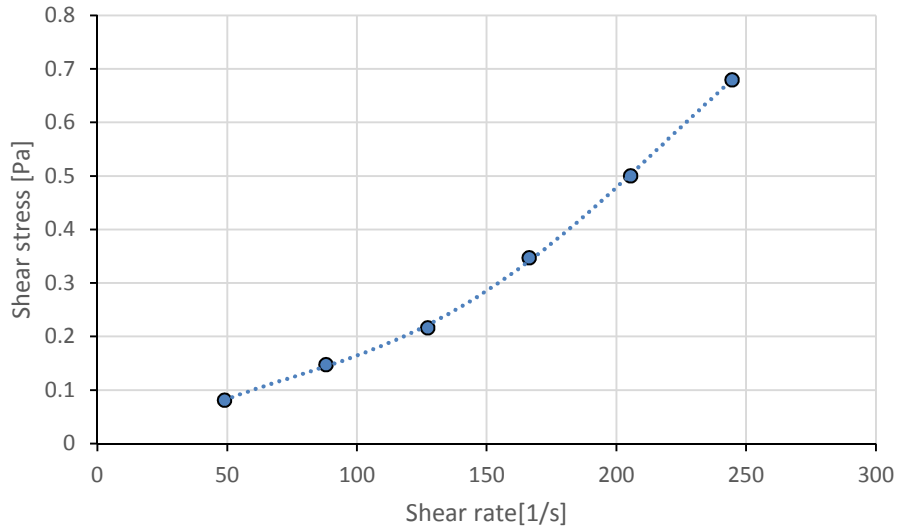
Figure 10. Results of shear stress for varying shear rate at 35 ℃

When the shear stress on a non-Newtonian fluid is divided by the respective shear rate, apparent viscosity is obtained. In Figure 11 to Figure 14, apparent viscosities at varying shear rates are plotted for nanofluid at 20 ℃, 25 ℃, 30 ℃ and 35℃. From these figures it is obvious that the apparent viscosity of SiO_2 nanofluid increases with increase in shear rate. Non-Newtonian fluid which exhibit such behavior is termed as a dilatant non-Newtonian fluid or shear thickening non-Newtonian fluid.
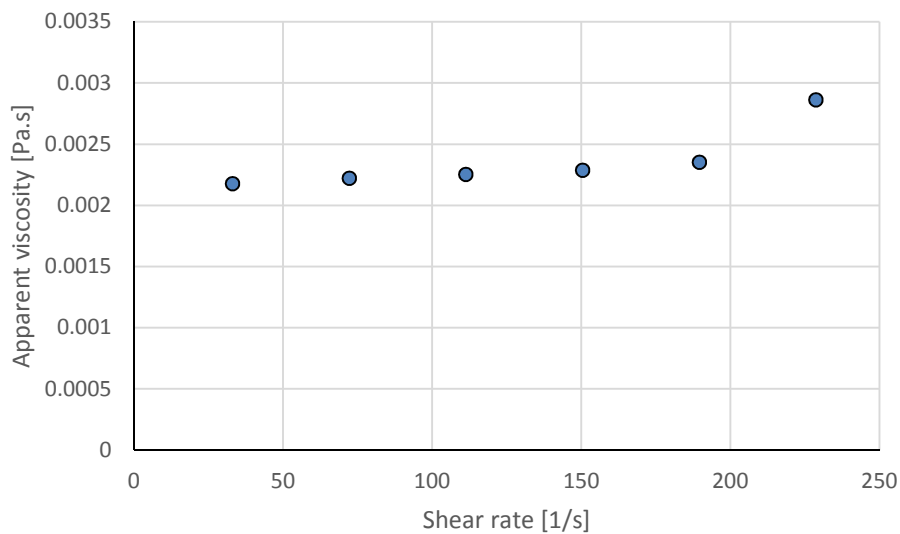
Figure 11. Apparent viscosity at varying shear rate for 20℃

52
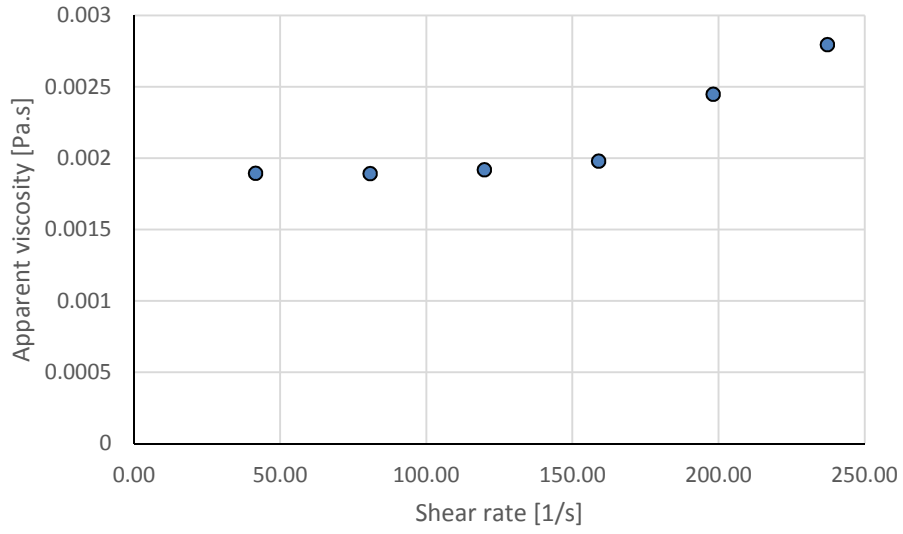
Figure 12. Apparent viscosity at varying shear rate for 25℃
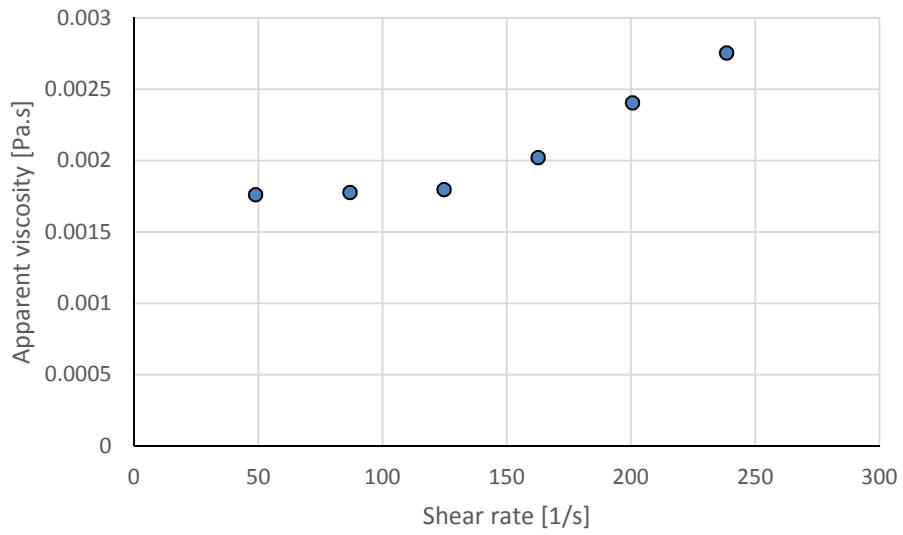
Figure 13. Apparent viscosity at varying shear rate for 30℃
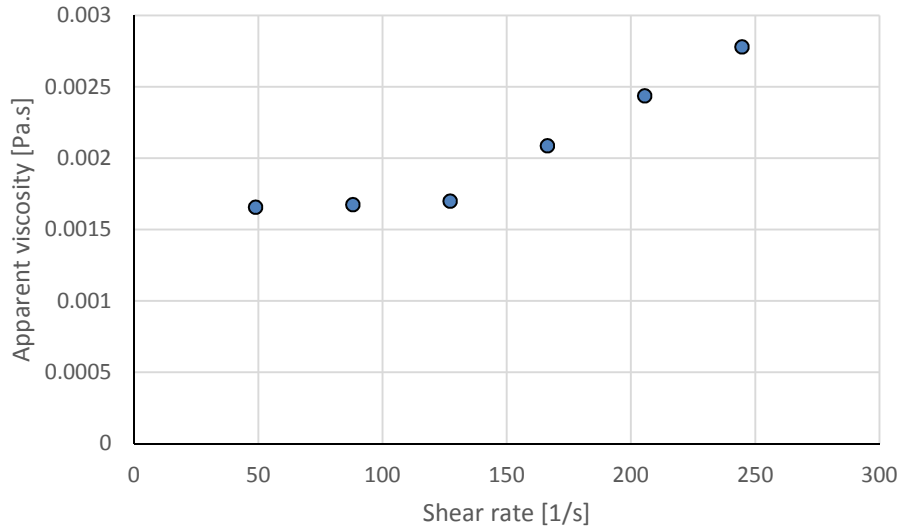
Figure 14. Apparent viscosity at varying shear rate for 35℃

4.3   Flow loop validation with water

To check the reliability of the experimental setup distilled water was run through the test sections. Measured mass flow rate, pressure drop, and dimension of the tubes were used to calculate the experimental friction factor using Equation (2.1.5). Reynolds number was calculated which was used to predict the theoretical friction factor for laminar flow using Equation (2.1.6) for the circular tubes and Equation (2.1.10) for the square tubes. Experimental and theoretical friction factors were plotted against Reynolds number for circular tubes in Figure 15 and for square tubes in Figure 16. The results show that theoretical equation has predicted the experimental results within $\pm$ 15%. This validates the experimental setup for pressure drop measurements.

54
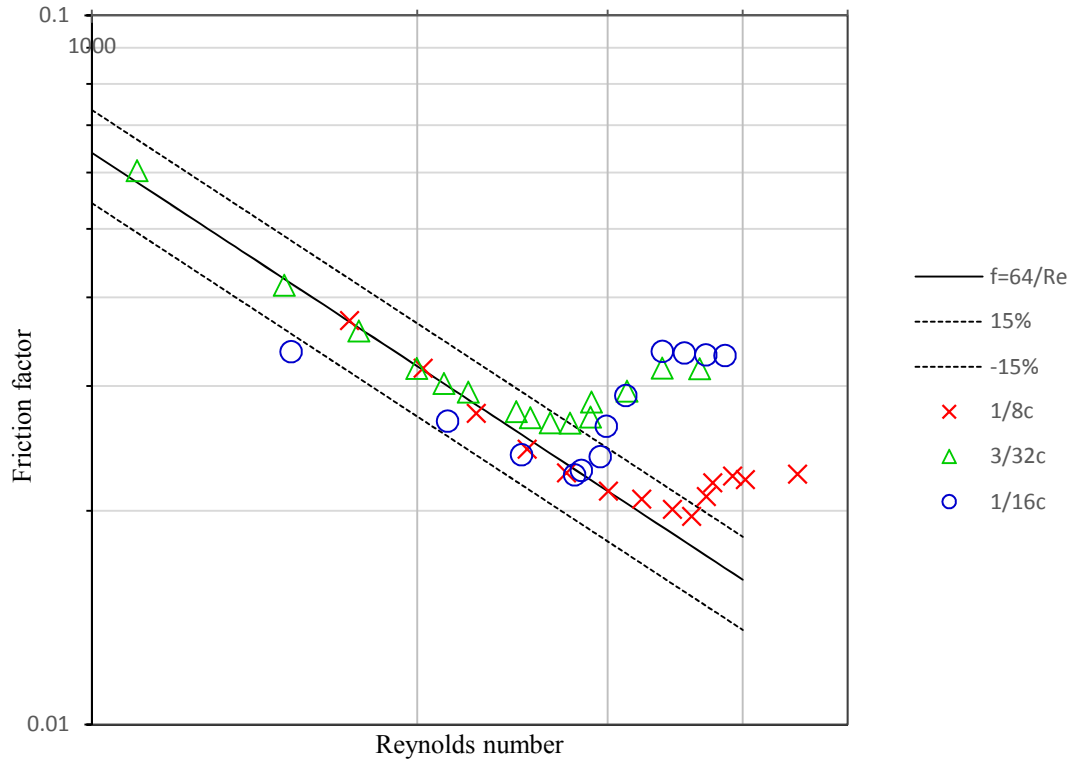
Figure 15. Friction factor versus Reynolds number for water in circular tubes
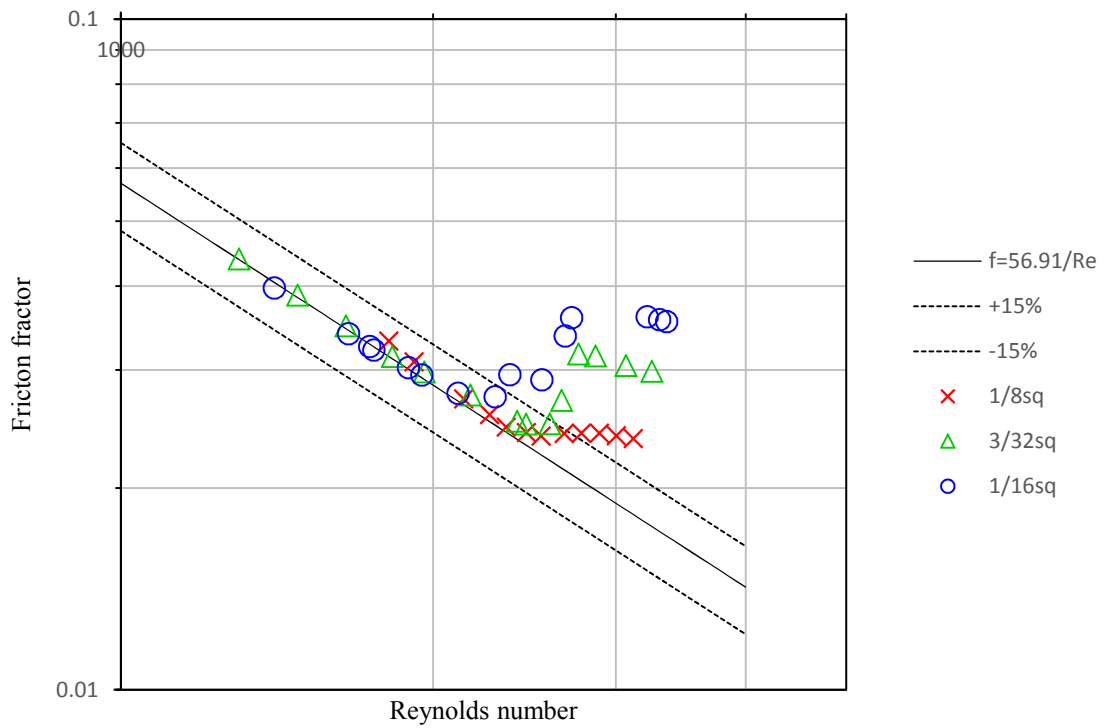
Figure 16. Friction factor versus Reynolds number for water in square tube

Nusselt number from experimental data was calculated using Equation (2.1.16) and Equation (2.1.20). These Nusselt number for Reynolds number in laminar regime was compared with theoretical Nusselt number calculated from Leinhard and Leinhard correlation [8], Equation (2.1.22) and was plotted against dimensionless distance from the entrance which is given by the value 2/Gz. The plots of six different tubes are shown Figure 17 to Figure 22. Since the experimental values of the Nusselt number are within ±15% of the Nusselt numbers estimated by Lienhard and Leinhard correlation [8] for Nusselt number, we can conclude that the experimental setup for heat transfer measurements are reliable.
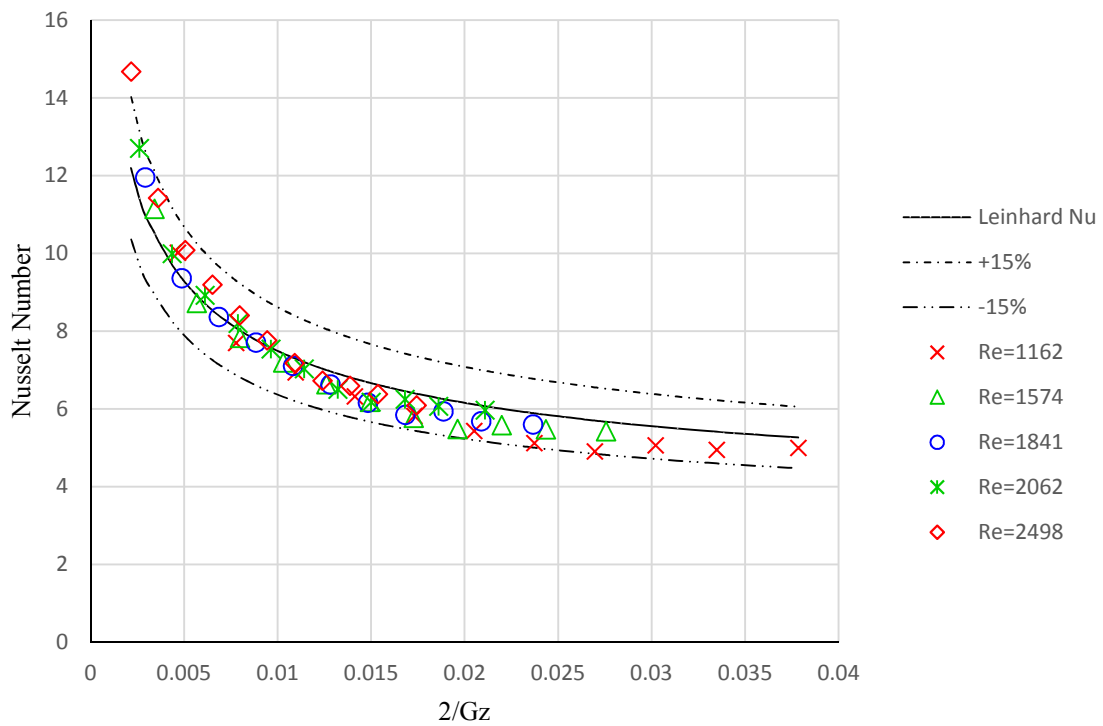
Figure 17. Nusselt number plotted against 2/Gz for water in 1/8c
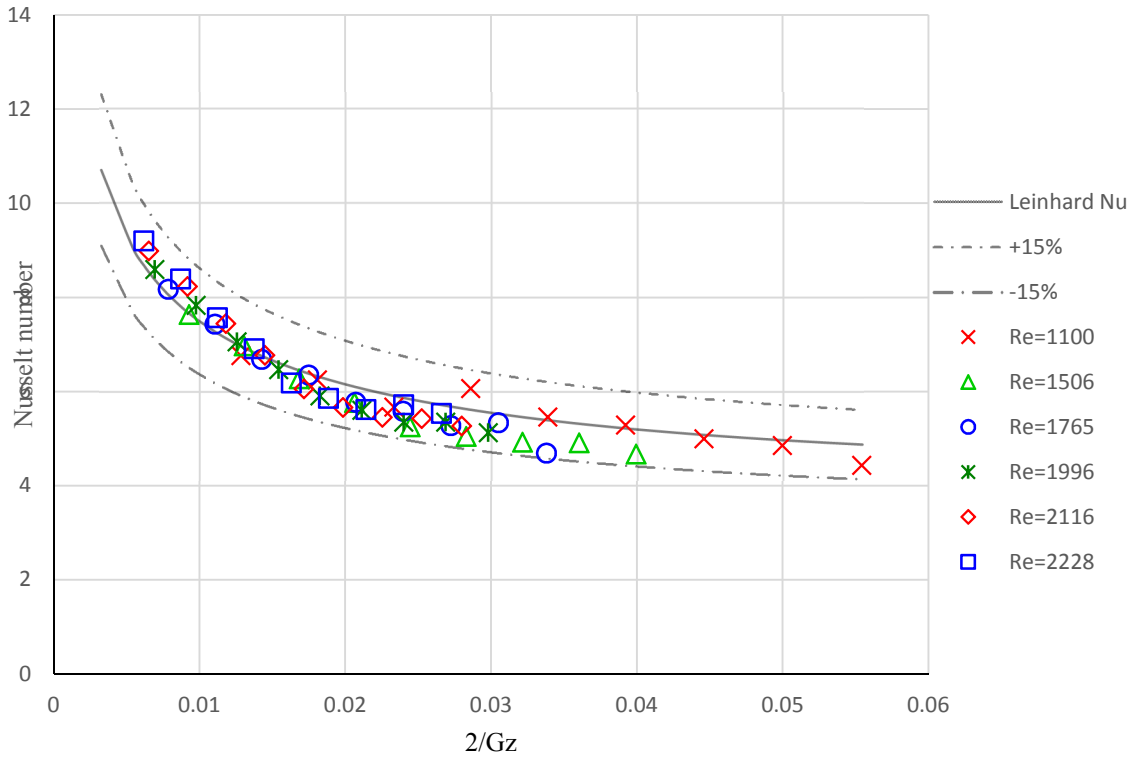
Figure 18. Nusselt number plotted against 2/Gz for water in 3/32c
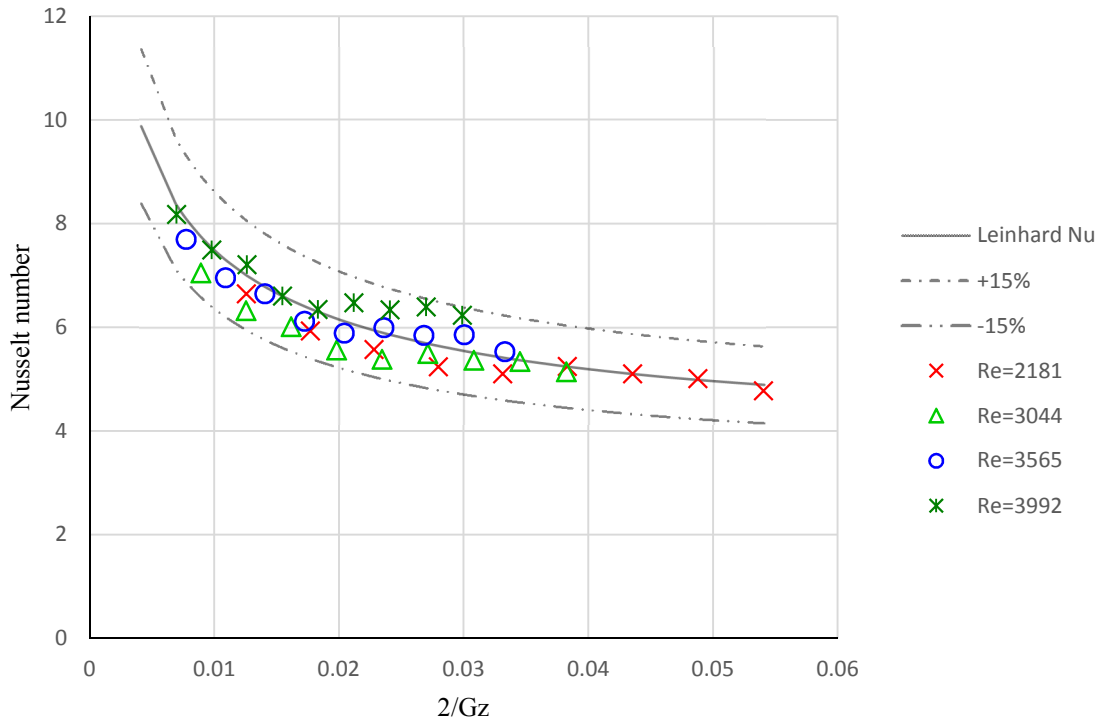
Figure 19. Nusselt number plotted against 2/Gz for water in 1/16c
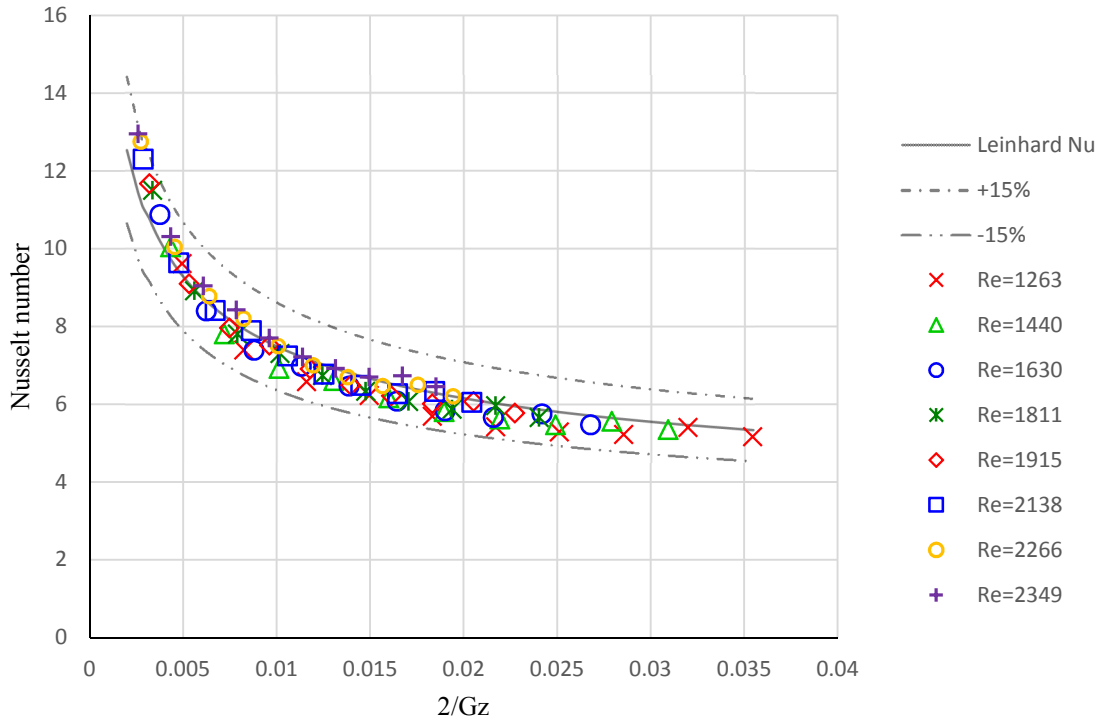
Figure 20. Nusselt number plotted against 2/Gz for water in 1/8sq
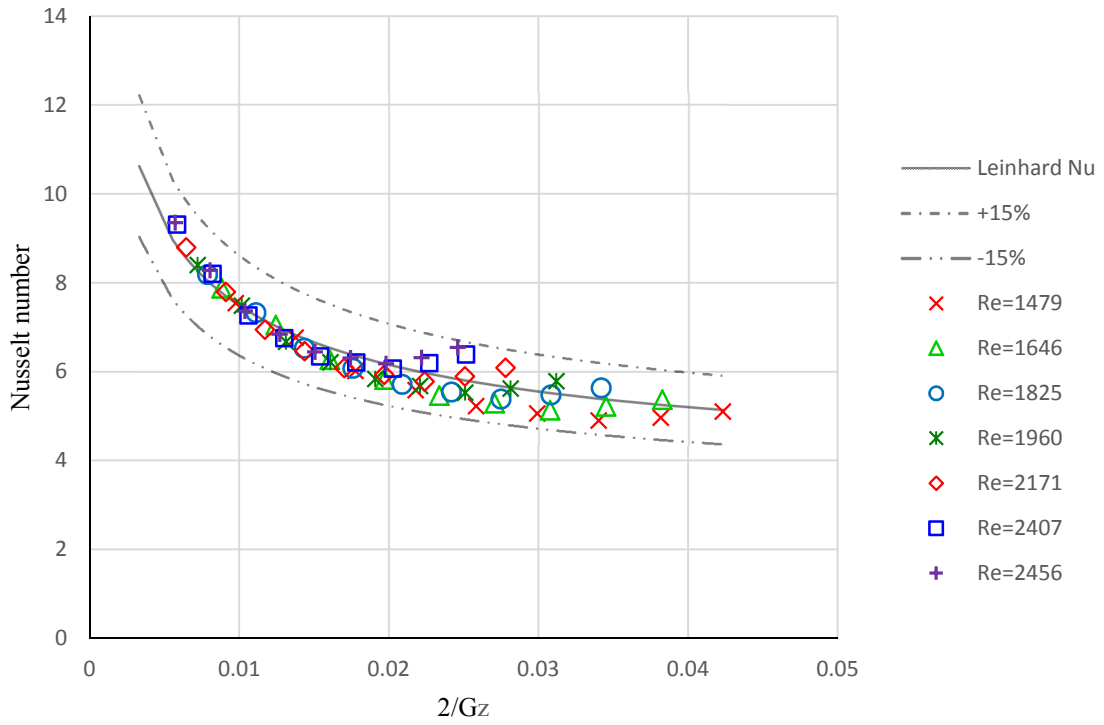
Figure 21. Nusselt number plotted against 2/Gz for water in 3/32sq
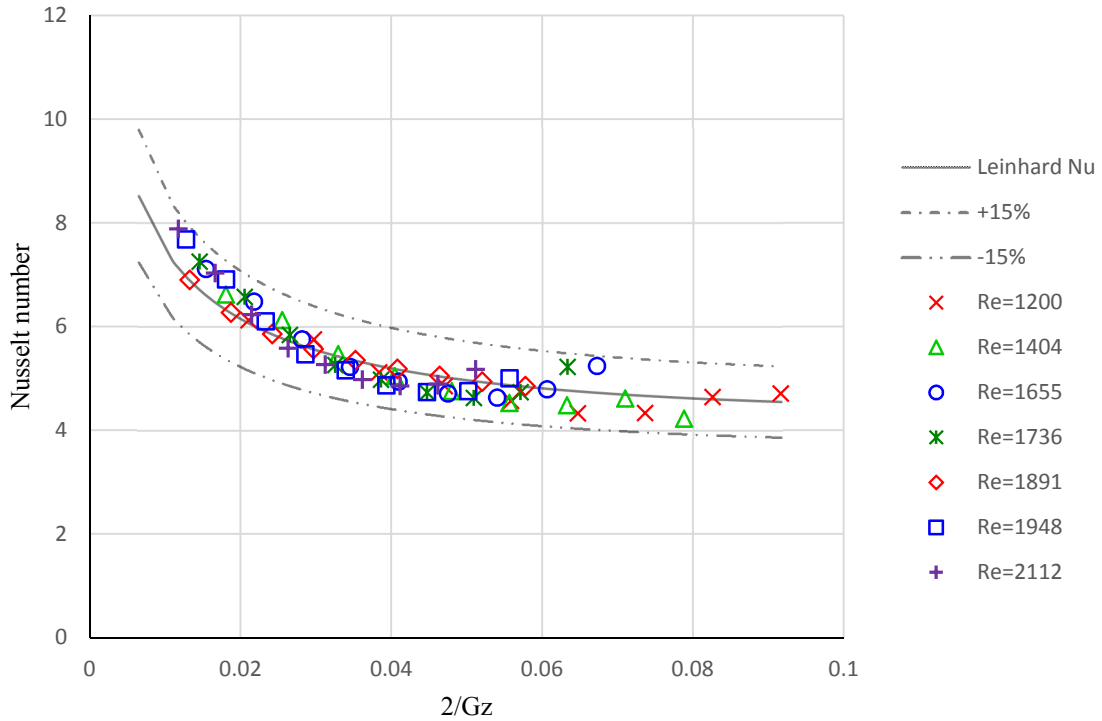
Figure 22. Nusselt number plotted against 2/Gz for water in 1/16sq

4.4   Fluid friction

Fluid friction for water and SiO_2 nanofluid was studied in six different test section. This was done by comparing friction factor at same Reynolds number and same mass flow rate. Effects of different fluids, different hydraulic diameters, and shapes are discussed in the following sub sections.

4.4.1   Effect of working fluid on friction factor

4.4.1.1   Circular tubes

Friction factor for water and SiO_2 nanofluid for the three circular tubes plotted against the Reynolds number are presented in Figure 23, Figure 24 and Figure 25. On a log scale the change of flow regime from laminar to transition is more distinct than in conventional scale so they are plotted a log scale. In laminar regime, the plot (on a log scale) of friction factor versus Reynold number can be represented by a straight line with a negative slope. As the

59

Reynolds number is increased, eventually the flow regime changes from laminar to transition with higher friction factor than the ones predicted by the line in laminar regime. This deviation on the plot indicates the change of regime. In the laminar regime the friction factor for nanofluid overlaps the friction factor for water which means that there is no significant change or increase in fluid friction in laminar flow when compared at similar Reynolds number. At the same time in the post laminar regime (transition and early turbulence) the friction factor for nanofluid is slightly lower than that of water and this difference is increasing with the decrease in hydraulic diameter of the tube. For 1/16c the higher Reynolds number data points are missing because of the limitation of the pump. For a given tube size both water and nanofluid, the transition occur at about the same Reynolds number. This behavior of non-Newtonian fluid is similar to the results of [9] and indicates that there is less fluid friction in nanofluid than that in water at same Reynolds number in turbulent regime
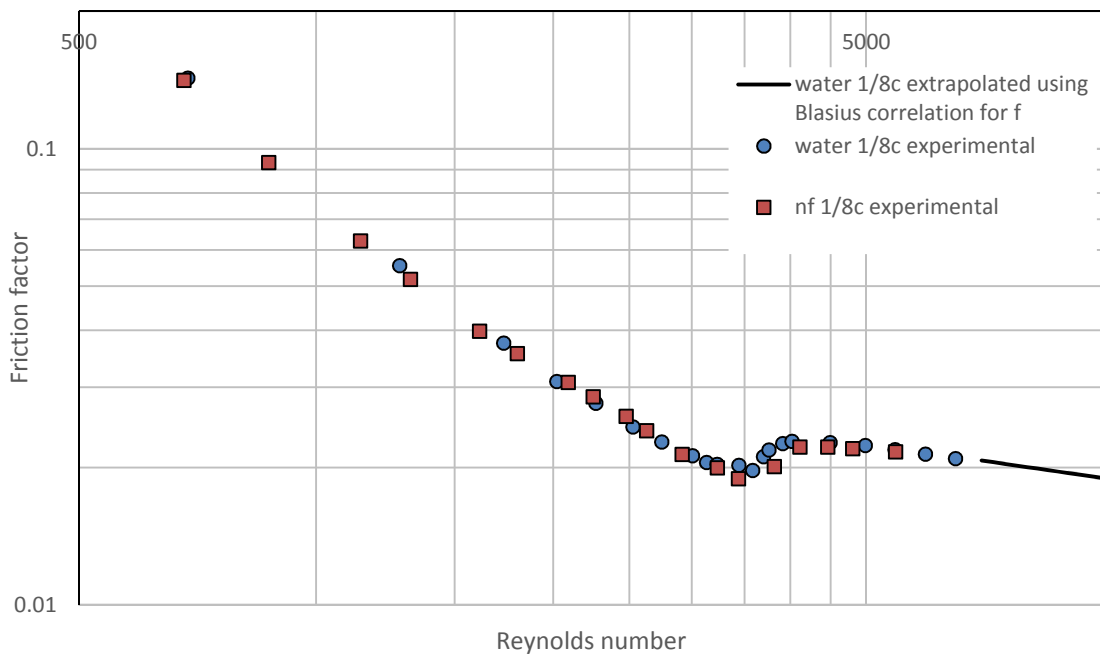
Figure 23. Friction factor versus Reynolds number for water and SiO_2 nf in 1/8c
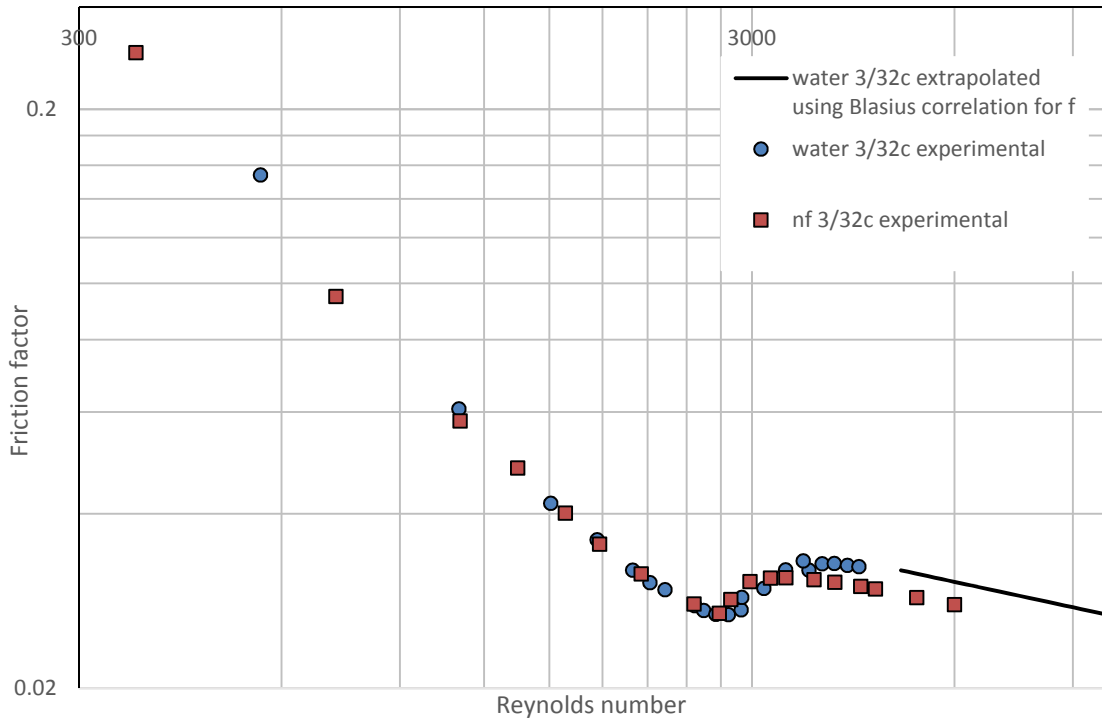
Figure 24. Friction factor versus Reynolds number for water and SiO_2 nf in 3/32c
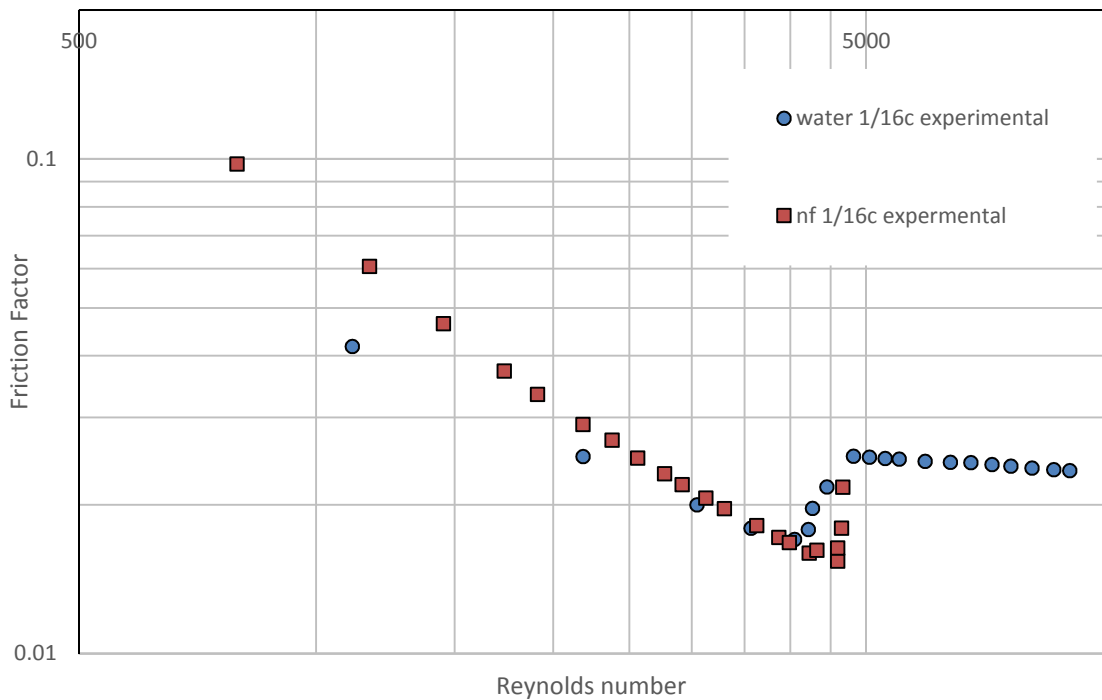
Figure 25. Friction factor versus Reynolds number for water and SiO_2 nf in 1/16

Friction factor plotted against the mass flow rate for water and nanofluid are presented in Figure 26, Figure 27 and Figure 28. For 1/8c and 3/32c the friction factors at higher mass flow rates for water are predicted by Blasius correlation for friction factor, Equation (2.1.7). These plots tell a different story than the plots for f v/s Re. When friction factors for nanofluid and water are compared at same mass flow rate, the friction factor for nanofluid is higher in both turbulent and laminar regime except for the range of mass flow rate at which water is already in turbulent regime and nanofluid is still in laminar regime. When friction factor for water is compared at same flow rate in laminar regime, it increases by 50 to 80 %. Also, it can be effortlessly observed that the transition for nanofluid occurs at higher mass flow rate than that of water. This can be attributed to higher viscosity of nanofluid. The range of mass flow rate for which the fluid friction of nanofluid is higher for water is as follows - for 1/8c this range is 1.82 g/s, for 3/32c it is 2.12 g/s and for 1/16c it is 2.25 g/s. For 1/8c the difference between the mass flow rates of water and nanofluid at which transition occurs is 37.1% of mass flow rate of water at which transition occurs. This value for 3/32c and 1/16c are 92.5% and 100.1% respectively. This would mean that the range of mass flow rate for which fluid friction of nanofluid is lower than that of water is wider for smaller hydraulic diameters.
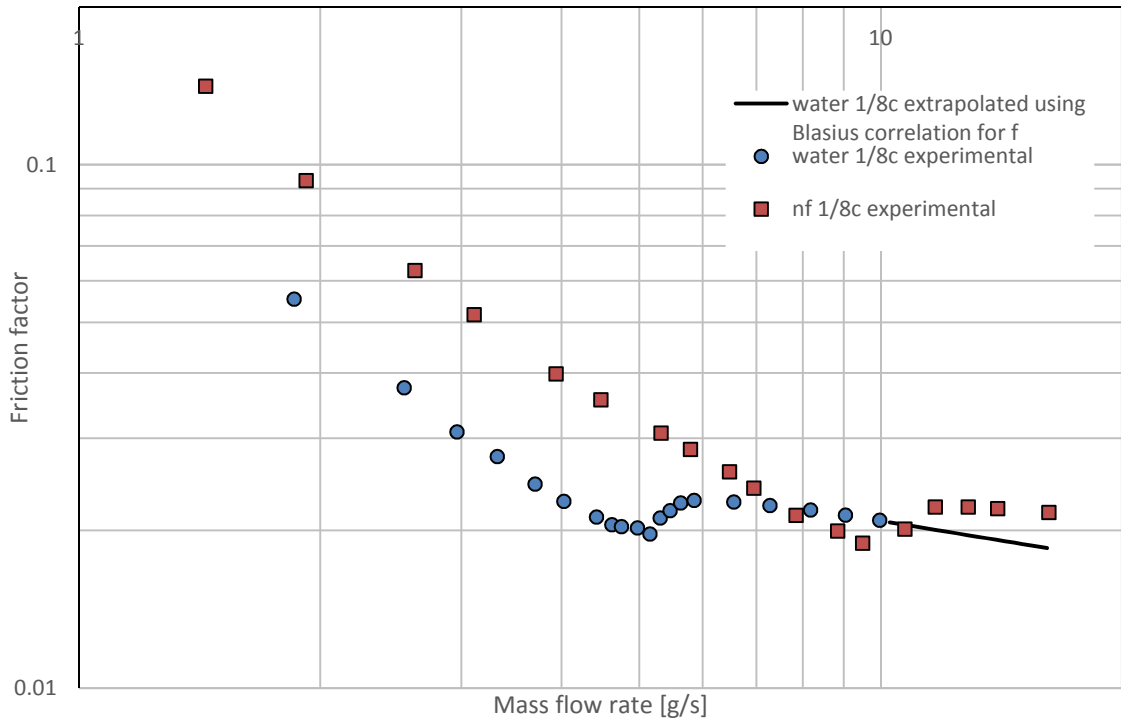
Figure 26. Friction factor versus mass flow rate for water and SiO_2 nf in 1/8c
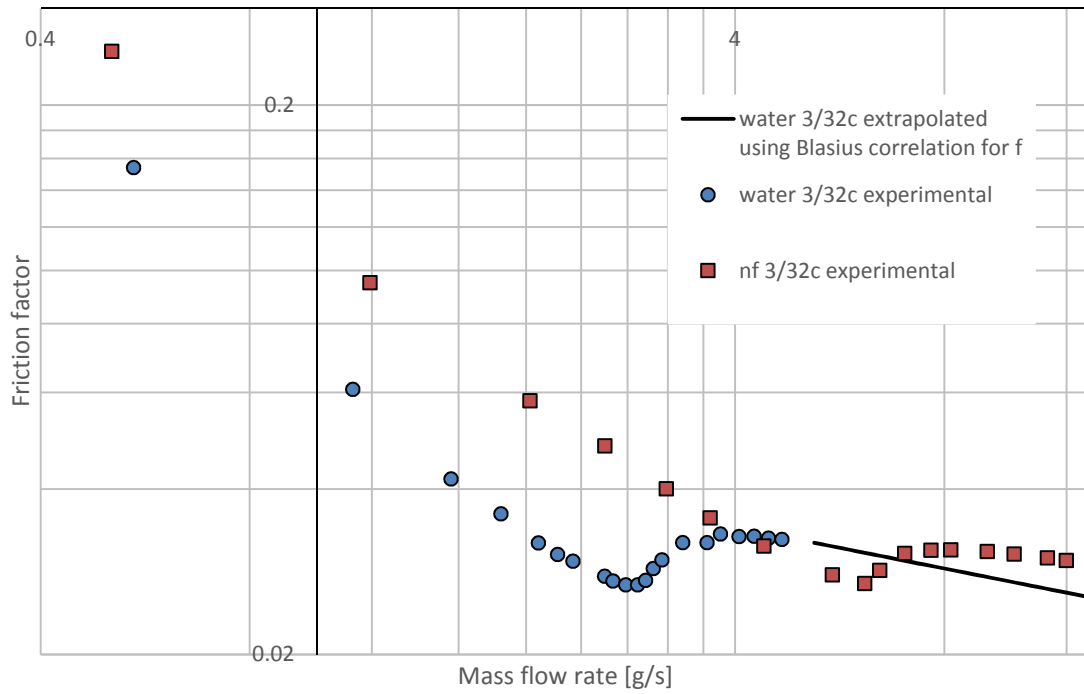

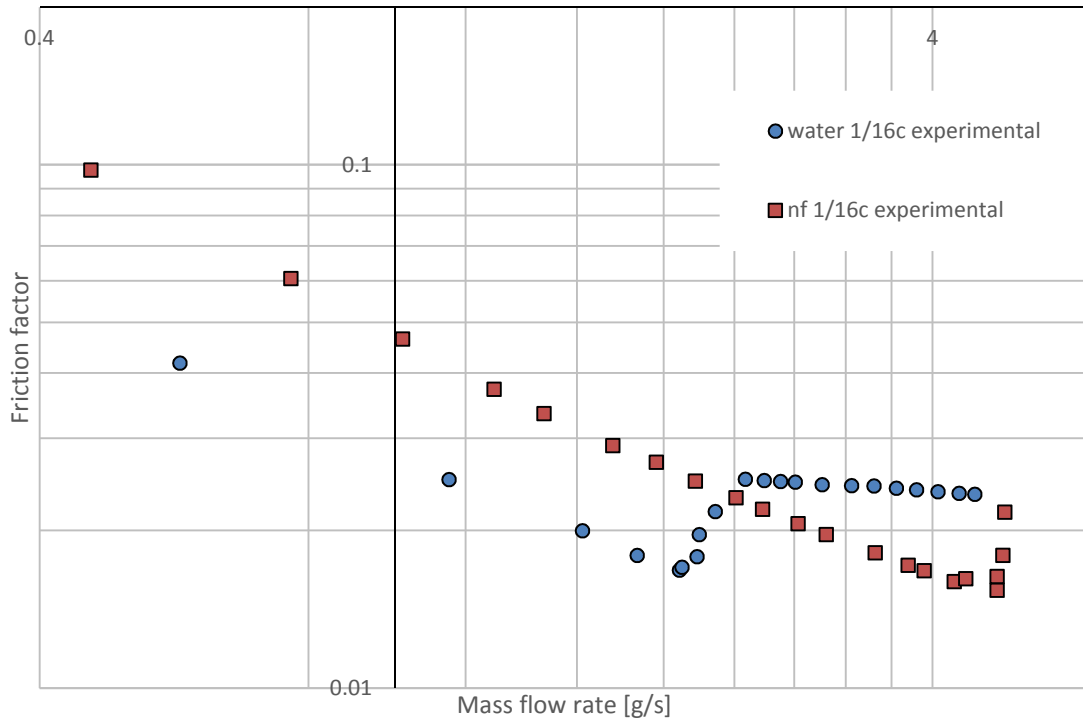Figure 27. Friction factor versus mass flow rate for water and SiO_2 nf in 3/32c

Figure 28. Friction factor versus mass flow rate for water and SiO_2 nf 1/16c

4.4.1.2 Square tubes

Friction factors for water and SiO_2 nanofluid flowing in square tubes were plotted against Reynolds number in log scale. The plots for 1/8sq, 3/32sq and 1/16sq are presented in Figure 29, Figure 30 and Figure 31, respectively. In laminar region, friction factor of nanofluid overlaps the friction factor for water. For 1/8sq the transition from laminar to turbulence is smoother then in smaller hydraulic diameter tubes and the degree of abruptness in transition is observed to increase with decrease in hydraulic diameter. The reason may be the extra turbulence added at the corner.

Unlike in circular tubes, where for both water and nanofluid transition occurred at around same Reynolds number, in square tube the Reynolds number at which the transition occurs for water and nanofluid is different. For 1/8sq the transition for nanofluid occurs at higher Reynolds number than that of water (Figure 29). For 3/32sq the transition occurs at similar

Reynolds number and for 1/16sq transition for nanofluid occurs at lower Reynold number than that of water (Figure 30 and Figure 31). Thus, for square tubes no distinct pattern could be observed, as of, if transition for nanofluid would occur earlier or later than that of water in terms of Reynolds number. At this point it would be worthwhile to mention that the Reynold number at which a flow would embark on transition depends various parameters, such as flow surface roughness, vibrations, noise and other disturbances. And during the experiment, these parameters were not controlled. Further in these plots it can be observed that in post laminar regime the trend of friction factor for nanofluid is, to some degree, shifted to the lower end of the friction factor axis. This would mean that in post laminar regime friction factor for nanofluid in square tubes are lower than that of water.
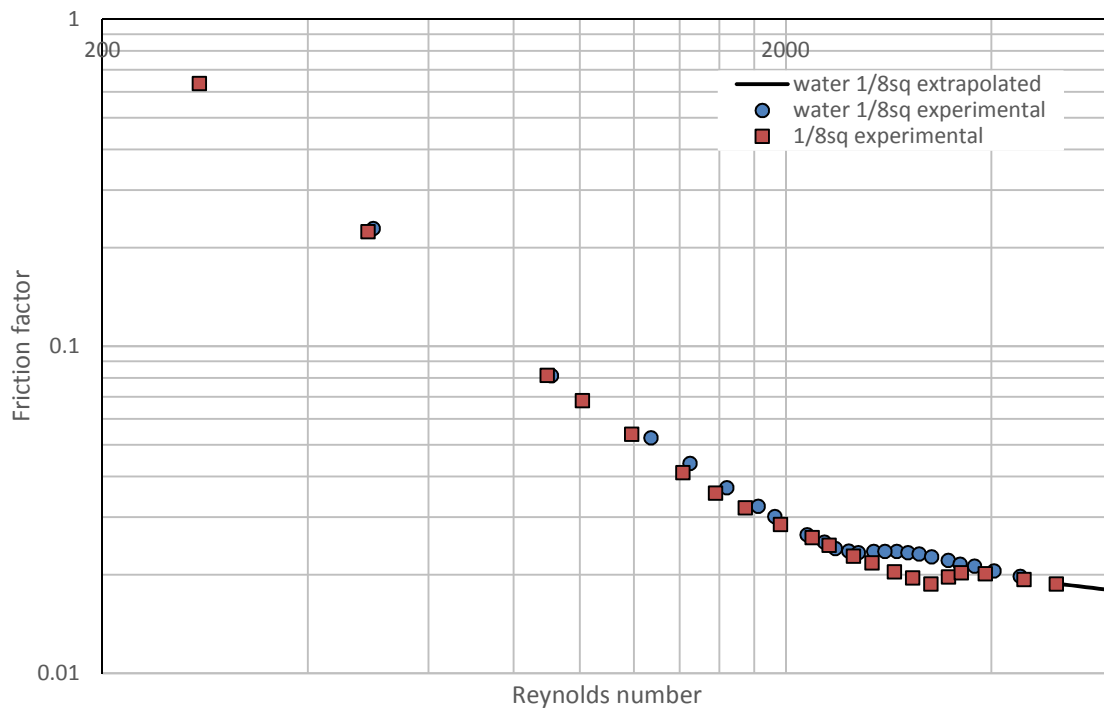
Figure 29. Friction factor versus Reynolds number for water and SiO_2 nf in 1/8sq
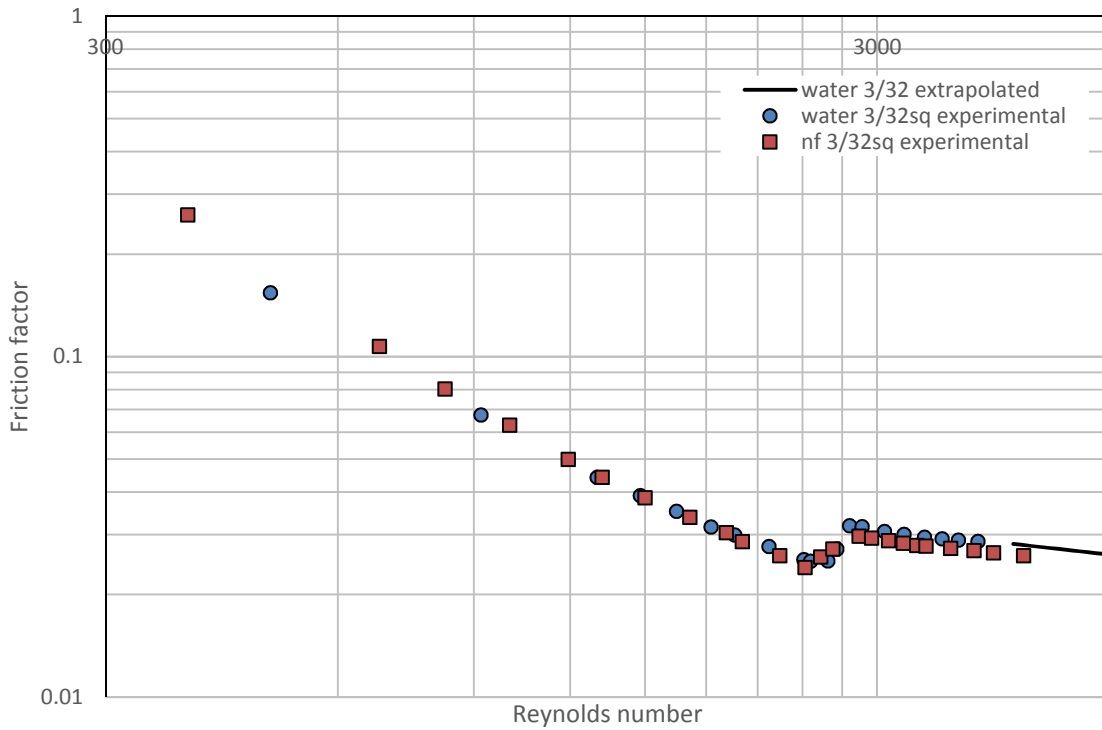
Figure 30. Friction factor versus Reynolds number for water and SiO_2 nf in 3/32sq
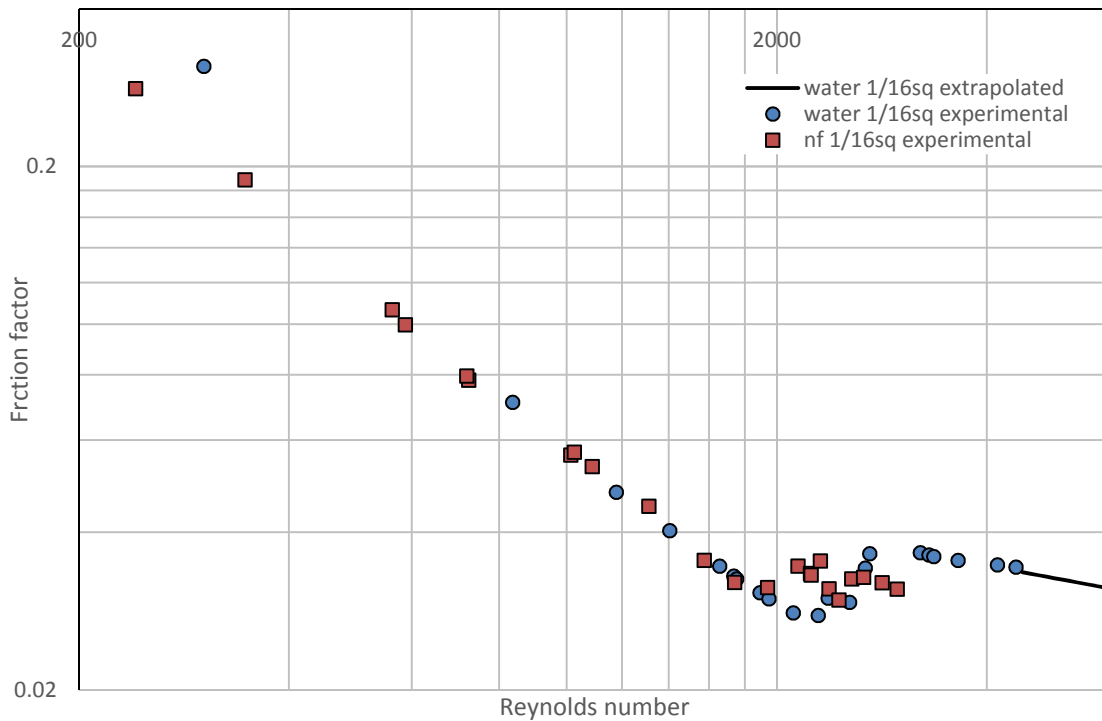

Figure 31. Friction factor versus Reynolds number for water and SiO_2 nf in 1/16sq

Friction factor plotted against mass flow rate for water and SiO_2 nanofluid are shown in Figure 32, Figure 33 and Figure 34. Friction factor for water at higher Reynold number was extrapolated using Blasius friction factor correlation, Equation (2.1.7). When both water and nanofluid are in laminar regime the friction factor is higher by 50 to 80 % for nanofluid than that of water. Also from these plots it can be observed that transition for nanofluid happens at larger mass flow rate than that of water. For 1/16sq the difference between the mass flow rate of nanofluid and water at which transition occurs in 116.4% of mass flow rate at which transition occurs in water. (Figure 32). This value for 3/32sq and 1/16sq are 101% and 97% respectively (Figure 33 & Figure 34).
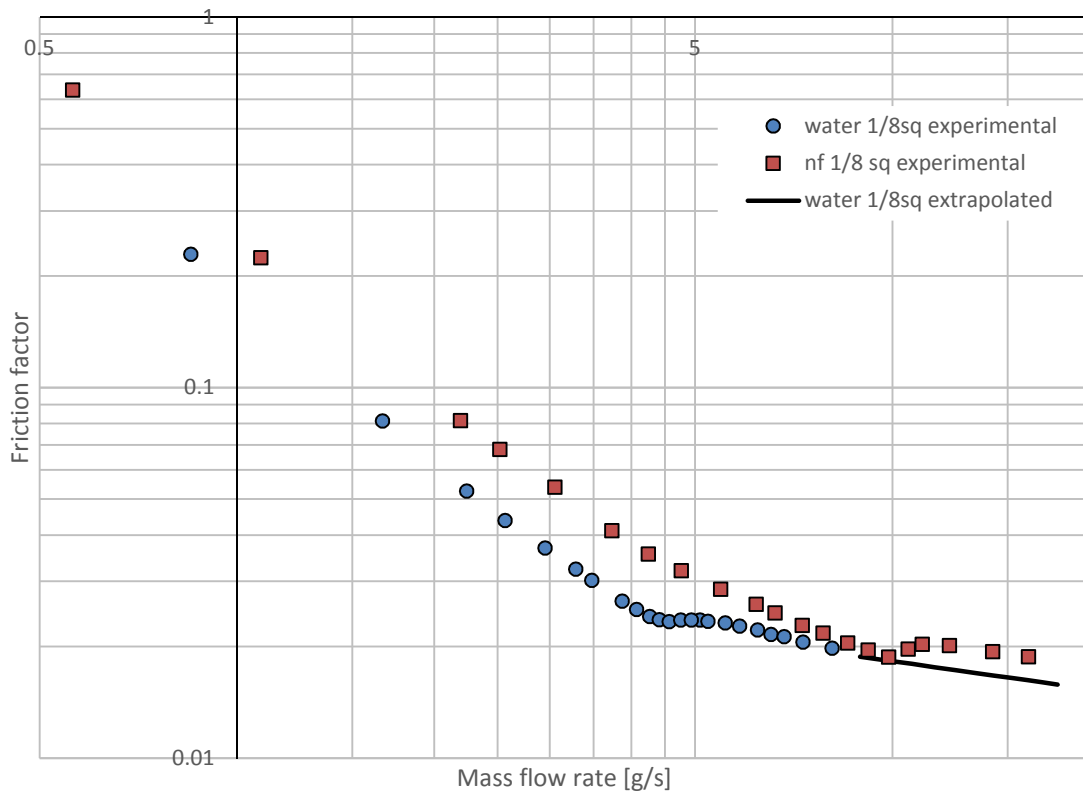
Figure 32. Friction factor versus mass flow rate for water and SiO_2 nf in 1/8sq
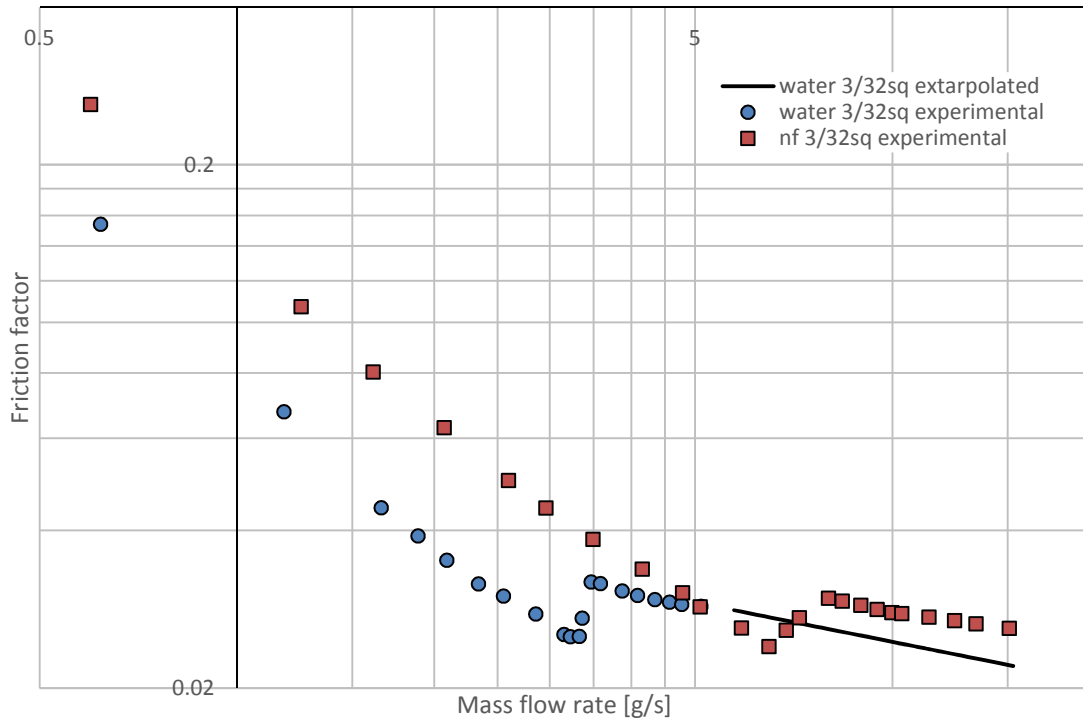
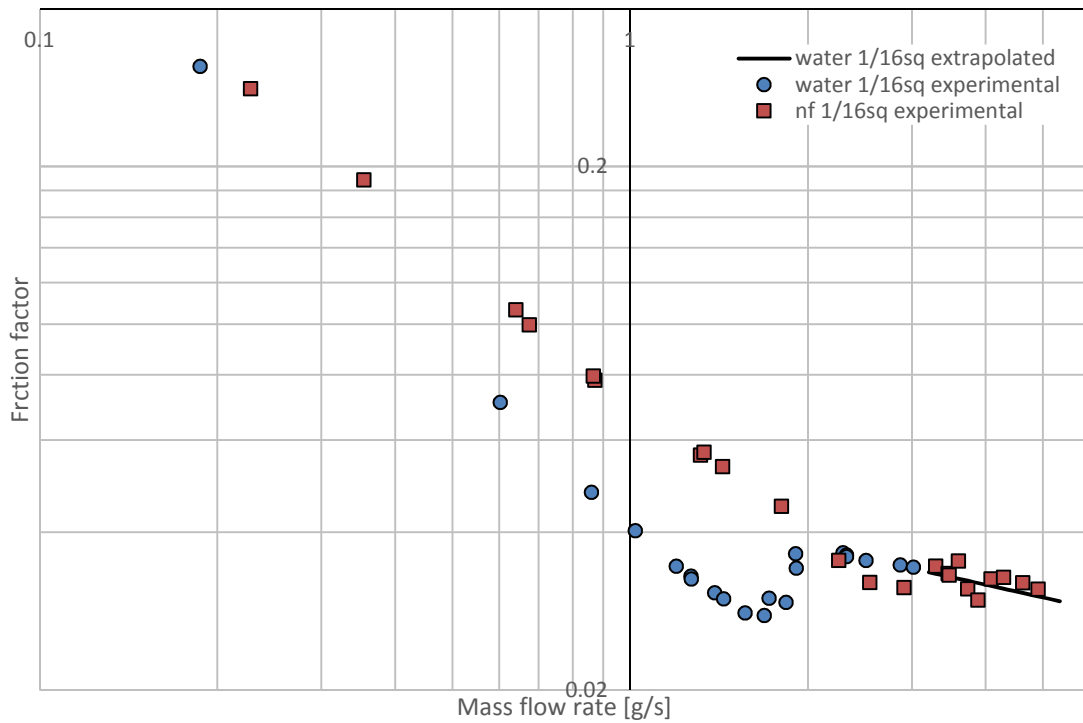Figure 33. Friction factor versus mass flow rate for water and SiO_2 nf in 3/32sq

Figure 34. Friction factor v/s mass flow rate for water and SiO2 nf in 1/16sq

4.4.2 Effect of hydraulic diameter D_h on friction factor

4.4.2.1 Circular tubes

In Figure 35 friction factor for 1/8c, 3/32c, and 1/16c are plotted against the Reynolds number on a log scale. This plot compares friction factor at different hydraulic diameters of circular tube. And it also shows that at which Reynolds number the flow changes from laminar to transition regime. Here, 3/32c has the earliest transition at Reynolds number of 2460 followed by 1/8c and 1/16c at Reynolds number of 3440 and 4590, respectively. These data obviously suggest that transition Reynolds number cannot be related to hydraulic diameter size. However it cannot be concluded that transition Reynolds number is not affected by diameter of the tube as there is another factor which have strong effect on transition Reynolds number. This factor is the roughness of the internal tube surface which is not studied this research. Besides surface roughness, transition Reynolds number is also affected by vibrations, noise and other disturbances.
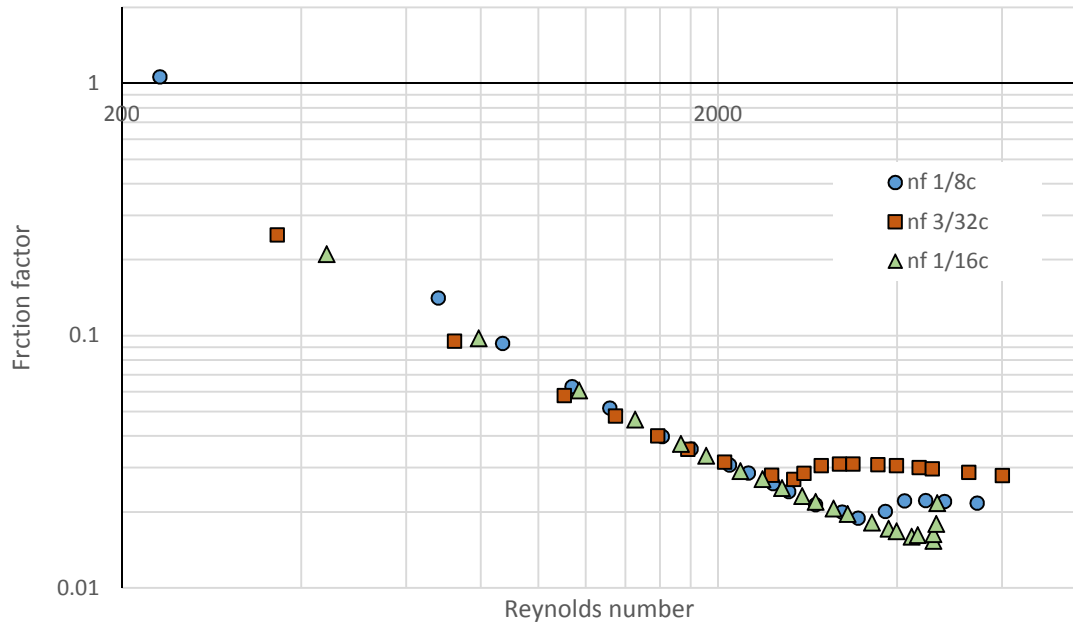

Figure 35. Friction factor versus Reynolds number for SiO_2 nf for circular tubes with different hydraulic diameters

In Figure 36 friction factor for 1/8c, 3/32c and 1/16c is plotted against mass flow rate on a log scale. This plot can be used to compare friction factors for of 3 circular tube of different hydraulic diameter at similar mass flow rate. For example at a mass flow rate of 3.1 g/s friction factor for 1/8c is 0.051, for 3/32c it is 0.040 and for 1/16c it is 0.019. Thus at a given mass flow rate in laminar regime friction factor is higher for larger hydraulic diameter tube. This can be explained from Equation (3.3.1) and Equation (3.3.2) which imply that friction factor is directly proportional to the fifth power of hydraulic diameter.
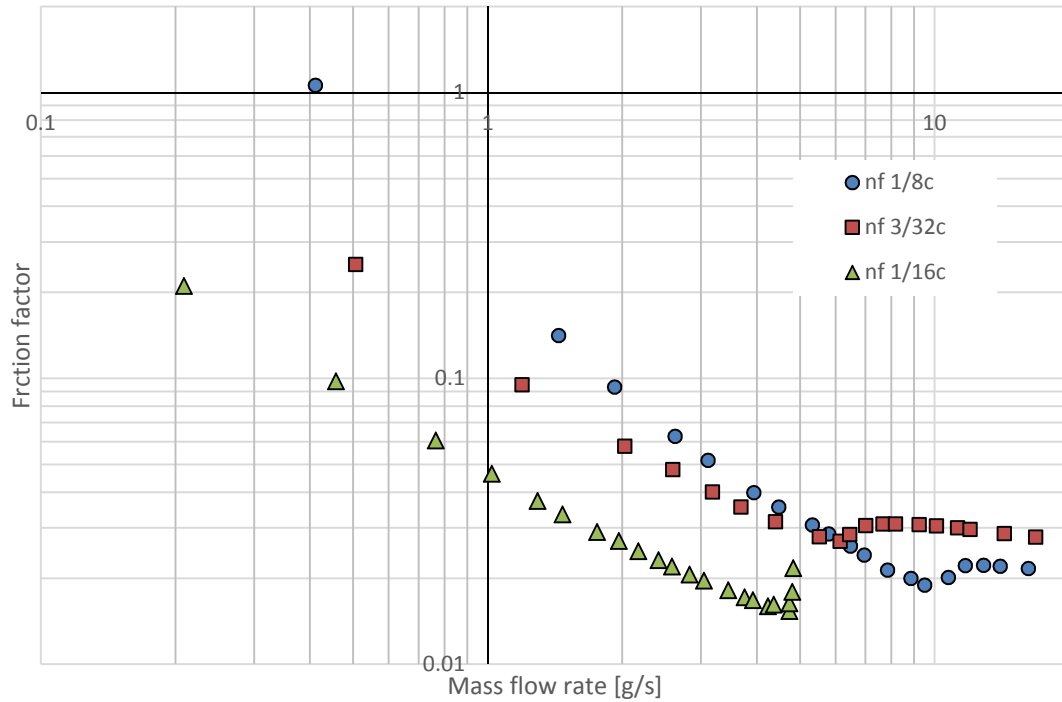
Figure 36. Friction factor versus mass flow rate SiO_2 nf in circular tubes with different hydraulic diameters
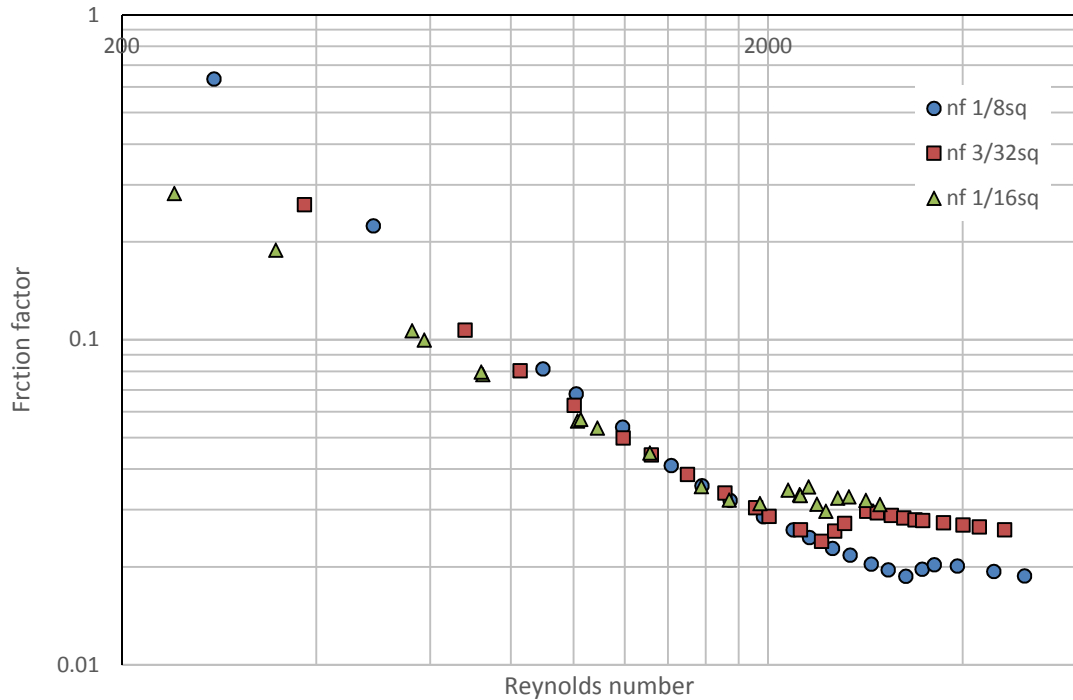
4.4.2.2 Square tubes

Figure 37. Friction factor versus Reynolds number for SiO$_2$ nf for square tubes with different hydraulic diameters

In Figure 37 friction factor for SiO$_2$ nanofluid flowing in 1/8sq, 3/32sq and 1/16sq are plotted against the Reynolds number. This plot compares friction factor at similar Reynolds number for different hydraulic diameter. For Reynolds number between 1000 and 2000, when the flow in all the 3 tubes are in laminar regime, the friction factors overlaps. For Reynolds number lower than 1000, the friction factor deviate from each other, with smaller diameter tube having the lower friction factor. This plot also can be used to see at what Reynolds number the flow regime is changing from laminar to transition. For 1/6sq the flow embarks on transition regime at a Reynolds number around 1950. For 3/32sq and 1/16sq the onset of transition occurs at around 2400 and 3200 Reynolds number. These values of Reynolds number suggest that for smaller diameter tube the transition occurs at

lower Reynolds number. However, since the roughness of the internal surface of the test

section had been studied, the effect of the hydraulic diameter cannot be concluded.

In Figure 38, friction factor of SiO_2 nanofluid for different hydraulic diameter square tubes

are plotted respectively against mass flow rates. This plot can be used to compare friction

factor at similar mass flow rate different hydraulic diameter tubes. For example at a mass

flow rate of 2.9 g/s friction factors for 1/8sq, 3/32sq and 1/16sq are 0.053, 0.044, and 0.031

respectively. Similar to the circular tubes, the square tubes with largest hydraulic diameter

has the largest friction factor because of larger flow cross section area.
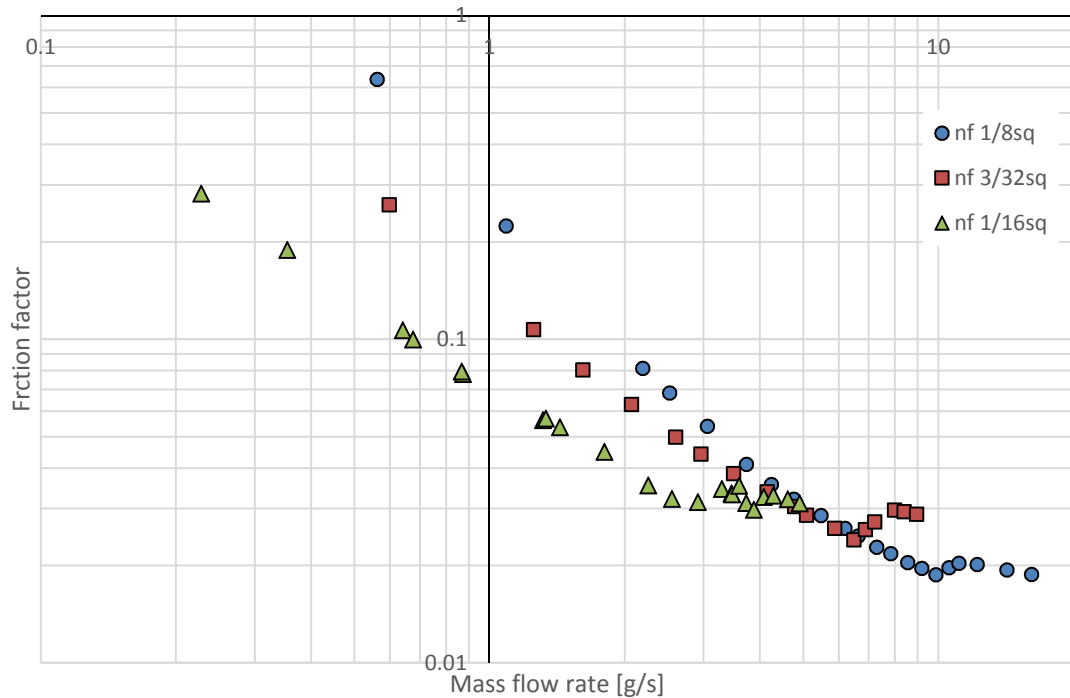
Figure 38. Friction factor versus mass flow rate for SiO_2 nf in square tubes with different hydraulic diameters

4.4.3 Effect of shape on friction factor

4.4.3.1 Friction factor versus Reynolds number

In Figure 39 friction factor is plotted against the Reynolds number for SiO_2 nanofluid flowing in circular and square tube of size 1/8 inch external tube dimensions (hydraulic diameters used for calculations are 0.088 inch for 1/8c and 0.086 in for 1/8sq). Similarly Figure 40 and Figure 41 are for tube size 3/32 inch external tube dimensions (D_h for 3/32c is 0.064 in and for 3/32sq it is 0.0638) and 1/16 inch external tube dimension (D_h for 1/16c is 0.034 in and for 1/16sq it is 0.037in) respectively. In all the three plots the friction factor for square tube is less than that of circular tubes in laminar regime.
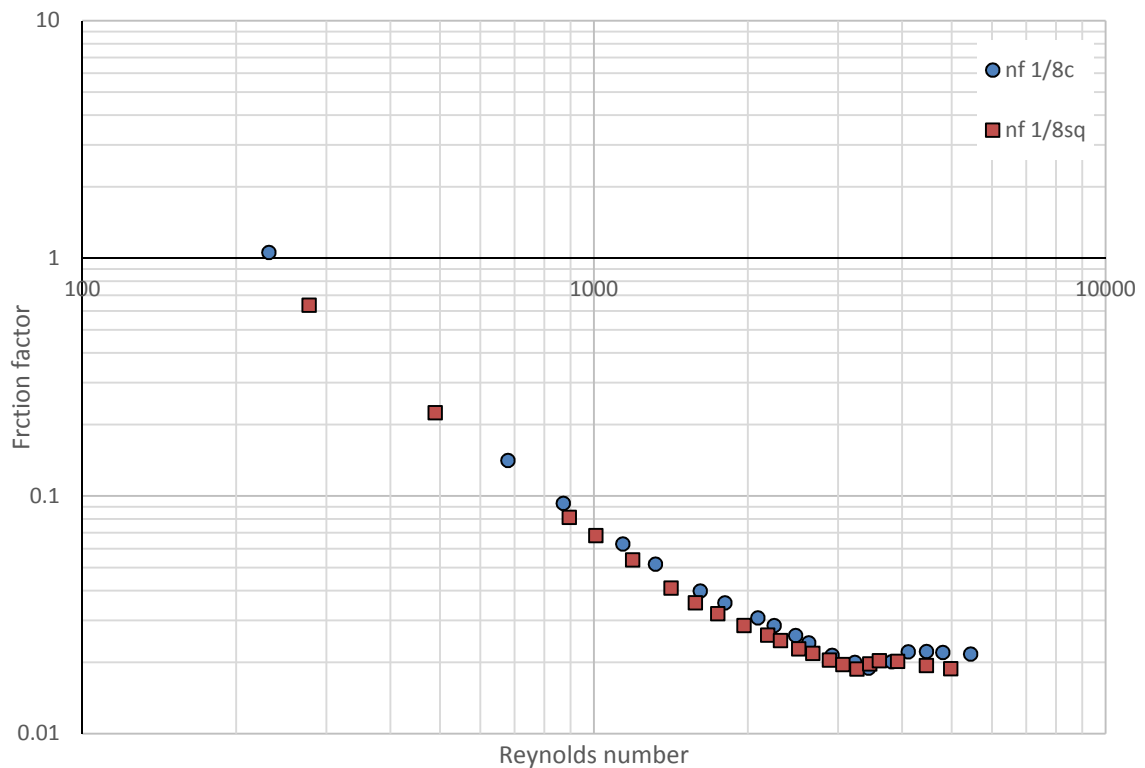
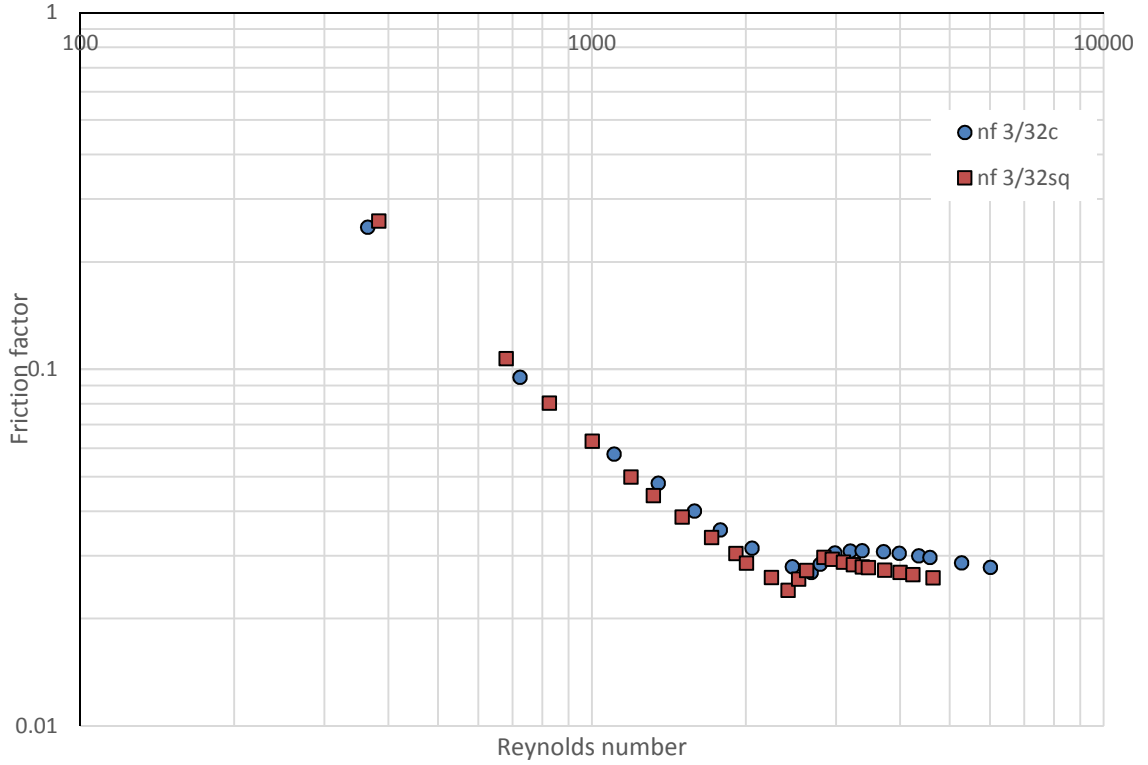Figure 39. Friction factor versus Reynolds number for SiO_2 nf in 1/8c and 1/8sq

73

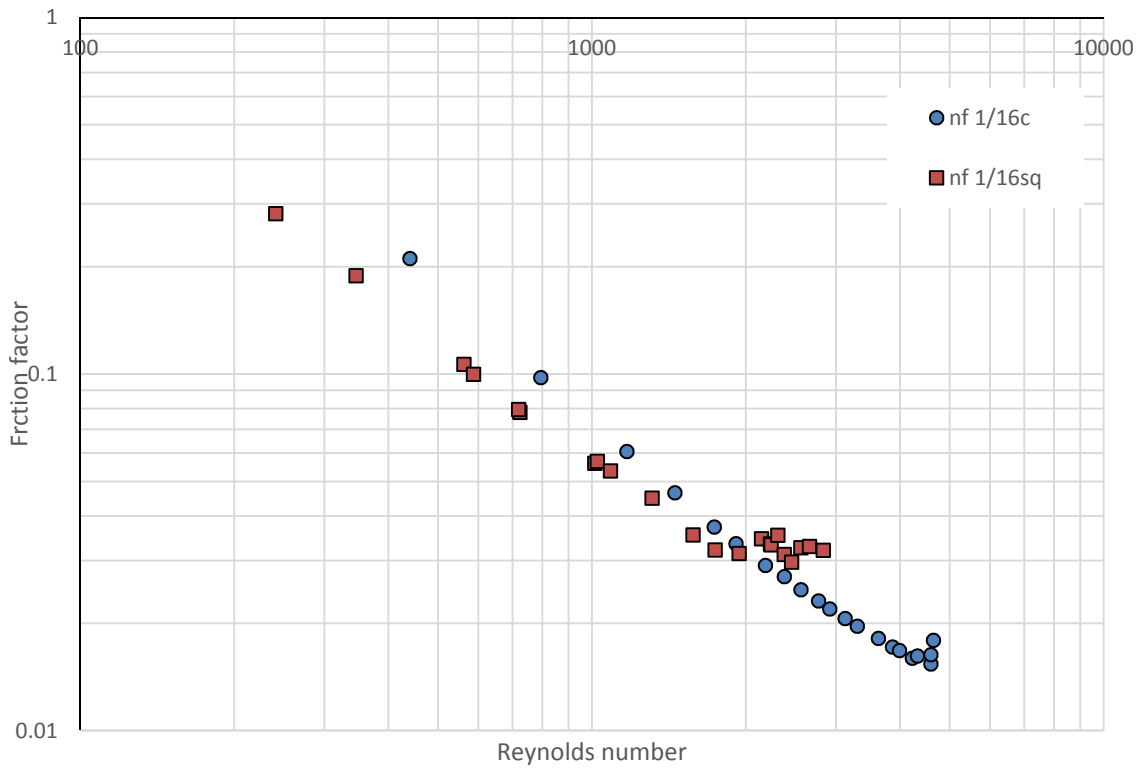Figure 40. Friction factor versus Reynolds number for SiO_2 nf in 3/32c and 3/32sq

Figure 41. Friction factor versus Reynolds number for SiO_2 nf in 1/16c and 1/16sq

4.4.3.2   Pressure drop versus mass flow rate

For SiO_2 nanofluid pressure drop for corresponding mass flow rate for a circular cross-section tubes are compared with a square tubes with same hydraulic diameter in Figure 42, Figure 43 and Figure 44. For a given mass flow rate the pressure drop in circular tube is higher. Furthermore, the difference between pressure drop in circular tube and the pressure drop in square increases with increase in mass flow rate. For same hydraulic diameter square has the larger cross-section area so average fluid velocity is lower (conservation of mass) and thus smaller pressure drop, (as pressure drop ΔP is directly proportional to square of fluid velocity.u^2. Further, in laminar regime (lower flow rate) boundary layer is a major contributor to pressure drop and square has larger perimeter. Thus, the pressure drop difference is lower in lower flow rate. When comparing 1/8c and 1/8sq at a mass flow rate of 16 g/s pressure drop in 1/8c is 68% higher than the pressure drop in 1/8sq. At this flow rate the flow is in turbulent regime. Also at a mass flow rate of 15g/s pressure drop in 3/32c is 58% higher than that of 3/32sq.
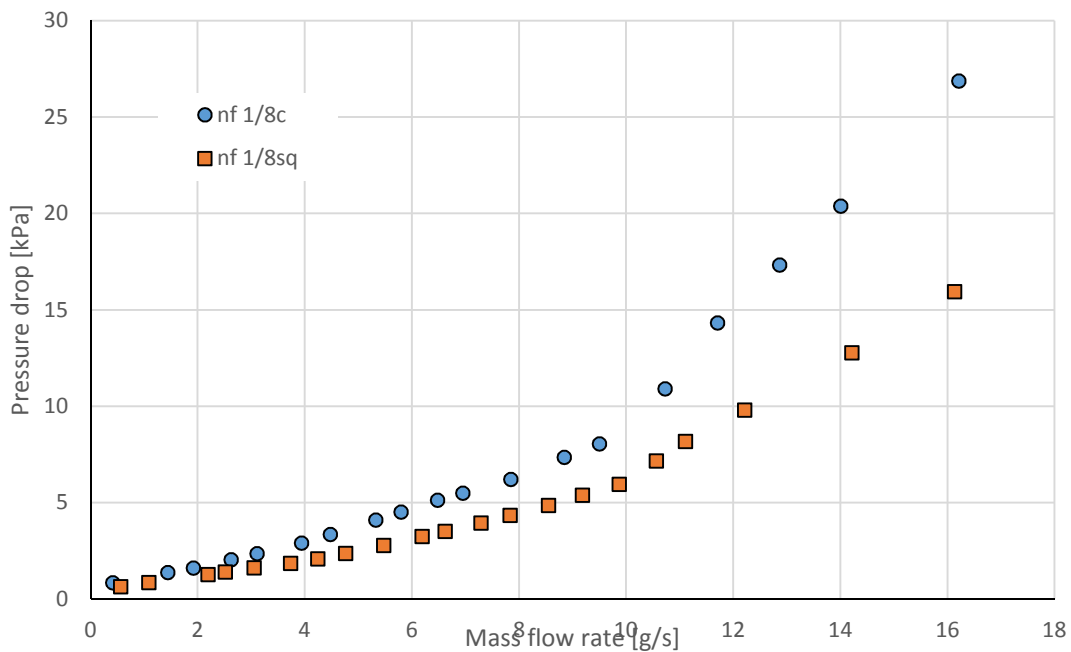

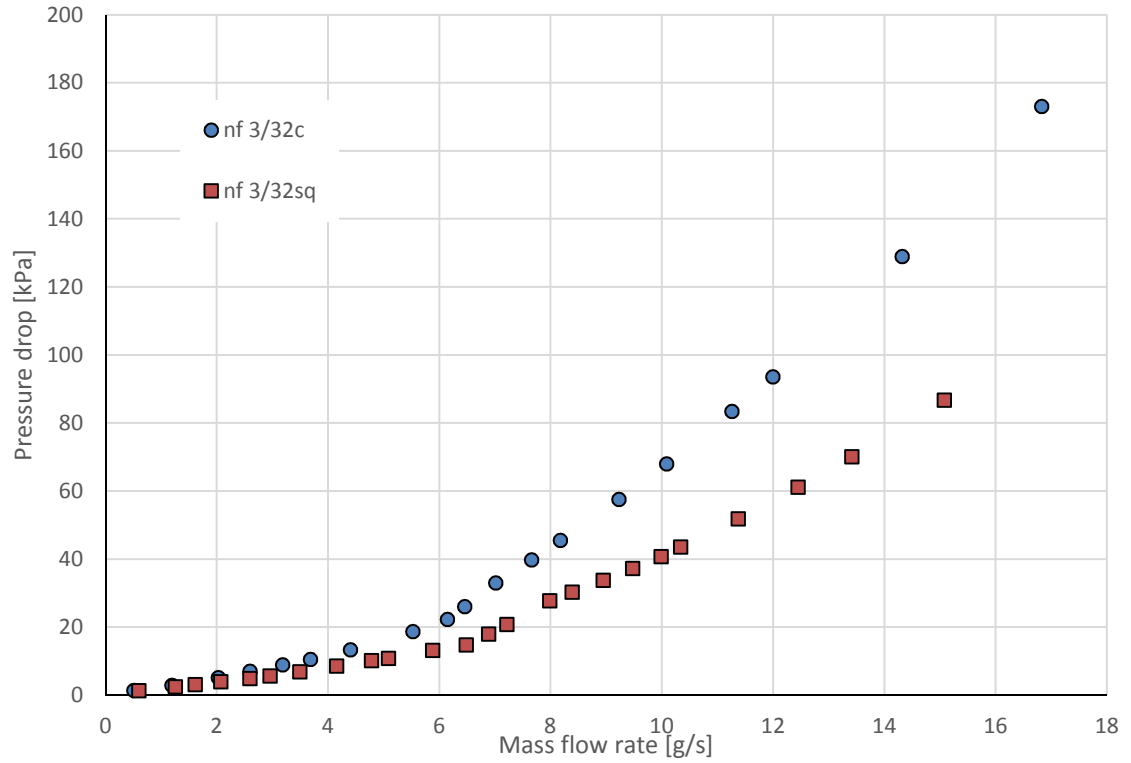Figure 42. Pressure drop versus massflow rate for SiO_2 nf in 1/8c and 1/8sq

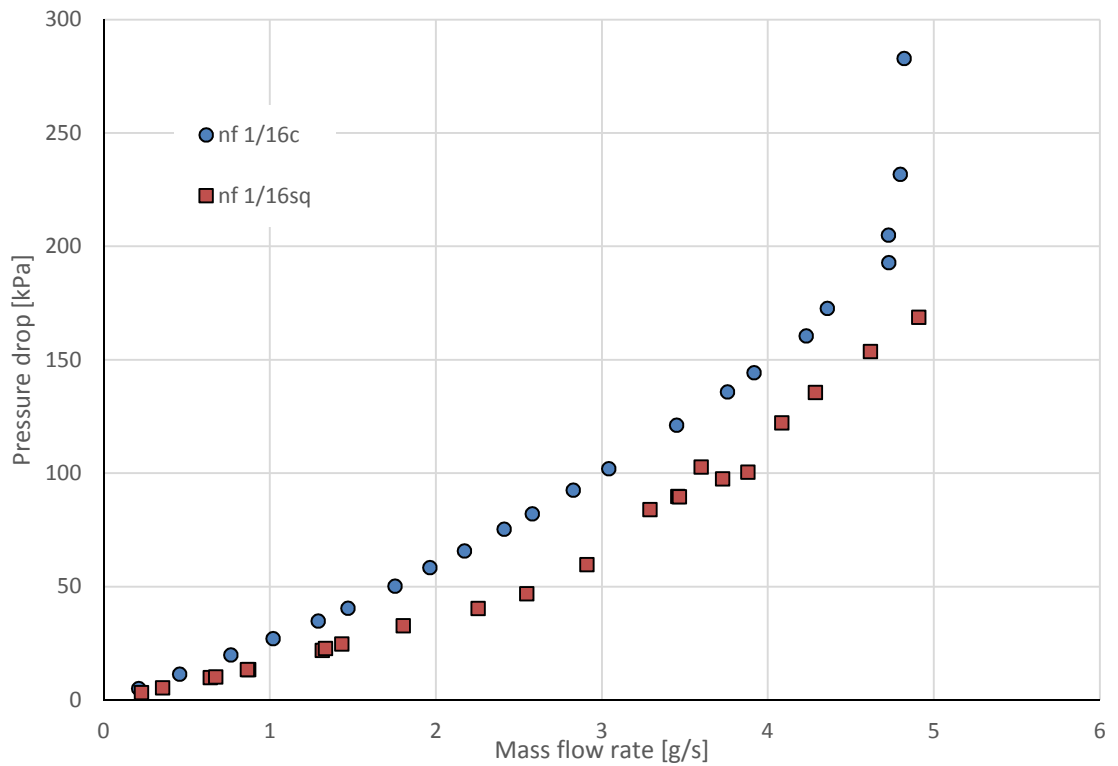Figure 43. Pressure drop versus mass flow rate for SiO_2 nf in 3/32c and 3/32sq

Figure 44. Pressure drop versus massflow rate for SiO_2 nf in 1/16c and 1/16sq

4.5   Heat transfer

Heat transfer behavior of water and 9.58% by volume Silicon Dioxide (SiO_2) nanofluid was studied in circular and square channel of hydraulic diameters at three different levels. The experimental data were analyzed and the effect of working fluid, effect if hydraulic diameter and effect of cross-section on heat transfer are discussed in the following sub-sections of this section.

4.5.1   Effect of working fluid on heat transfer

Study of effect of working fluid on heat transfer is carried out by comparing local Nusselt number for water and SiO_2 nanofluid at same Reynolds number along the dimensionless distance from the inlet. Also the overall Nusselt numbers for the two fluids for was plotted along their respective Reynolds number. In addition to that local heat transfer coefficient for the two fluids are compared at similar pumping power. The results are discussed in following sub-sections.

4.5.1.1   Circular tubes

The results for the analysis of effect of working fluid on heat transfer in circular channels are present in various plots and discussed in the following paragraphs of this sub-section.

4.5.1.1.1   Nu versus x/D at comparable Re

In Figure 45 local Nusselt number for water and SiO_2 nanofluid is plotted against non-dimensional distance from the entrance for 1/8c. This plot compares the local Nusselt number at 10 different locations along the length of the tube 1/8c for water and nanofluid with two different Reynolds number. Exact Reynolds number for water and SiO_2 nanofluid was not available from the current experimental data. Thus similar Reynolds number were used for comparison. Smaller level of Reynolds number for water and nanofluid was 2266

77

and 2249 respectively. The larger level of Reynolds number for which comparison was made was at 3441 for water and 3439 for nanofluid. The average of the smaller Reynolds numbers was 2257 and ratio of nanofluid Reynolds number to water Reynolds number was 0.992. For the bigger Reynolds number the average was 3440 and ratio 0.999. Even though the Reynolds number for water and nanofluid are not exact the difference is less than 1% so it is justifiable to make comparisons. For both the Reynolds number, local Nusselt number was higher for nanofluid. That would mean convective heat transfer for nanofluid is better than that of water.
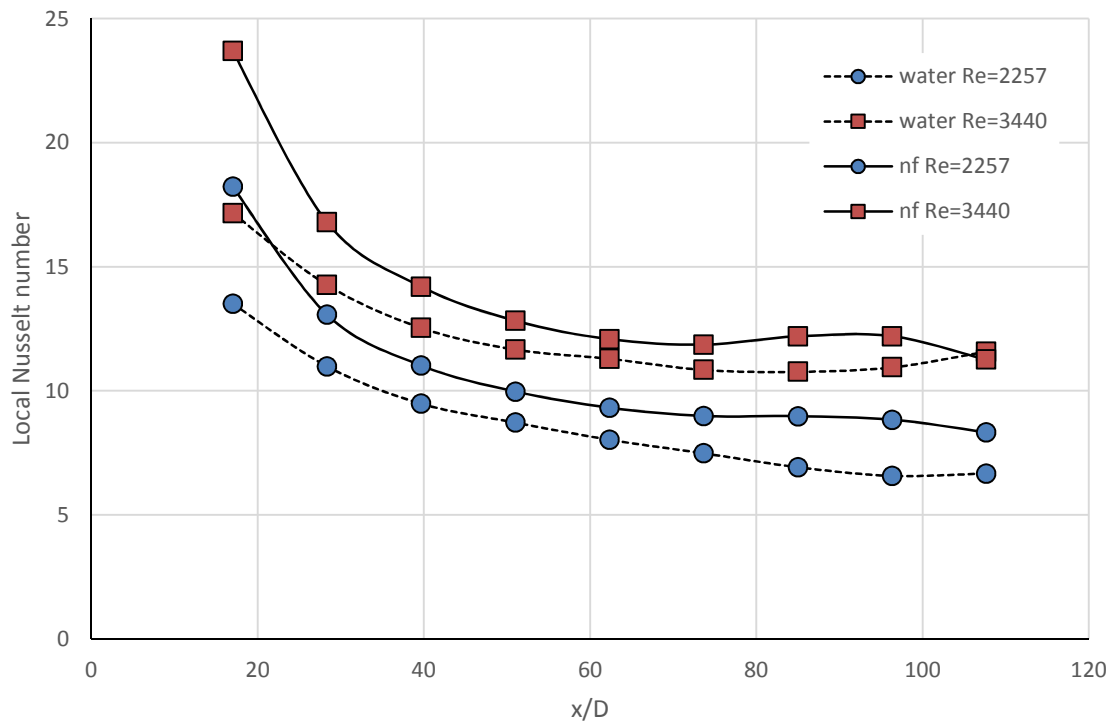

Figure 45. Local Nusselt number plotted against x/D for water and SiO_2 nf in 1/8c

In Figure 46 the ratio of local Nusselt number for SiO_2 nanofluid to local Nusselt number of water in 1/8c is plotted against non-dimensional length from the entrance. This plot can be used to quantify improvement in local Nusselt number when the working fluid is

changed from water to SiO_2 nanofluid. For instance when the value of the ratio is equal to 1 the local Nusselt number for nanofluid is equal to local Nusselt number of water at the given Reynold number and when this value 1.2 the local Nusselt number for nanofluid is 1.2 times more than that of water. From the plot it can be observed that the ratio is always greater than 1, with one exception, which indicate that the local Nusselt number for nanofluid is greater than that of water. This ratio, which is the indication of improvement of local Nusselt number, is highest at the location which is nearest to the inlet of the tube. At the location where x/D is equal to 16.9 (this is the location nearest to the inlet where thermocouple was cemented). The values ratios were 1.34 and 1.38 for Reynolds number 2257 and 3440 respectively. For Reynolds number of 2257 the value of the ratio was between 1.1 and 1.2 for most of the locations, except for the ones near the outlet, where the ratio increased. For Reynolds number of 3440 on the later part of the tube the value of the ratio was between 1.1 and 1.2 expect at the location near the outlet, where the value of the ratio dropped below 1. Since, at the locations near to the outlet, the value of the ratio increased for one of the Reynolds numbers and decreased for another, Nusselt number behavior in this location is inconclusive. This may be attributed to flow instability at the outlet of the tube. On the whole, the improvement in Nusselt number (an indicator of heat transfer behavior) is highest at the location nearest to the inlet and at locations near to the outlet, the Nusselt number behavior is inconclusive.
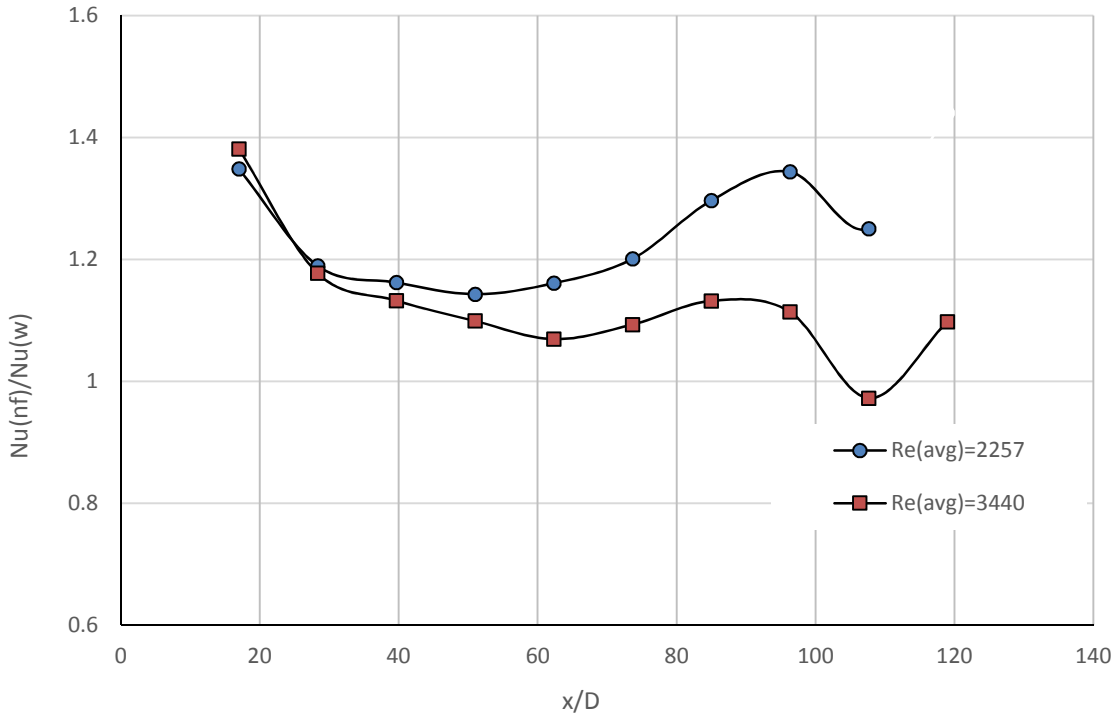
Figure 46. Ratio of Nu(nf) to Nu(w) plotted against x/D for 1/8c

In Figure 47 the negative slopes of the line joining two consecutive local Nusselt number in Figure 45 is plotted against the dimensionless distance from the inlet. This gives an idea of how the local Nusselt numbers are changing along the length of the tube. In this plot -$\Delta Nu/\Delta(x/D)$ is plotted against average of the two consecutive (x/D) values used in the ratio. The value of the term -$\Delta Nu/\Delta(x/D)$ represents the negative slope of the line joining the two consecutive local Nusselt numbers along the length of the tube. Here ΔNu is the difference between the consecutive local Nusselt numbers and $\Delta(x/D)$ is the difference between their respective dimensionless distances from the entrance. The positive value of the negative slope would indicate that there is decrease of Nusselt number along the length and higher the value, sharper the decrease in Nusselt number. Likewise, when the value of the negative slope is negative it would indicate that there is increase of Nusselt number along the length of the tube. Also when the value of the slope is equal to zero, this would indicate that the

Nusselt number does not change along the length of the tube. For a flow in laminar regime, when the value of the slope becomes zero the flow is said to be "thermally developed" and the length between the inlet of the tube and this point is termed as thermal entrance length. For laminar and turbulent regime the thermal entrance length can easily observed from the plot such as Figure 47. For transition regime the thermal entrance length cannot be observed easily due to instability of the flow behavior. Figure 47 contains plots of slope for both water and SiO_2 nanofluid. For comparable Reynolds number, slope of the line joining the consecutive Nusselt numbers is clearly higher for SiO_2 nanofluid than for water between the inlet and location where x/D is equal to 60. Beyond the location where x/D is equal to 60 the value is fluctuating above and below zero. Here the fluctuations in the slope indicate the instability in the flow. Thus for the flow with Reynolds number of 2257 and 3440 for both water and nanofluid in 1/8c the flow is still in thermal entry length. In other words, the thermal entry length is longer than the length of the tube.
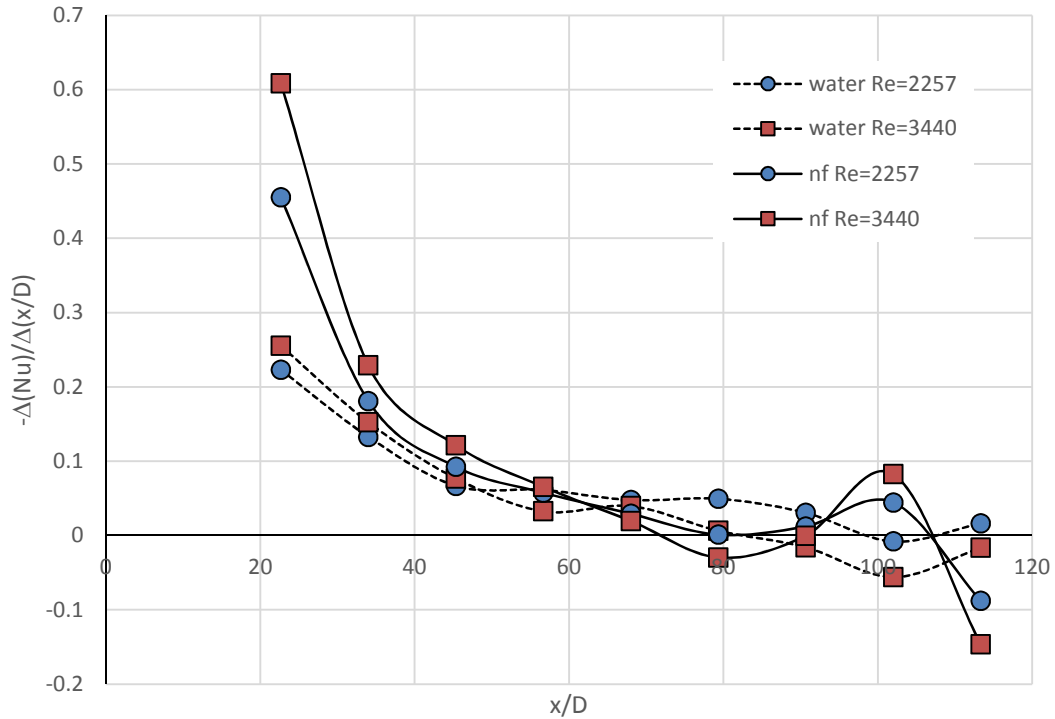
Figure 47. Nusselt number gradient plotted against x/D for 1/8c

Figure 48 can be used to compare change in local Nusselt of water and SiO_2 between the Reynolds numbers of range 500 to 5000. This figure contains two contour plots of local Nusselt number plotted against Reynolds number and non-dimensional axial distance x/D for water and nanofluid. Both the plots have same range of Reynolds number i.e. 500 to 5000 and the color of a contour on both of the plots have same range (numerical value) of Nusselt number. In the contour plot dark blue indicates a low Nusselt number and dark green indicates a high Nusselt number. Single color represents Nusselt numbers between 3 units. Observing the thickness of the contour we can see how Nusselt of number is changing with the Reynolds number. Wide contour would mean that to achieve a change of 3 units of local Nusselt number, a large change in Reynolds number is required. Similarly thin contour would mean that the 3 unit change in Nusselt number can be obtained with small change in Reynolds number. Contour plots in Figure 48 show that the Nusselt number for

82

both water and SiO_2 increases with increases in Reynolds number. In these contour plots the laminar, transition and turbulent flow regime can be distinguished from the width of the contours. In laminar regime the contour are widest and the value of the local Nusselt number is less than 10. The width of the contours are narrowest in the transition regime. In turbulent regime the width of the contours are wider than in transition and narrower than in laminar. This would mean that the change in Nusselt number with Reynolds number is most rapid in transition followed by turbulent and laminar regime. Furthermore, the change in local Nusselt number is more rapid for SiO_2 nanofluid than that for water in turbulent regime. This may be due to better mixing of particles in turbulent flow regime which would allow the nanofluid to transfer more heat from the tube inner surface. Thus if nanofluid has to be used as a heat transfer fluid it would be more effective if its flow over the heat exchanging surface in turbulent regime.
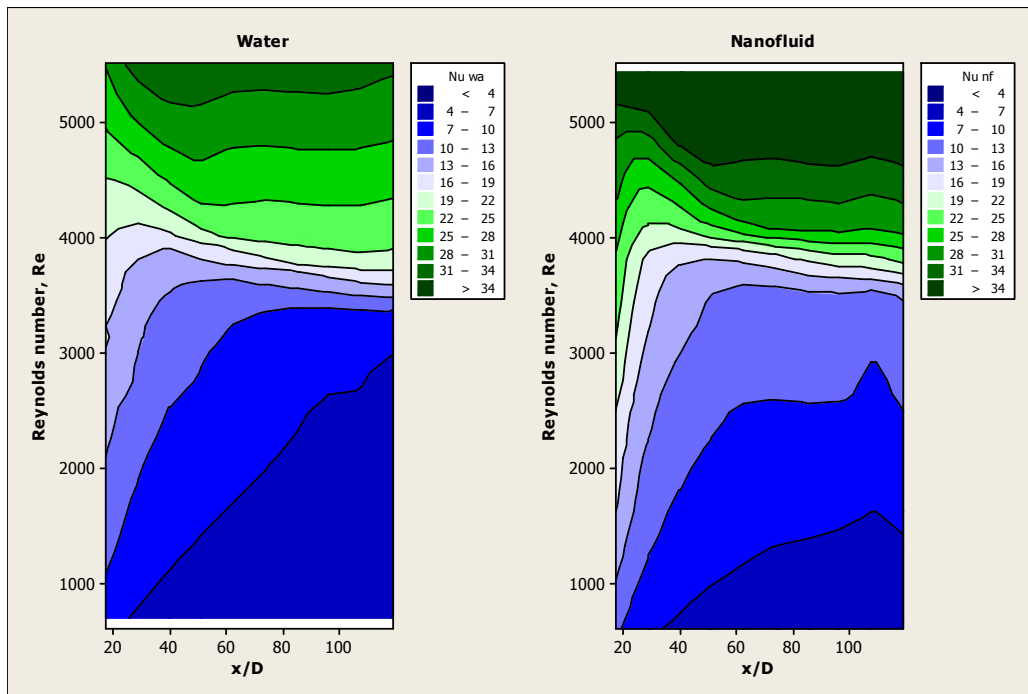
Figure 48. Contour plots for Nusselt number versus x/D & Reynolds number for water and nf in 1/8c

Overall Nusselt number for water and SiO$_2$ nanofluid is plotted against the Reynolds number flowing through 1/8c in Figure 49. The overall Nusselt number at each Reynolds number was calculated by integrating local Nusselt number over the length of the tube using trapezoidal rule. This plot can be used to compare overall Nusselt number for water and SiO$_2$ nanofluid at similar Reynolds number. At a Reynolds number of 1300 overall Nusselt number for nanofluid is 17% higher than that of water and at a Reynolds number of 5450 the overall Nusselt number for nanofluid is more than 30% higher than that of water. Thus the increase in Nusselt number is higher in higher Reynolds number when working fluid is changed from water to SiO$_2$ nanofluid. This is in agreement with comparisons made earlier for local Nusselt number.
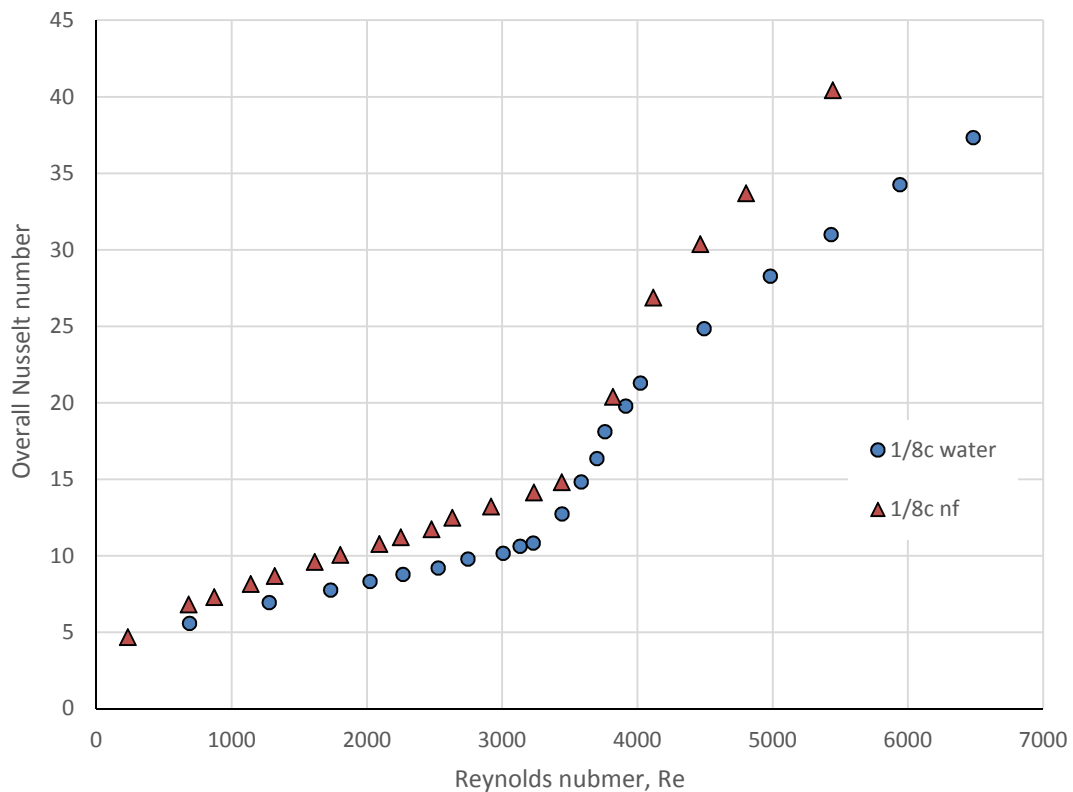
Figure 49. Overall Nusselt number versus Reynolds number for water and nf in 1/8c

In Figure 50 local Nusselt number is plotted against dimensionless distance from the inlet for water and SiO_2 nanofluid in 3/32 c. Comparison between water and nanofluid is made at three different Reynolds numbers. As in 1/8c the exact Reynolds number for both nanofluid and water was not available among the experimental data. So the comparisons were made between the comparable Reynolds numbers. Local Nusselt number for water were plotted at Reynolds numbers of 1100, 2467 and 3367 and for SiO_2 nanofluid local Nusselt numbers were plotted at Reynolds numbers of 1105, 2467 and 3371. For the lowest level of Reynolds number the local Nusselt number for nanofluid is greater than that of water only for the first half of the tube. For Reynolds number of 2467 local Nusselt number for nanofluid is higher than that for water for the whole length of the tube. Also for the highest level of Reynolds number (among the three) the local Nusselt number for nanofluid is higher than that of water for the whole length. Further a distinct jump of local Nusselt number can be observed when Reynolds number is increased from 2467 to 3367 for both the working fluids. This is due to the change in flow regime. When the flow embarks on the transition regime the streamline flow changes to disorganized flow lines and the lateral mixing of fluid layers occurs. As a result of this disorganized flow line there is better mixing of fluid layers which causes a significant increase in local Nusselt number. Furthermore, trend of local Nusselt number along the length for water at Reynolds number of 3367 is different than that the trend at other Reynolds number. A normal trend for local Nusselt would have a maximum near the inlet, then it would decrease till the thermal entry length and then tend to remain constant. In this case the local Nusselt number is increasing along the length of the tube. This may be due to gradual onset of transition along the length of the tube.
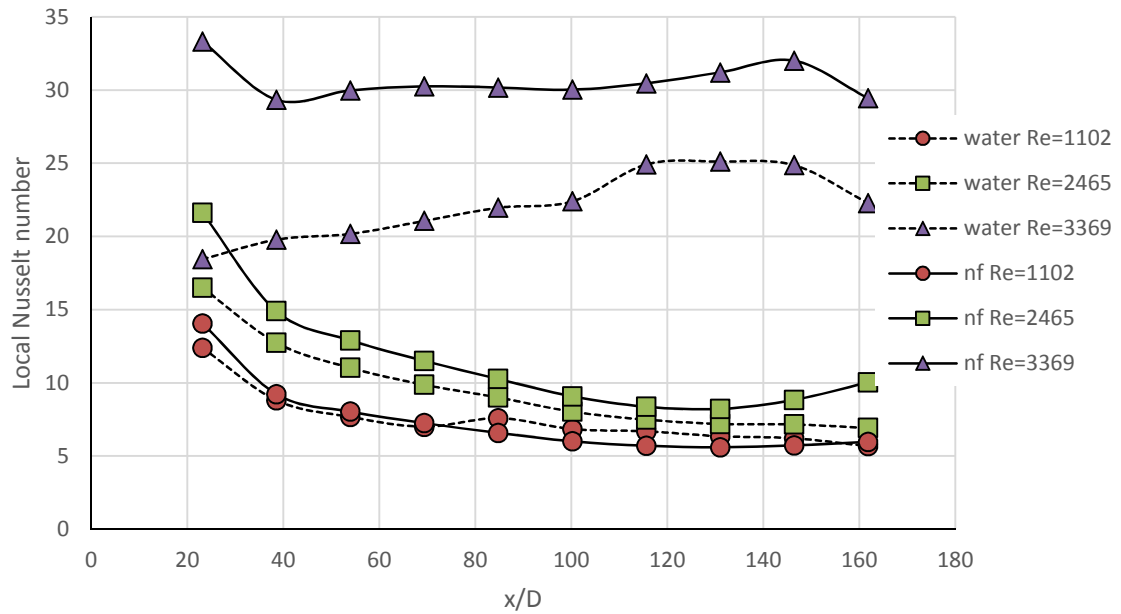
Figure 50. Local Nusselt number plotted against x/D for water and nf in 3/32c

In Figure 51 ratio of local Nusselt number of SiO_2 nanofluid to local Nusselt of water is plotted against the dimensionless distance from the inlet for three levels of Reynolds number for which comparison was made in Figure 50. For the lowest level of Reynolds number, increase in local Nusselt number can be observed from the inlet to the dimensionless distance of 69.3. After that local Nusselt number is higher for water. At Reynolds number of 2465 the maximum increase in Nusselt number is 44% which is at the nearest location at which the heat transfer was measured. For the highest level of Reynolds, number the maximum increase in local Nusselt number is 80% and this is at the location nearest to the inlet at which heat transfer to fluid was measured.
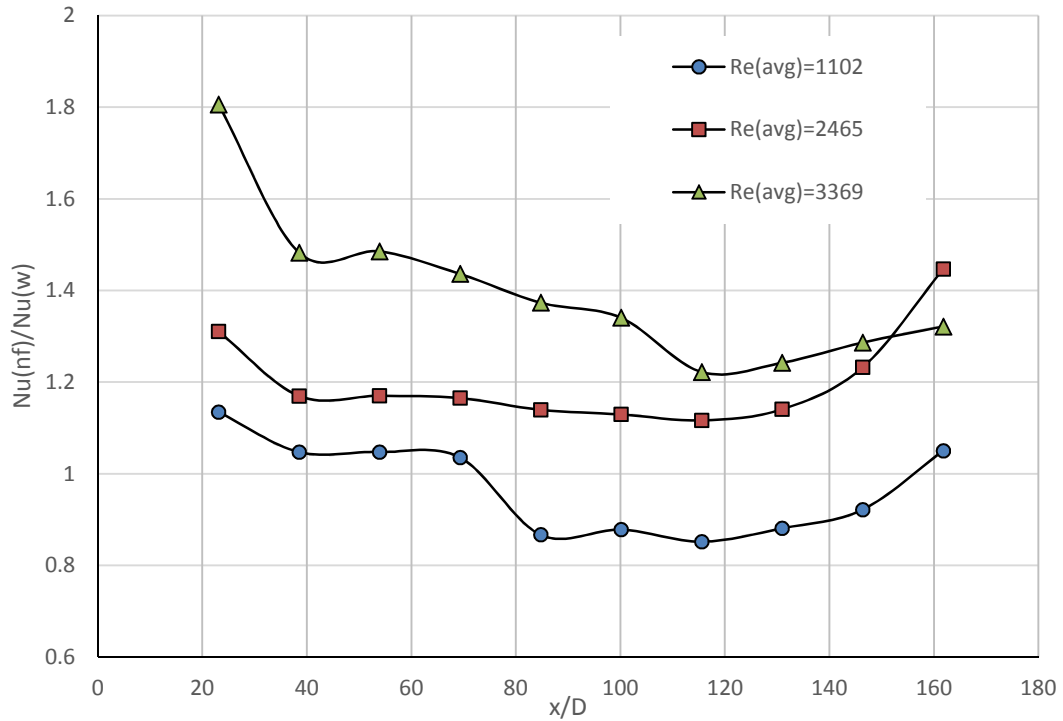
Figure 51. Ratio of Nu(nf) to Nu(w) plotted against x/D for 3/32c

Figure 52 is for test-section 3/32c and is similar to Figure 47 in which slope of line joining

two consecutive local Nusselt numbers are plotted along the dimensionless distance from

the inlet. For higher value of Reynolds number the fluctuations of the slope observed is

again due to onset of transition flow. As in 1/8c the slope is higher at the locations near

inlet. For the given Reynolds numbers thermal entrance length is longer than the length of

the tube. Figure 53 consists of two contour plots, one for water and other for SiO_2

nanofluid. In these plots local Nusselt number is plotted against Reynolds number and

dimensionless distance from the inlet for 3/32c and in Figure 54 overall Nusselt number is

plotted against Reynolds number for 3/32c. These plots are similar to plots for 1/8c.
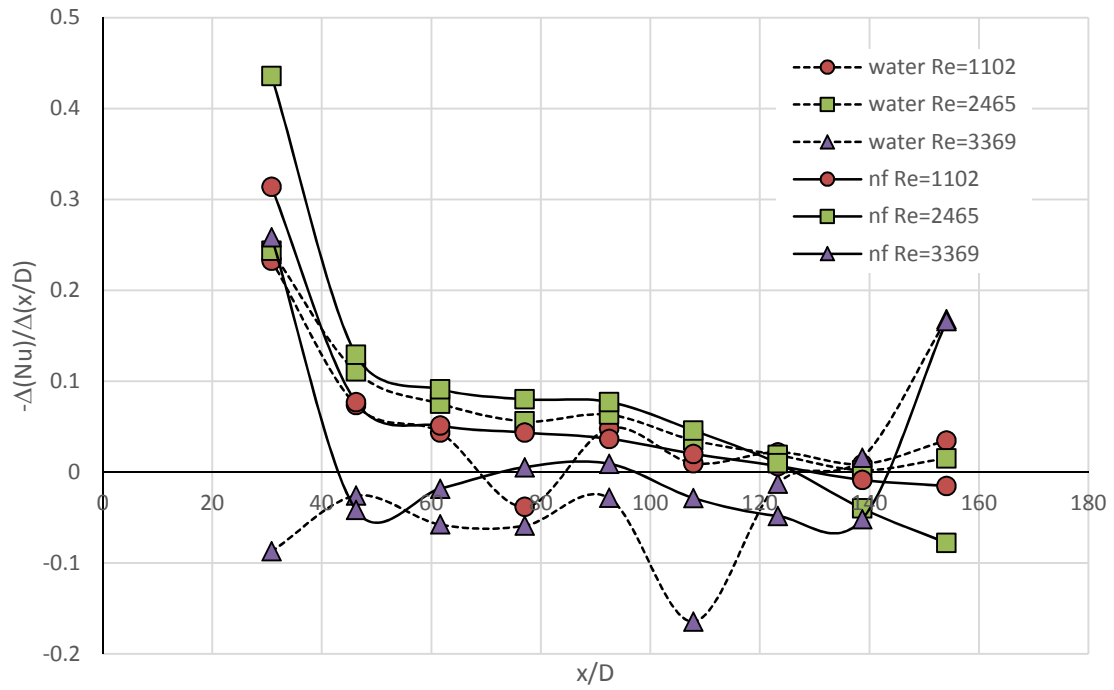
Figure 52. Nusselt number gradient plotted against x/D for water and SiO_2 nf in 3/32c
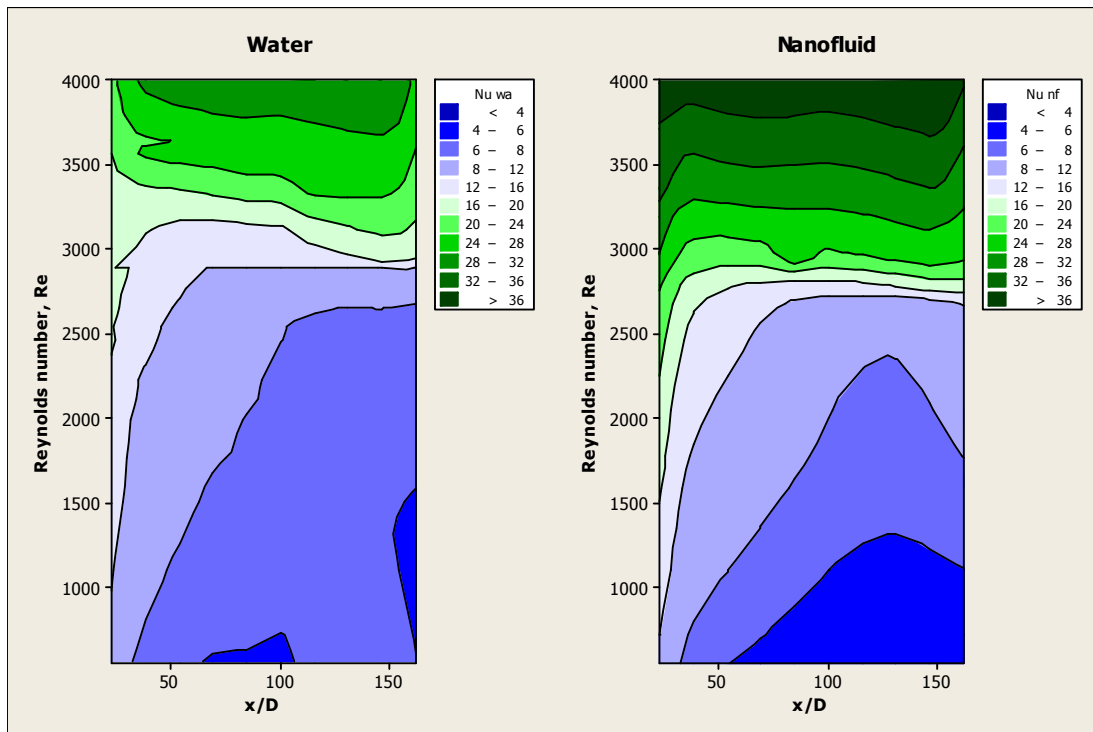
Figure 53. Contour plots for Nussetl number versus x/D & Reynolds number for water and nf in 3/32c
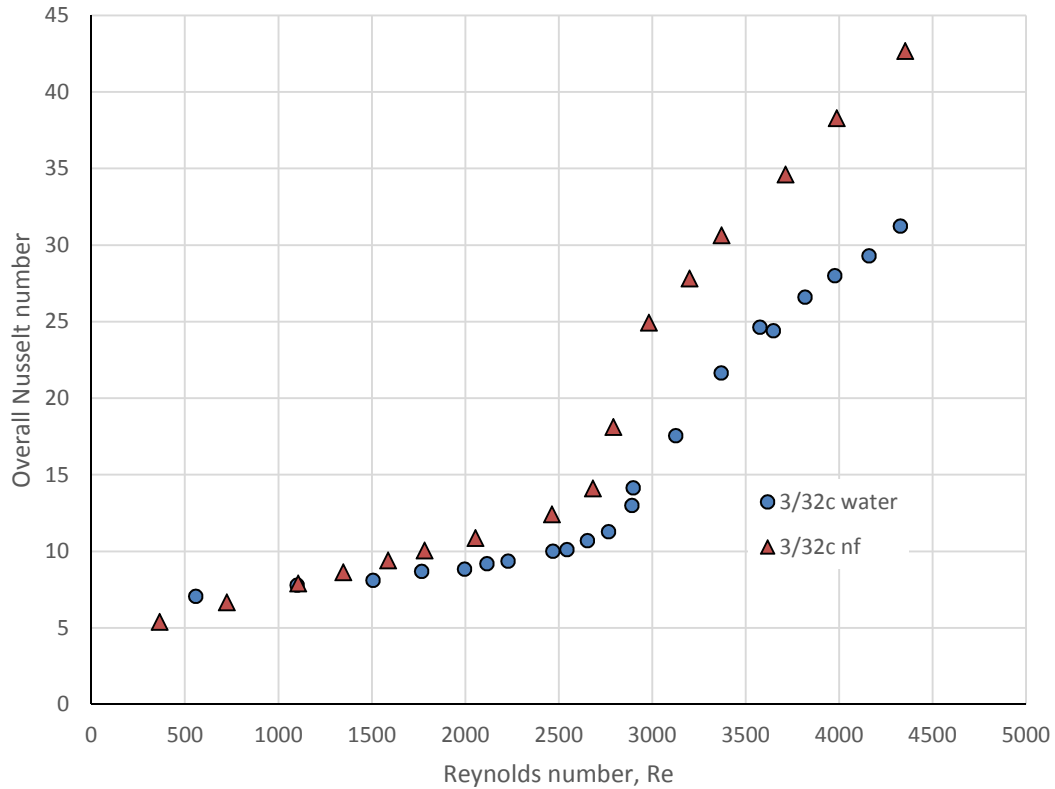
Figure 54. Overall Nusselt number versus Reynolds number for water and nf in 3/32c

Figure 55, Figure 56, Figure 57 and Figure 58 are the plots in which local Nusselt number for water is compared with local Nusselt number of SiO_2 nf in 1/16c test section. Figure 59 compares overall Nusselt number of SiO_2 nanofluid with water in 1/16c test section. Due to limitations in experimental setup heat transfer data could not be obtained at higher Reynolds number. For 1/16c at lower level of Reynolds number for which flow is laminar, increase in local Nusselt number was not observed when working fluid was changed from water to SiO_2 nanofluid. However for the first two locations, at which heat transfer was measured, increased by 6 to 15%. The dimensionless distance from the entrance for these two locations were 44.2 and 73.6.
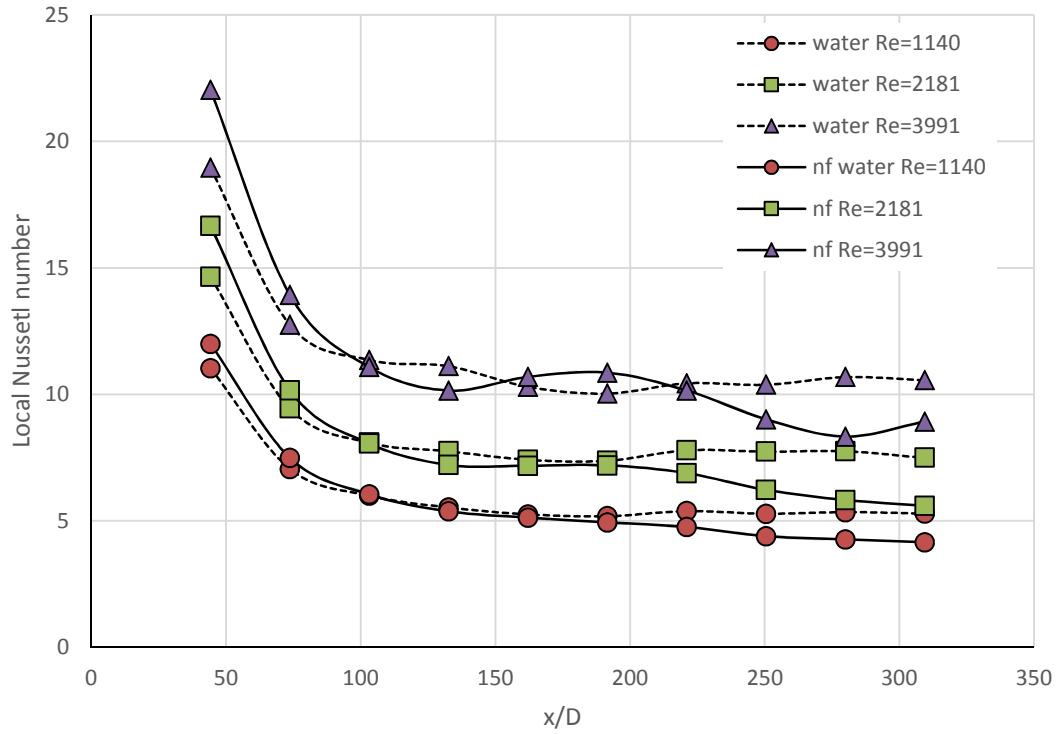
Figure 55. Local Nusselt number plotted against x/D for water and nf in 1/16c
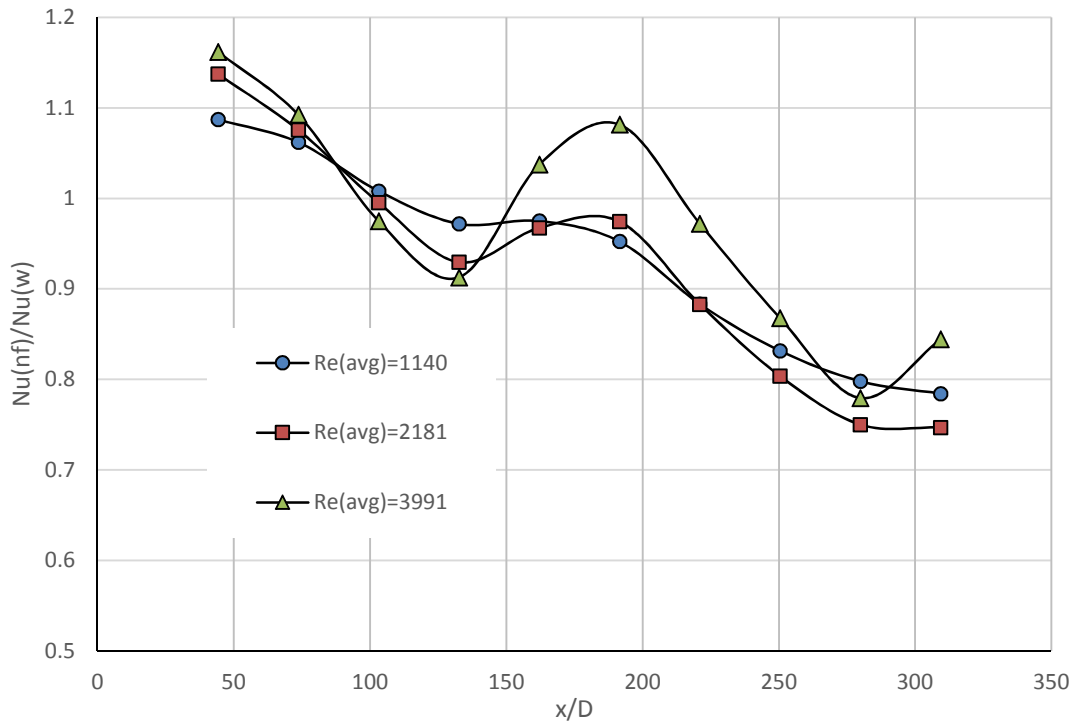
Figure 56. Ratio of Nu(nf) to Nu(w) plotted against x/D for 1/16c
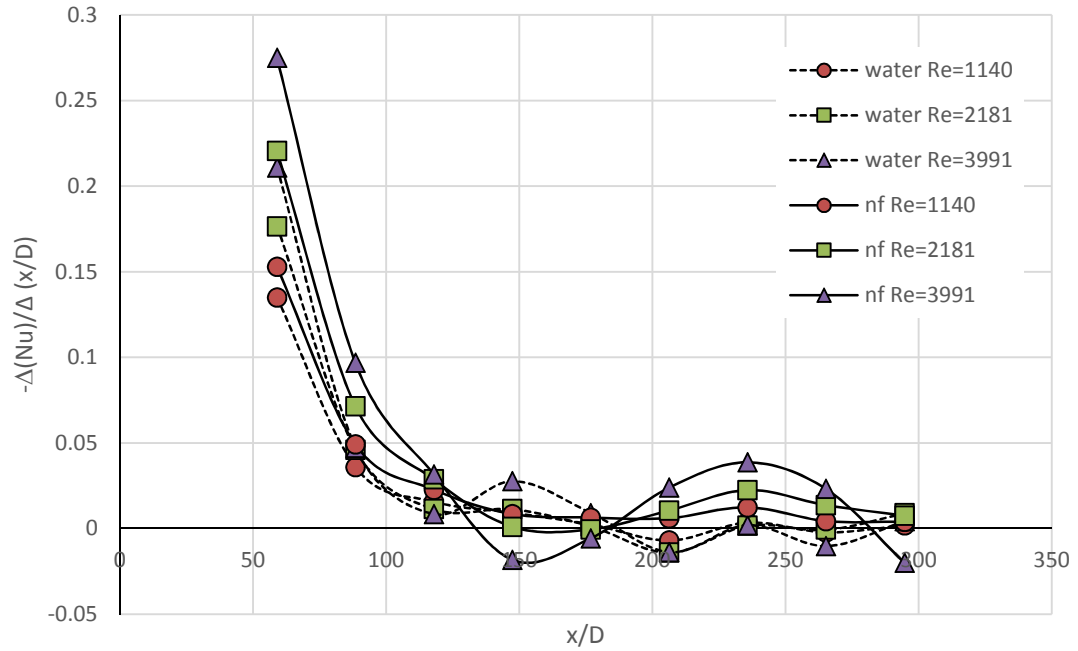
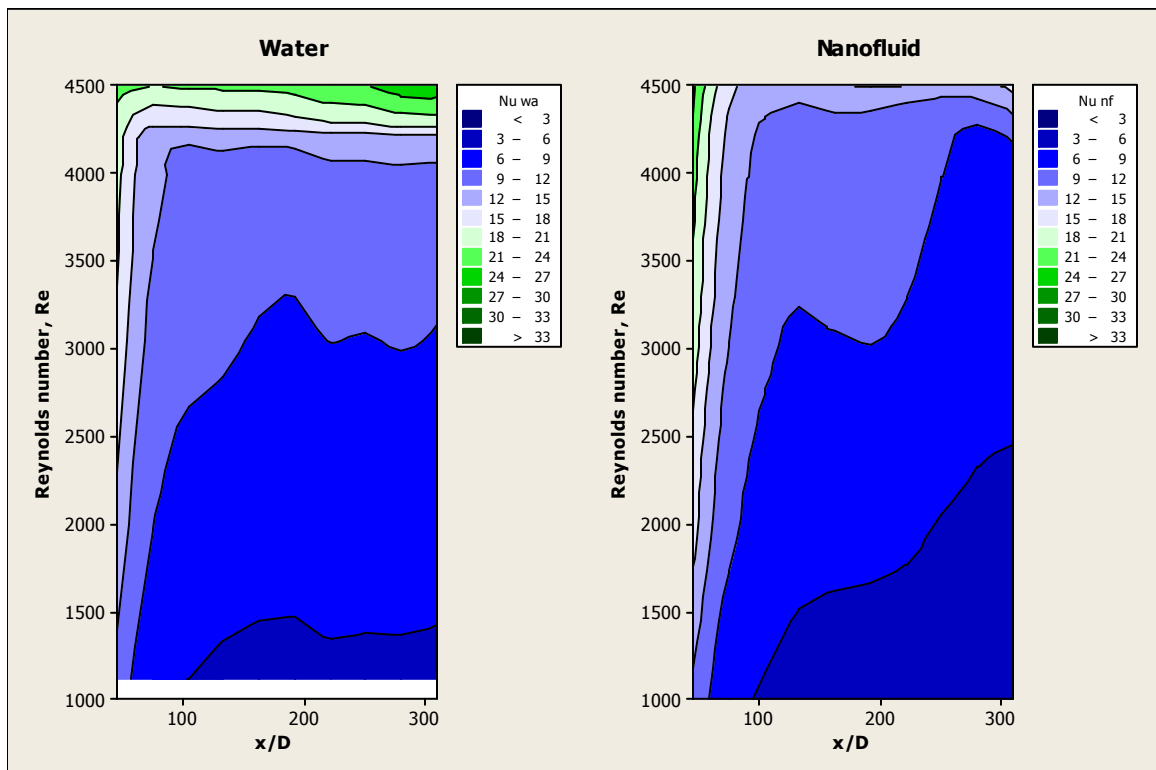Figure 57. Nusselt number gradient plotted against x/D for 1/16c

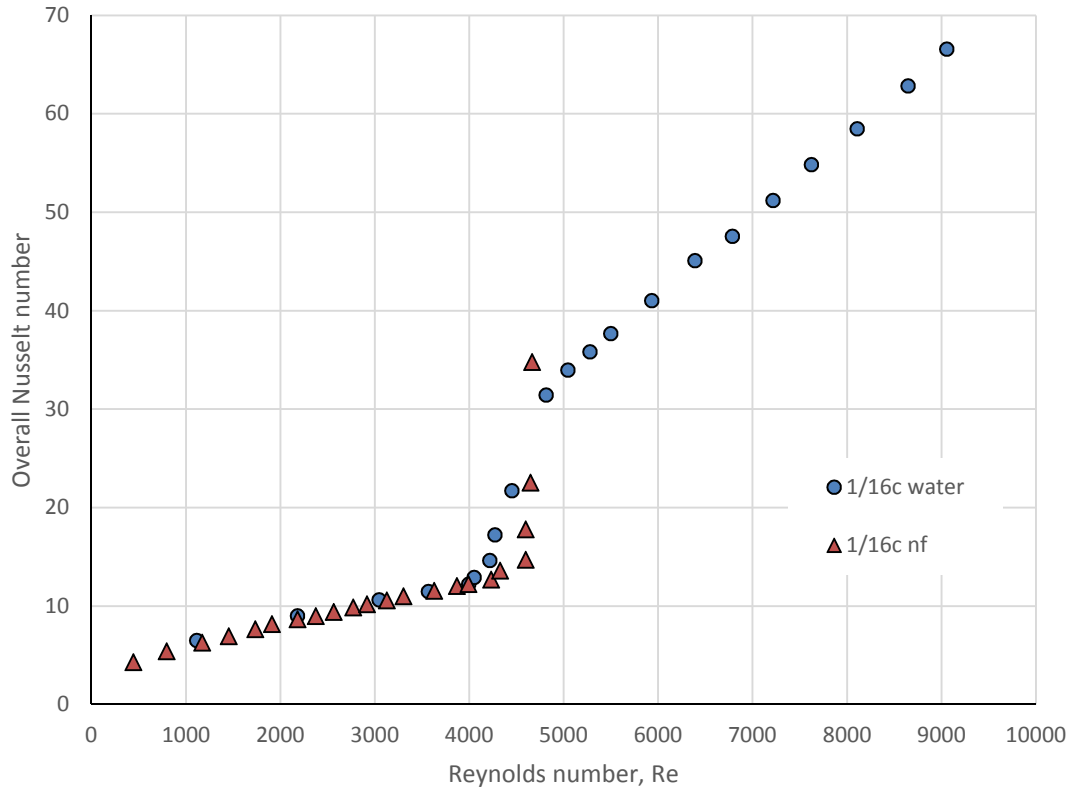Figure 58. Contour plots for Nussetl number versus x/D & Reynolds number for water and nf in 1/16c

Figure 59. Overall Nusselt number versus Reynolds number for water and nf in 1/16c

From the results and discussions presented in this section it is evident that SiO_2 nanofluid

has higher value of local Nusselt number at same Reynolds number than that of water.

Furthermore, with the increase in Reynolds number the difference between the local

Nusselt number for SiO_2 nanofluid and water increases. Although this may be true, it is not

enough evidence for us to say that SiO_2 is a better heat transfer fluid than water. The

dimensionless Nusselt number contains nanofluid's conductivity and therefore may not be

an appropriate indicator of increase in heat transfer by convection. Another important thing

to consider is the pressure drop penalty due to change (increase) in viscosity (apparent

viscosity in the case of non-Newtonian fluid) which offsets enhancement in heat transfer.

To put it in another way, nanofluid removes more heat energy from a heat transfer surface

than water, but at the same time nanofluid requires extra work energy to push it through

the flow passage. One of the ways to compare the heat transfer effectiveness of two different working fluid is to compare heat transfer coefficient at the same pumping power.

4.5.1.1.2   Pumping power v/s local heat transfer coefficient

Heat transfer coefficient of SiO_2 nanofluid is compared with that of water in 1/8c in Figure 60. Comparison was made for heat transfer coefficient along the dimensionless axial positon (x/D) at equal pumping powers. Exactly matching pumping power for water and SiO_2 nanofluid was not available among the experimental data. So, to compare heat transfer coefficient between the two working fluids, comparable pumping powers at two levels were considered in Figure 60. For water heat transfer coefficient was plotted for pumping power of 4.39 mW and 10.05 mW and for nanofluid the heat transfer coefficient was plotted at 4.64 mW and 9.93mW. At both of these pumping powers the flow regime was laminar for both the working fluids. The plot depicts that at same pumping power, heat transfer coefficient for water is higher than that for nanofluid. For a pumping power of about 4.5 mW and at a dimensionless distance from the inlet of 46.3, heat transfer coefficient of water is 18% higher than that of the nanofluid.
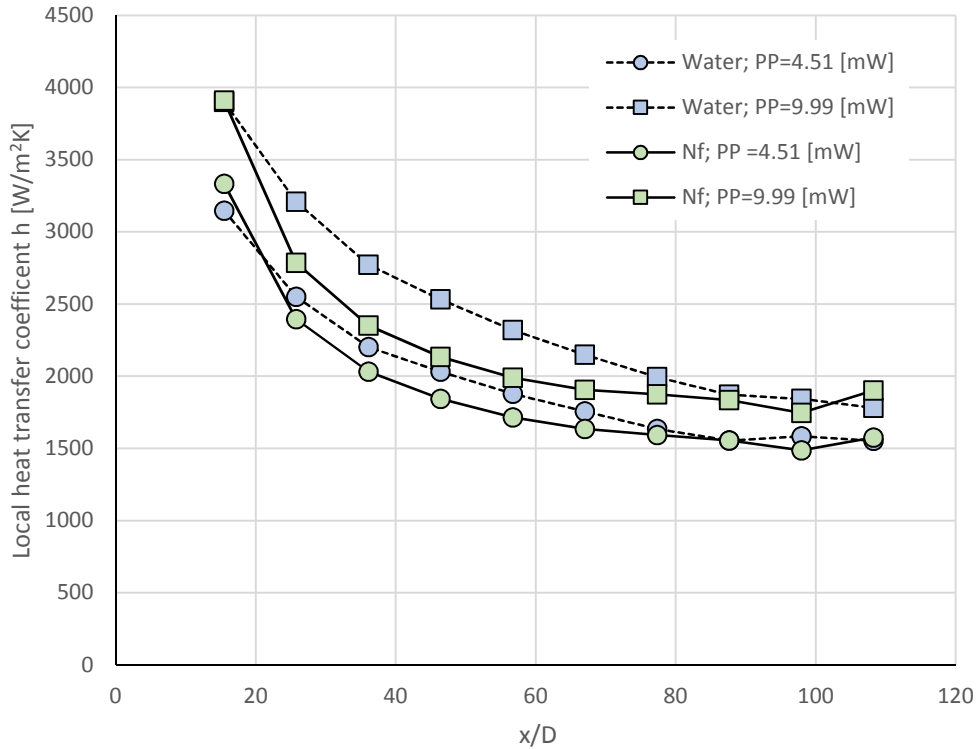
Figure 60. Local heat transfer coefficient h [W/m²K] versus x/D at comparable pumping power for 1/8c

Figure 61 consists of contour of plots local heat transfer coefficient of water and SiO$_2$ nanofluid in 1/8c test sections. In these contour plots, local heat transfer coefficient is plotted against pumping power and dimensionless distance from the inlet. The range of pumping power on both the plots is between 0 and 110 mW. On both contours plot same color represent same range of local heat transfer coefficient and each contour has a range of 800 W/m²K. From these contour plots for water and nanofluid, local heat transfer coefficient at equal pumping power can be compared. At around 10 mW pumping power, for both water and SiO$_2$ nanofluid, the local heat transfer coefficient is between 1600 and 2400 W/m²K. At this pumping power both the fluids are in laminar regime. Then for pumping power around 80 mW, the local heat transfer coefficient for water is between 8000 and 8800 W/m²K. while for nanofluid at same pumping power the local heat transfer

coefficient is between 3200 and 4000. Apparently at same pumping power local heat transfer coefficient is more than 100% higher at this pumping power. This substantial difference in the local heat transfer coefficient can be explained by the flow behavior of the fluids at this pumping power. At a pumping power of 80 mW water is clearly in turbulent flow regime and for the same pumping power the nanofluid is still in laminar regime due to is higher apparent viscosity or the friction between the fluid layers. And it is well established that for turbulent flow regime the heat transfer is significantly higher than in laminar flow due to the mixing of fluid layers Thus, when local heat transfer coefficient for water and nanofluid is compared at same pumping power heat transfer behavior of nanofluid does not look as much promising as it looked when local Nusselt numbers were compared at same Reynolds number. In Figure 62, Figure 63, Figure 64 and Figure 65 similar plots and contour plots for test sections 3/32c and1/16c were plotted and they tell the same story as the plots for 1/8c.
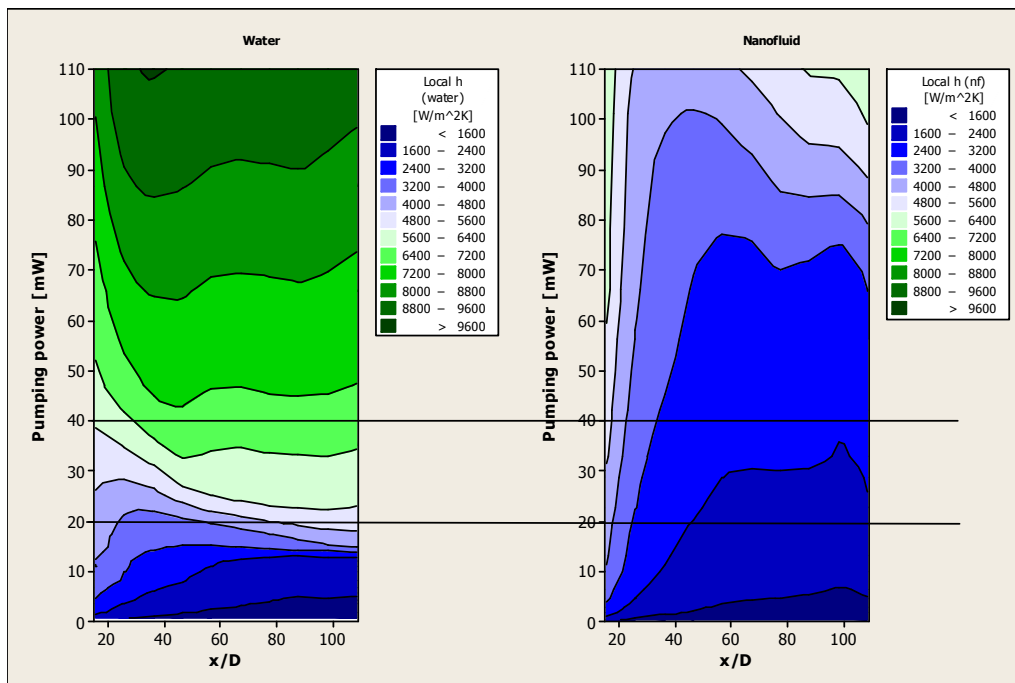

Figure 61. Contour plots for local heat tranfer coefficient, h [W/m^{2}K] versus pumping power [mW] & x/D for water and nf in 1/8c
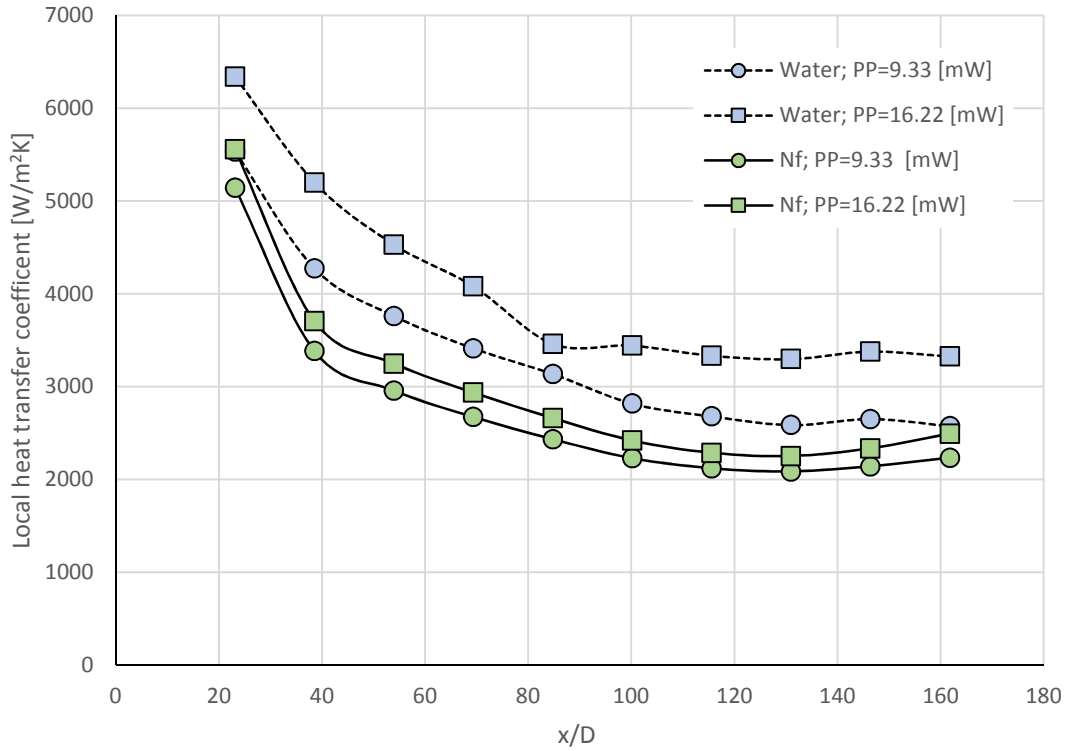
95

Figure 62. Local heat transfer coefficient h [W/m^{2}K] versus x/D at comparable pumping power [mW] in 3/32c
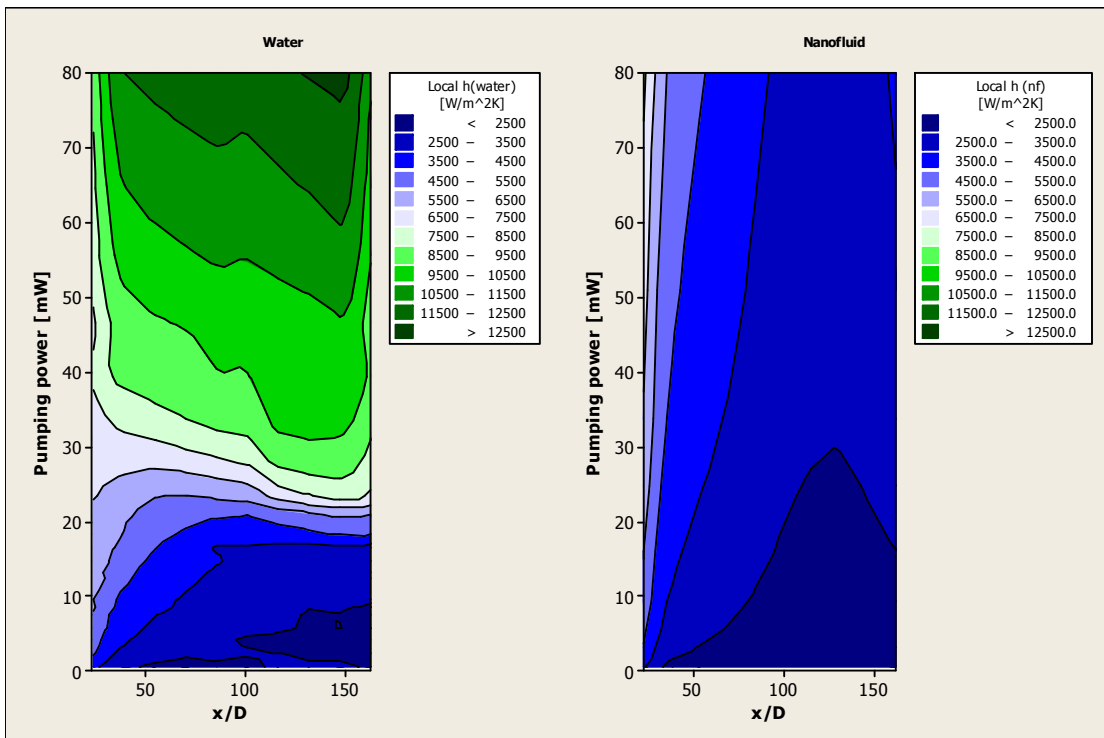

Figure 63. Contour plots for local heat trasnfer h [W/m^{2}K] versus pumping power [mW] & x/D for water and nf in 3/32c
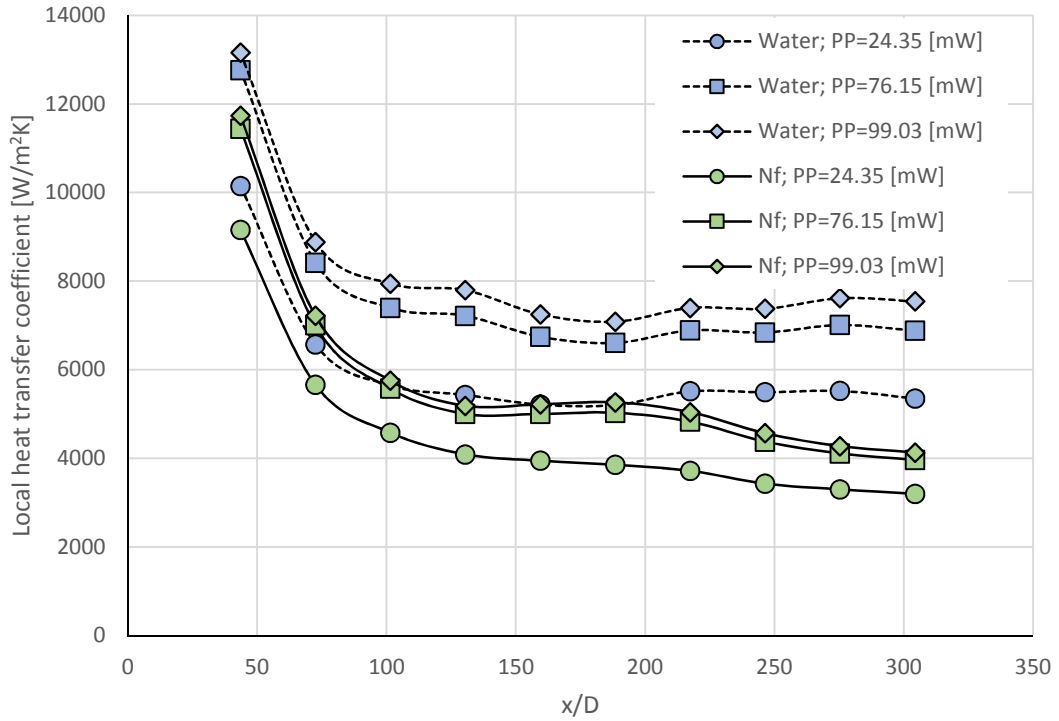
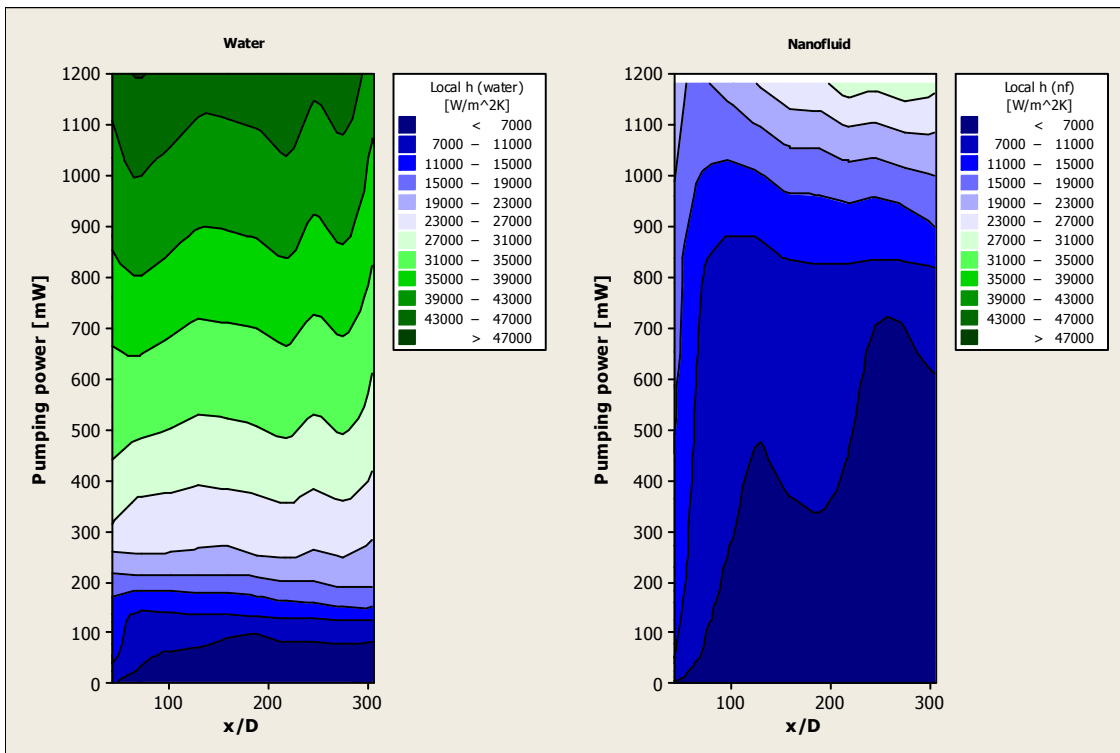Figure 64. Local heat transfer coefficient, h [W/m²K] versus x/D at comparable pumping power [mW] in 1/16 c

Figure 65. Contour plots for local heat transfer, h [W/m²K] versus pumping power [mW] & x/D for water and nf in 1/16c

97

4.5.1.2 Square Tubes

Heat transfer behavior of water and SiO_2 nanofluid were studied in square channels as well. And similar analysis were carried out as for circular channels. Local Nusselt numbers for water and SiO_2 nanofluid were plotted at similar Reynolds number along the dimensionless distance from the inlet. Also similar to circular tubes overall Nusselt numbers were plotted against their respective Reynolds number and local heat transfer coefficients were plotted against pumping powers. The results for effect of working fluids on heat transfer behavior in square channels was similar to that in circular channels. The results are presented in various plots in the following figures.
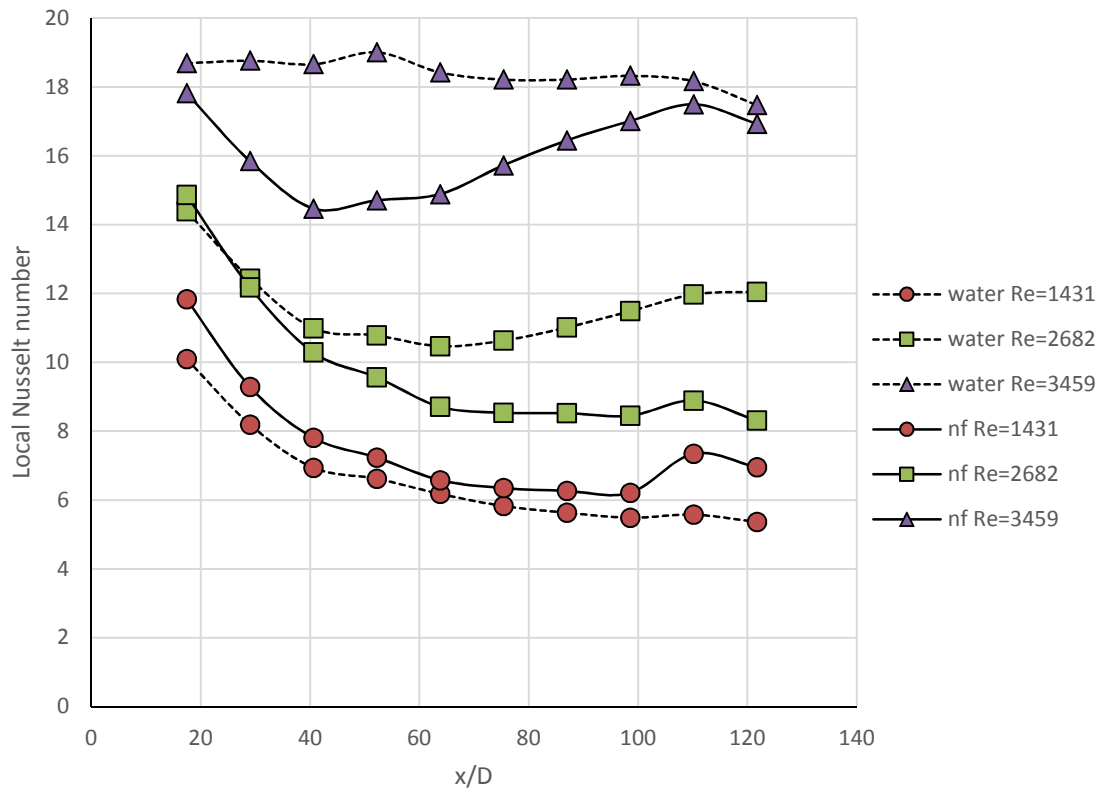
4.5.1.2.1 Nu versus x/D at comparable Re

Figure 66. Local Nusselt number plotted against x/D for water and nf in 1/8sq
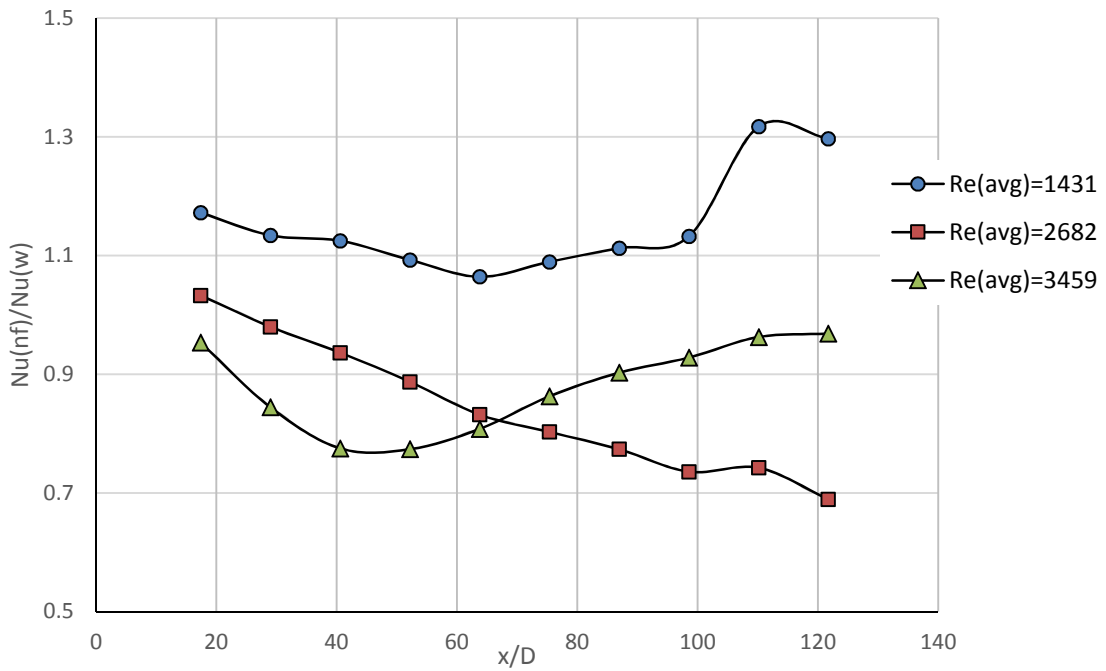
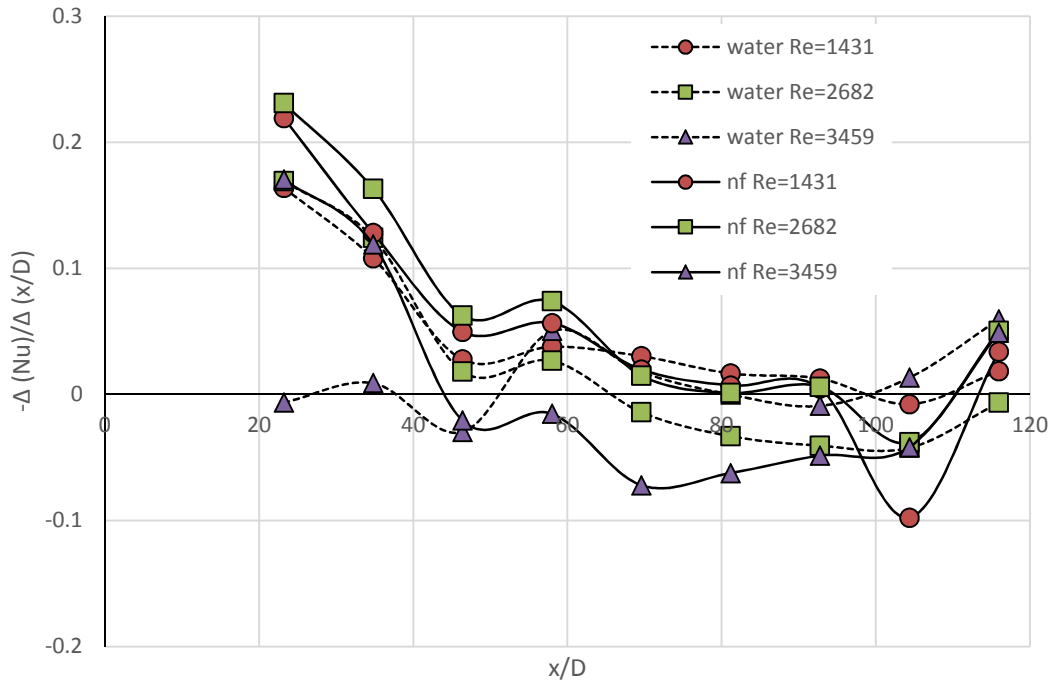Figure 67. Ratio of Nu(nf) to Nu(w) plotted against x/D for 1/8sq

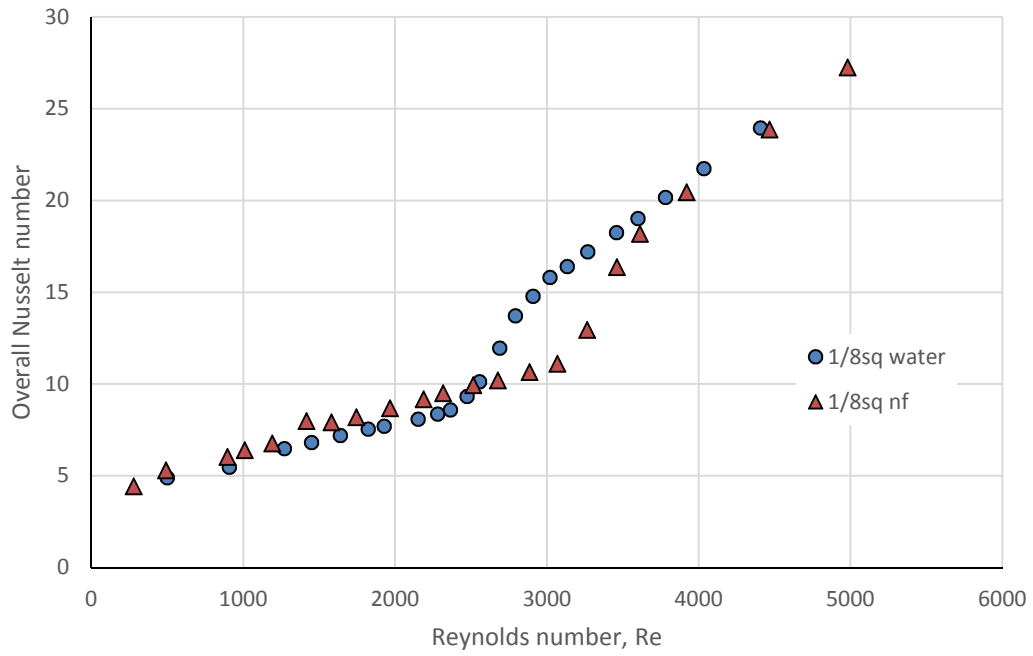Figure 68. Nusselt number gradient plotted against x/D for 1/8sq

99

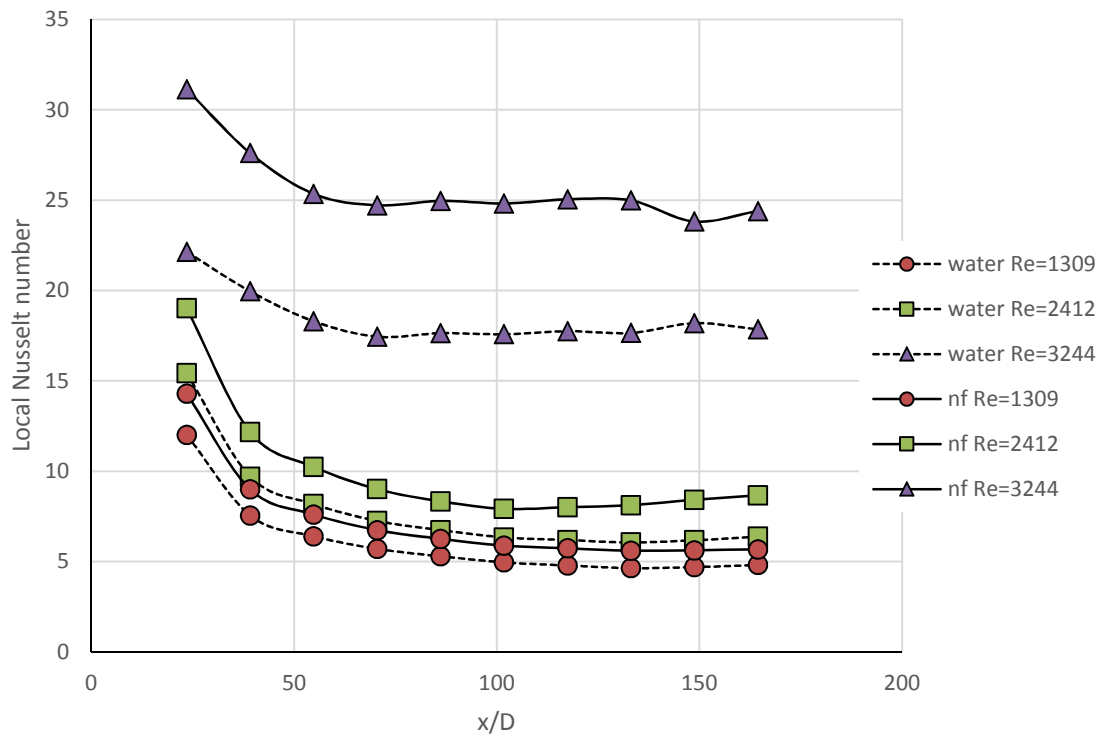Figure 69. Overall Nusselt number versus Reynolds number for water and nf in 1/8sq

Figure 70. Nusselt number plotted against x/D for water and nf in 3/32sq
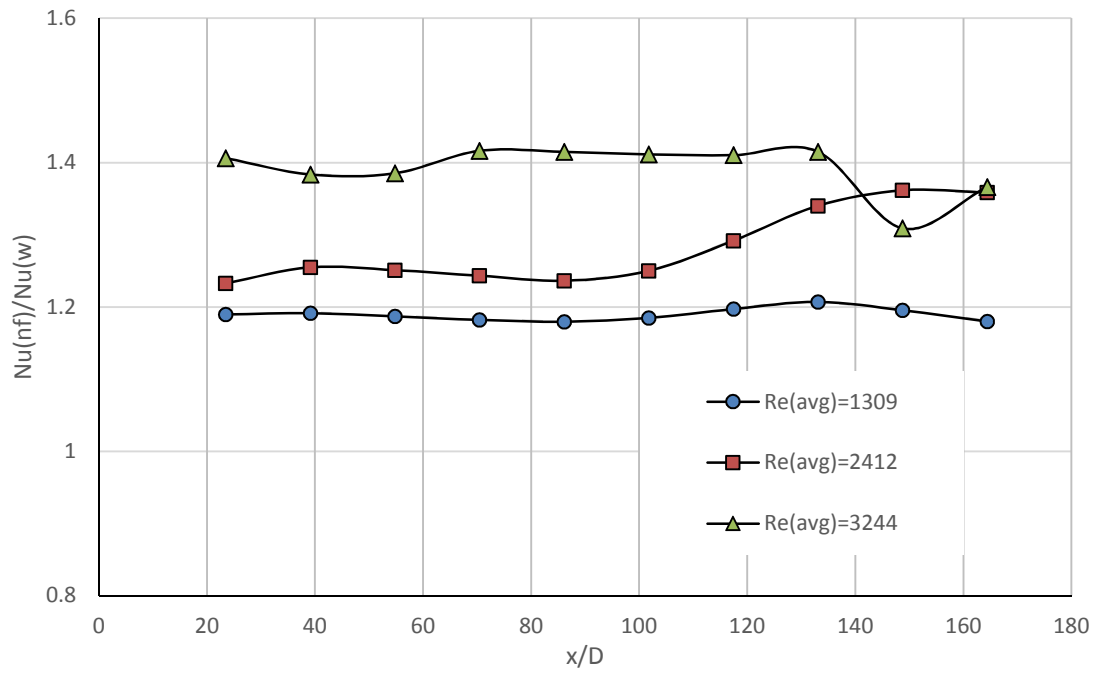
100

Figure 71. Ratio Nu(nf) to Nu(w) plotted against x/D for 3/32sq

Figure 72. Nusselt number gradient plotted against x/D for 3/32sq

101

Figure 73. Overall Nusselt number versus Reynolds number for water and nf in 3/32sq
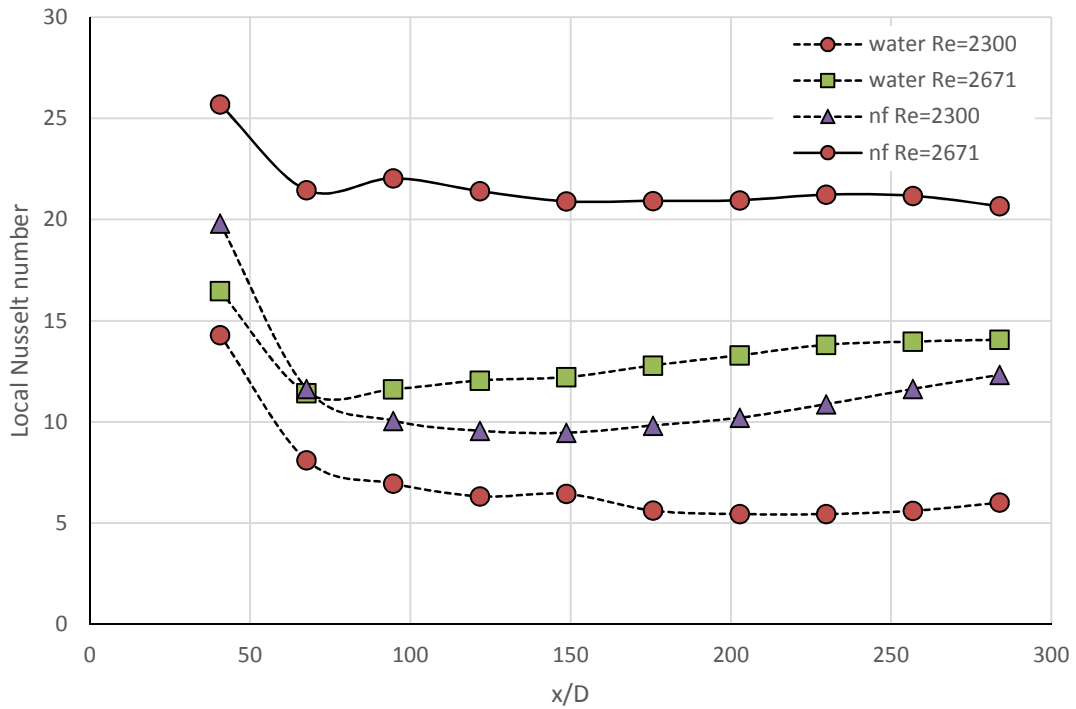
Figure 74. Local Nusselt number plotted against x/D for water and nf in 1/16sq

102

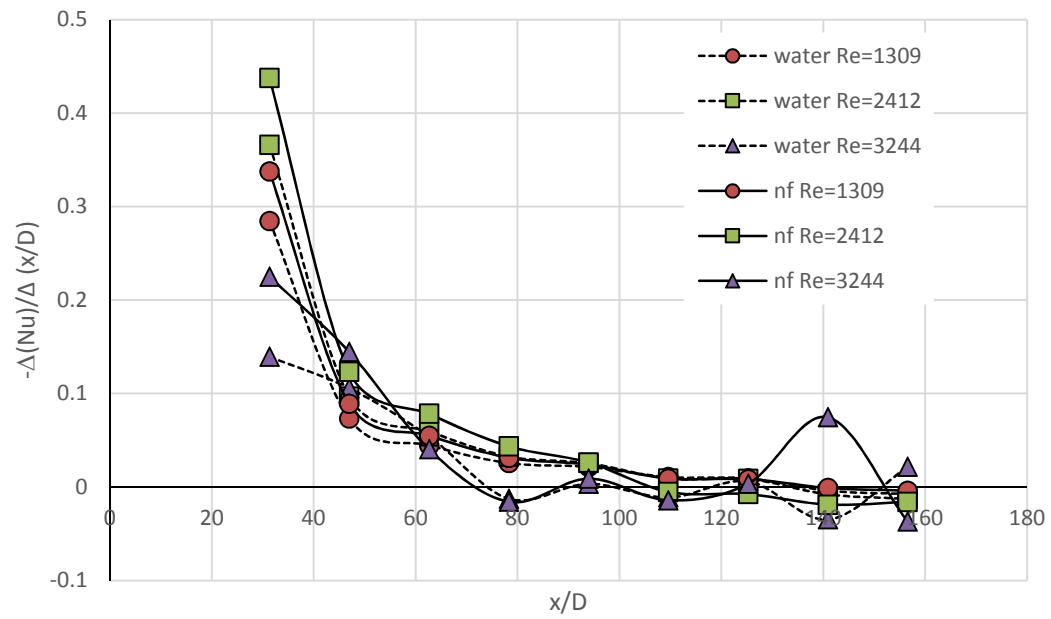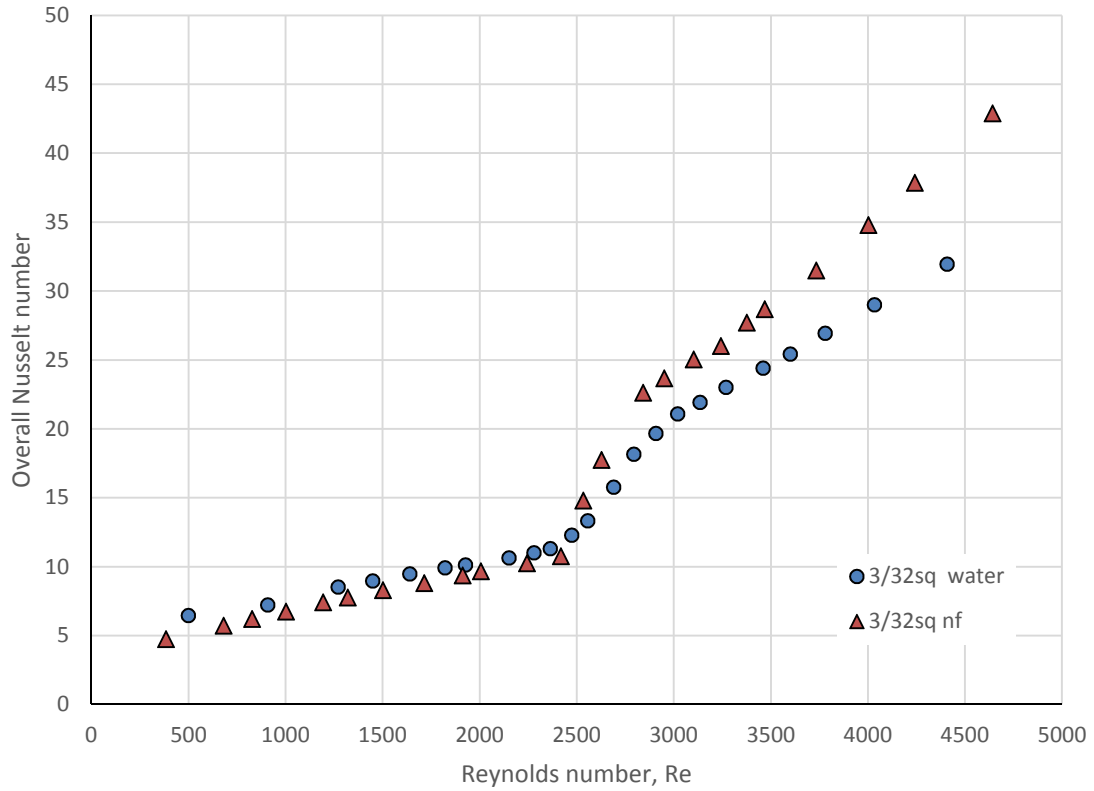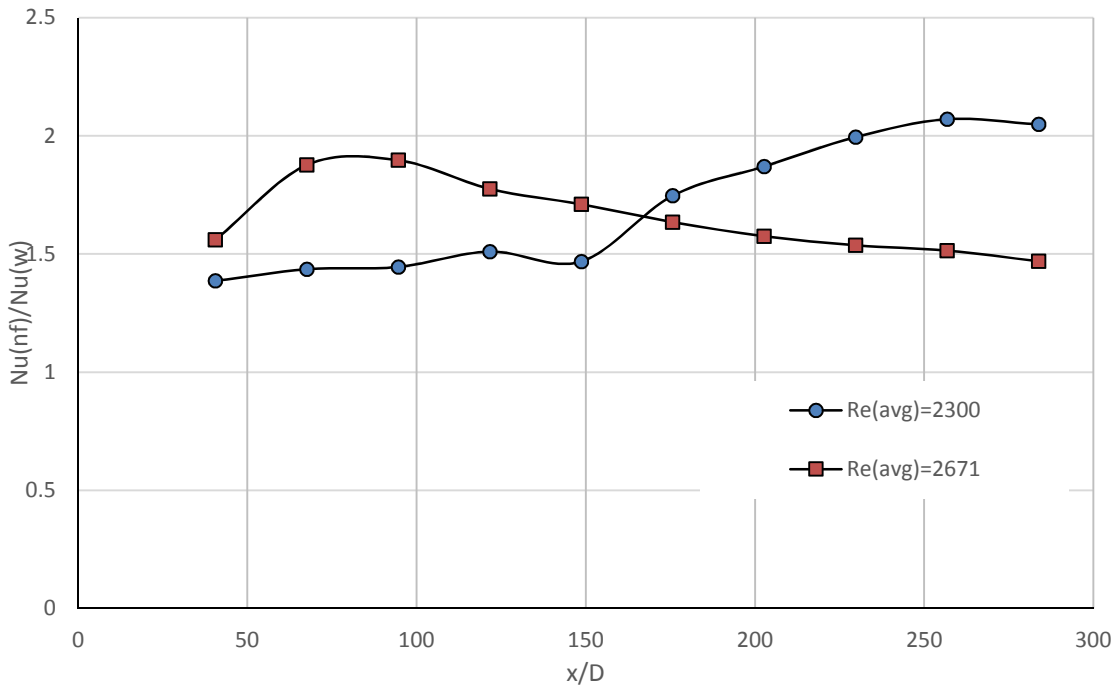Figure 75. Ratio of Nu(nf) to Nu(w) plotted against x/D for 1/16sq
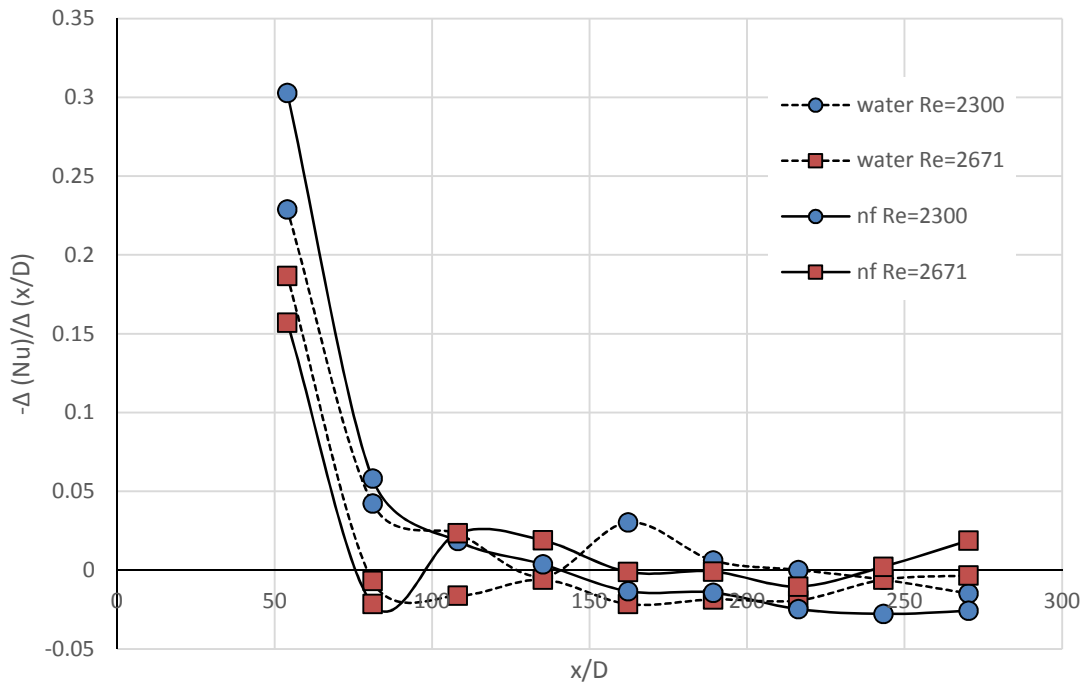
Figure 76. Nusselt number gradient plotted against x/D for 1/16sq
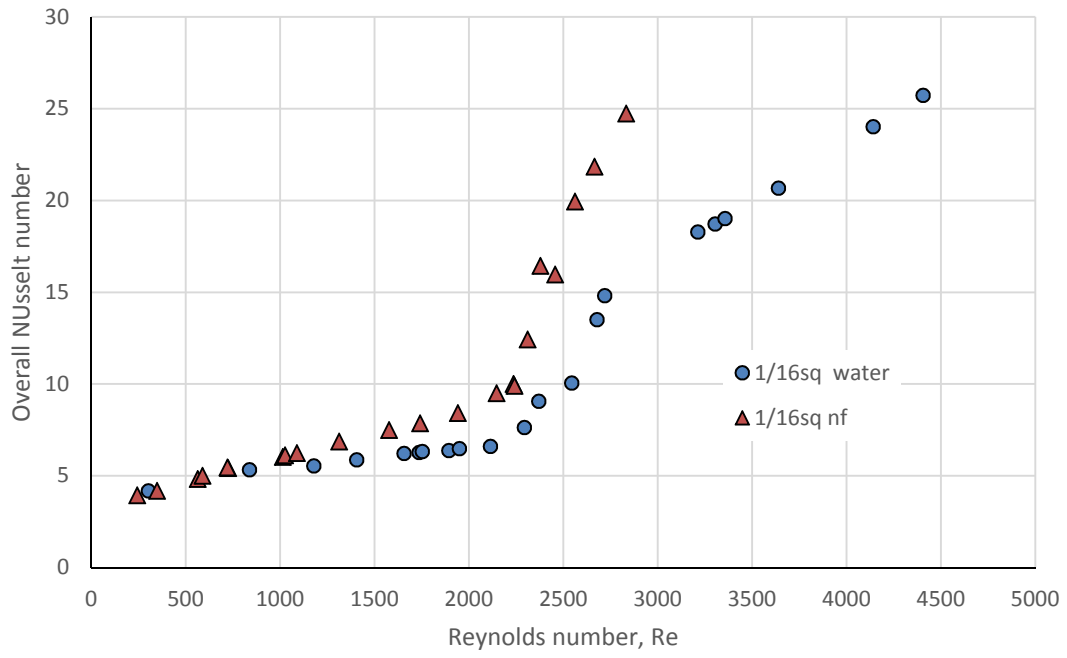
Figure 77. Overall Nusselt number versus Reynolds number for water and nf in 1/16sq

4.5.1.2.2 Pumping power v/s local heat transfer coefficient for square tubes
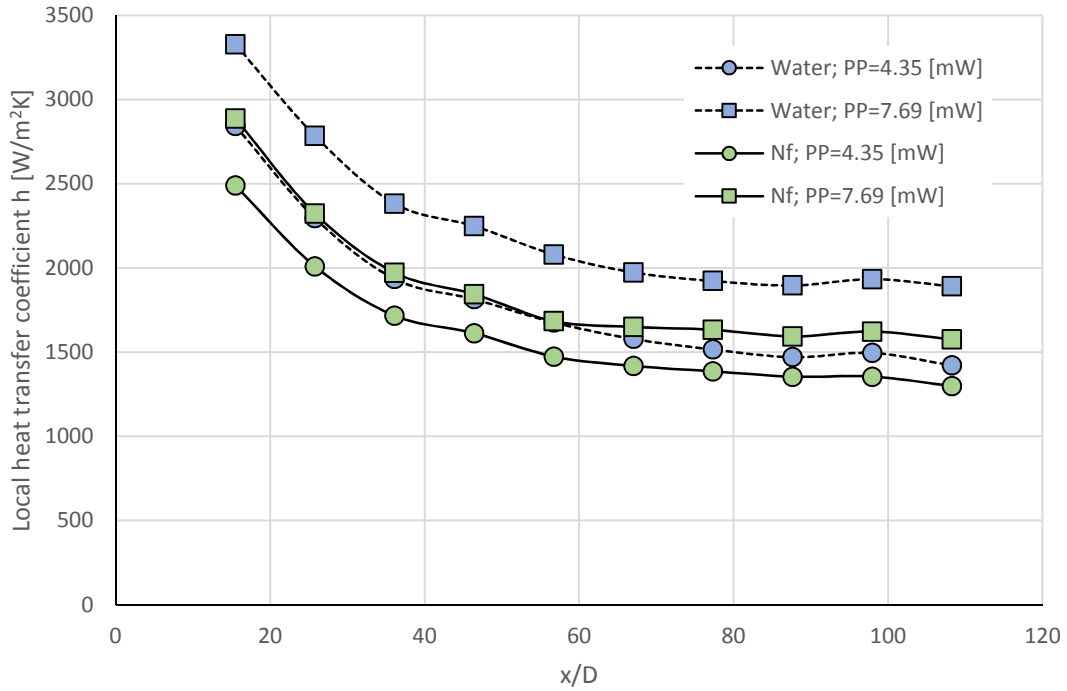
Figure 78. Local heat transfer coefficient, h [W/m^{2}K] versus x/d at comparable pumping power [mW] in 1/8 sq
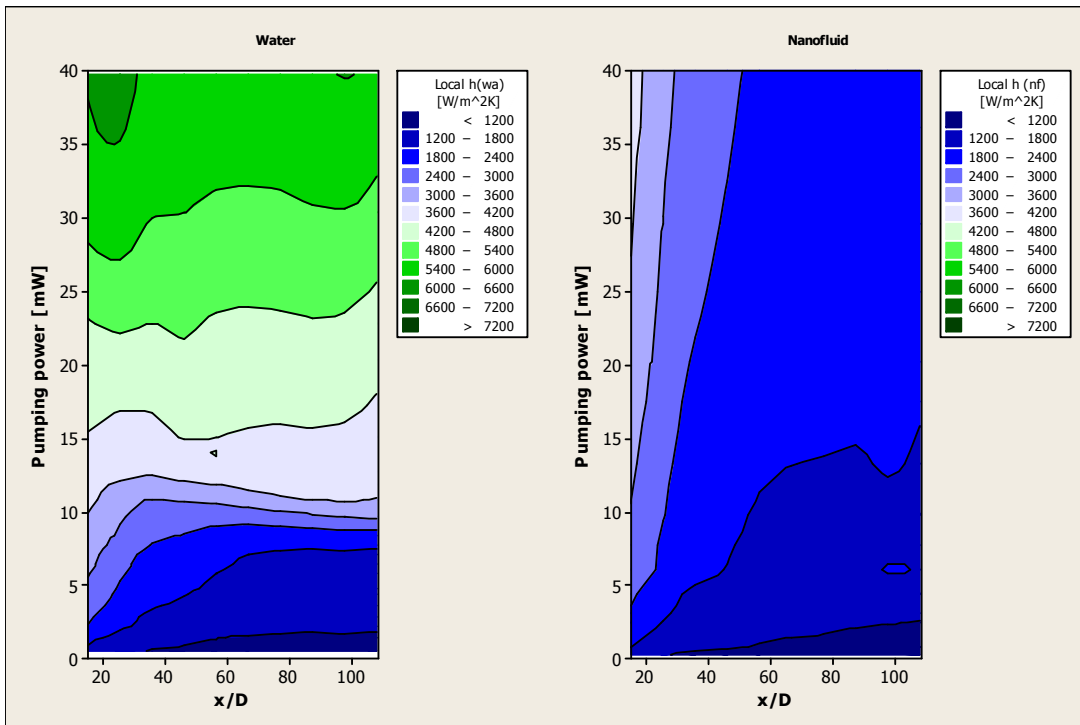
Figure 79. Contour plots for local heat transfer, h [W/m^{2}K] versus pumping power&x/D for water and nf in 1/8sq
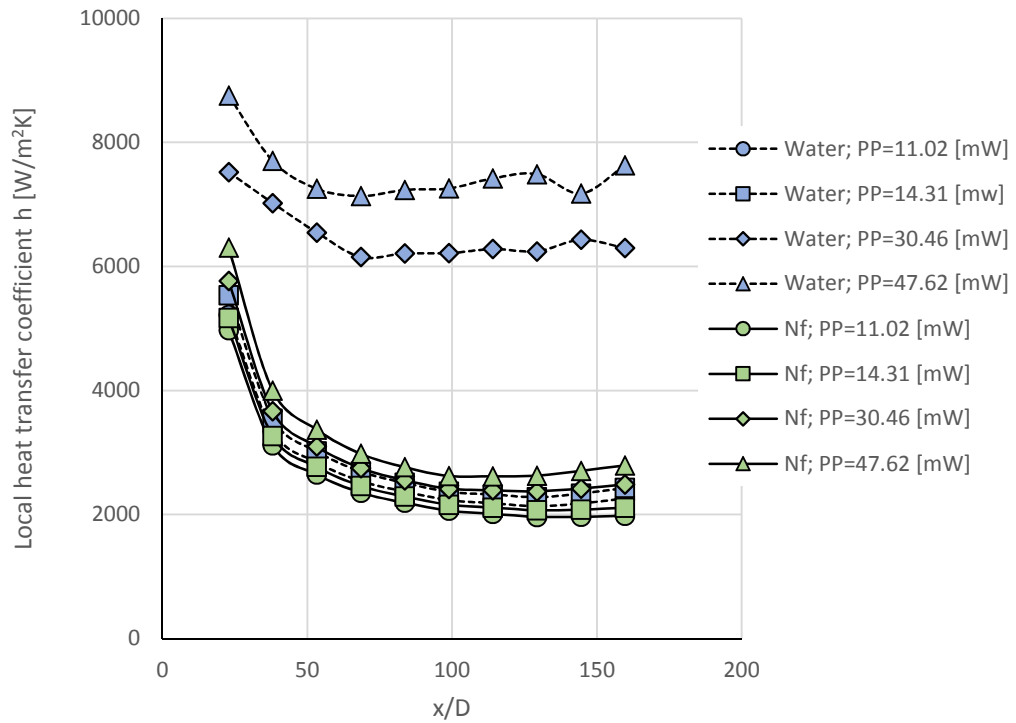
Figure 80. Local heat transfer coefficient h [W/m^{2}K] versus x/d at comparable pumping power 3by32 sq
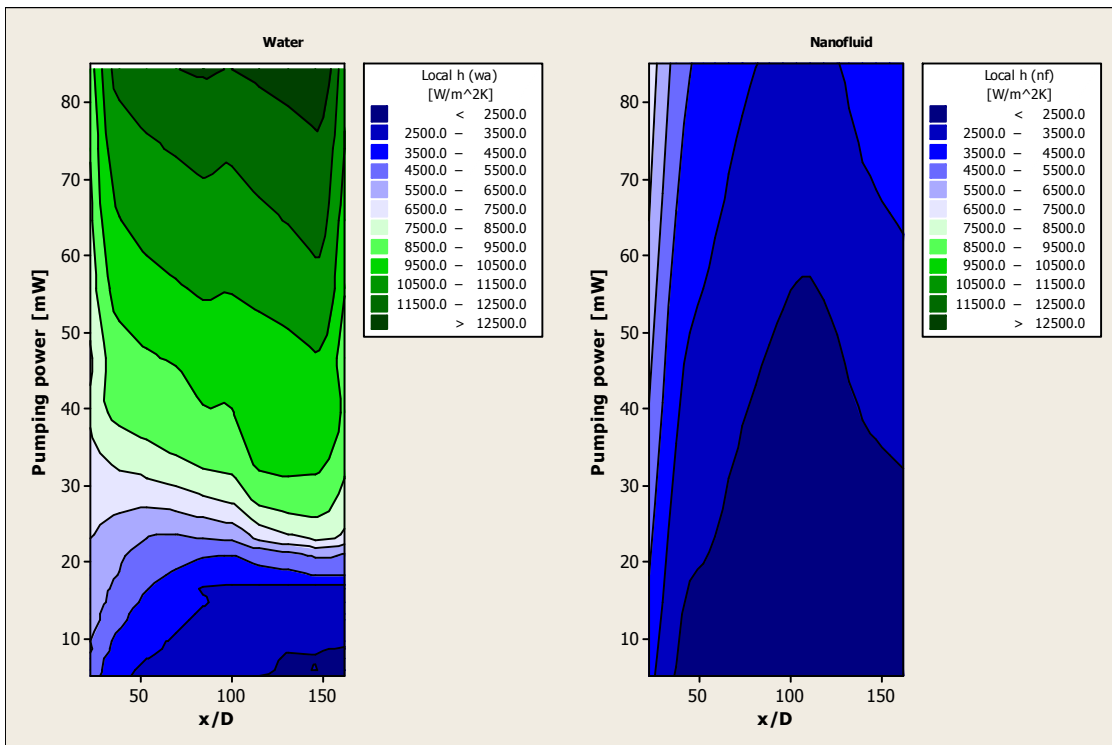
Figure 81. Contour plots for local heat transfer coefficient h [W/m^{2}K] versus pumping power & x/D for water and nf in 3/32sq

106
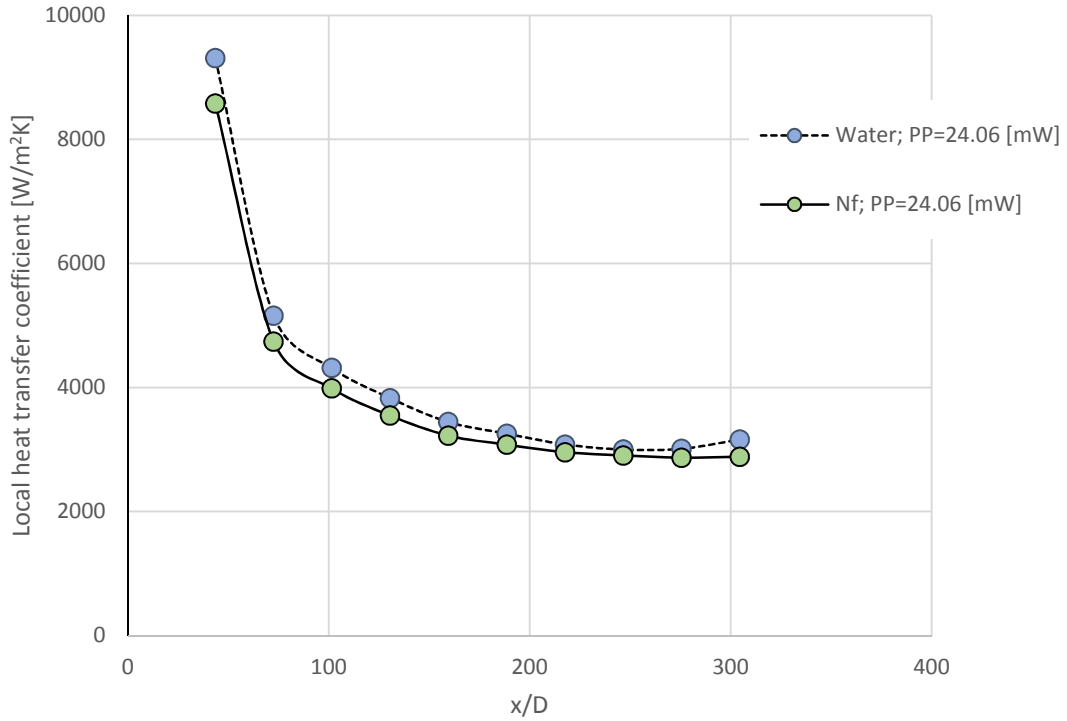
Figure 82. Local heat transfer coefficient h [W/m²K] versus x/D at comparable pumping power in 1by16 sq
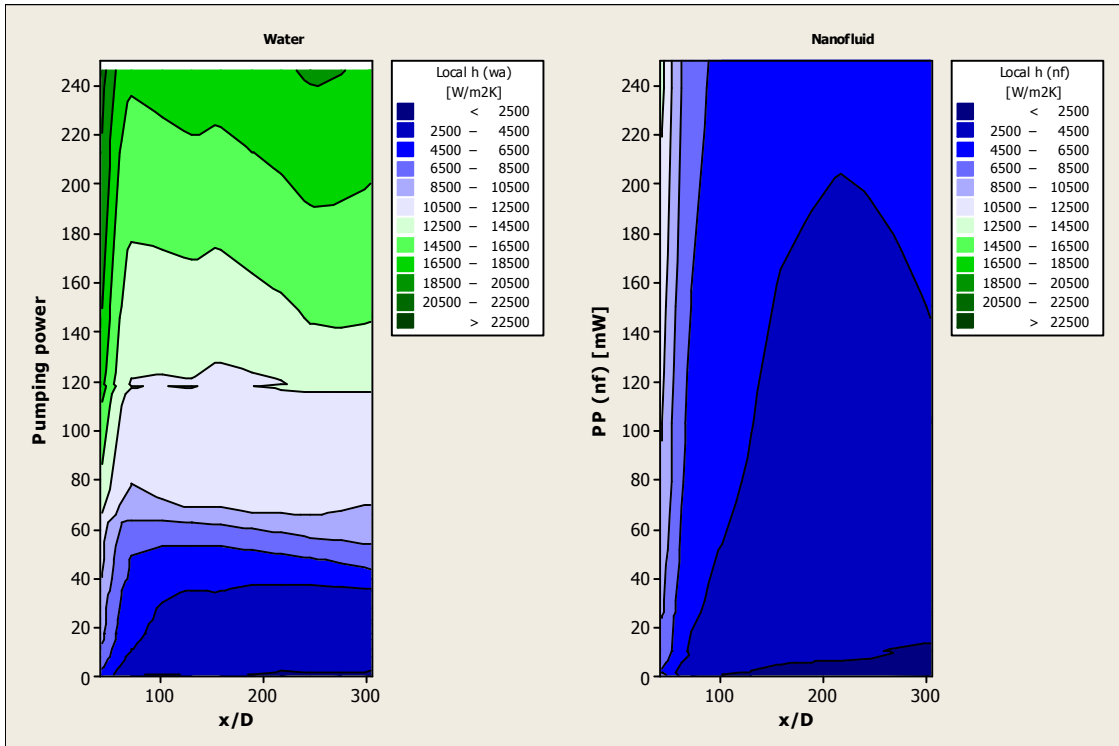
Figure 83. Contour plots for local heatransfer coefficient [W/m²K] h versus pumping power & x/D for water and nf in 1/16sq

4.5.2 Effect of hydraulic diameter D_h on heat transfer

The effect of hydraulic diameter on heat transfer behavior in circular and square channel is discussed in this sub-section. Three levels of hydraulic diameters were studied. The external dimensions provided by the manufacturer were as follows, 1/8" (0.125"), 3/32" (0.09375") and 1/16" (0.0625"). These dimensions were also used to name the test-sections. The hydraulic diameters (internal dimension of the cross-section) of circular test-sections used for analysis were 0.0881", 0649" and 0.0339". For square test-sections the hydraulic diameters used for analysis were 0.0862", 0.0638" and 0.037".

4.5.2.1 Circular tubes

In Figure 84 local Nusselt numbers are plotted against the dimensionless locations along the tube length for three sizes of circular tubes. For each tube size the local Nusselt number is plotted for three Reynolds numbers. For the three different sizes of tube, local Nusselt number at exact Reynolds number was not available, so comparable Reynolds numbers are presented in the plot. On this plot no discernable effect of hydraulic diameter on heat transfer behavior is observed. Local Nusselt number of 3/32c at Reynolds number of 2982 is higher than for others. This is because at this Reynolds number the flow is in turbulent regime.

Figure 84. Local Nusselt number versus x/D for SiO$_2$ nf in circular tubes of different hydraulic diameters

Overall Nusselt number of SiO$_2$ nanofluid flowing in different hydraulic diameter circular tubes (1/8c, 3/32 c and 1/16c) is presented in Figure 85. Here the overall Nusselt number is plotted against their respective Reynolds number. In the laminar regime the overall Nusselt number for all the three tube tend to overlap on each other. However, in post laminar Regime, which is marked by considerable increase in overall Nusselt number, a good difference in overall Nusselt number for the different test section can be observed. The earliest onset of transition can be observed for 3/32c and has the highest values for overall Nusselt numbers. It is then the followed by 1/8c for whose transition Reynolds number is between transition Reynolds numbers of 3/32c and 1/16c. For 1/8c the overall Nusselt numbers at Reynolds number in post laminar regime are lower than that for 3/32c. Then for 1/16c the onset of transition is actually at the lowest Reynolds number among the

three test-sections and the overall Nusselt numbers at higher Reynolds number is not available. For this test section the rate of increase in the overall Nusselt number in post laminar regime more rapid than that for other two test sections. Due experimental setup limitations overall Nusselt number at higher Reynolds number is not available.
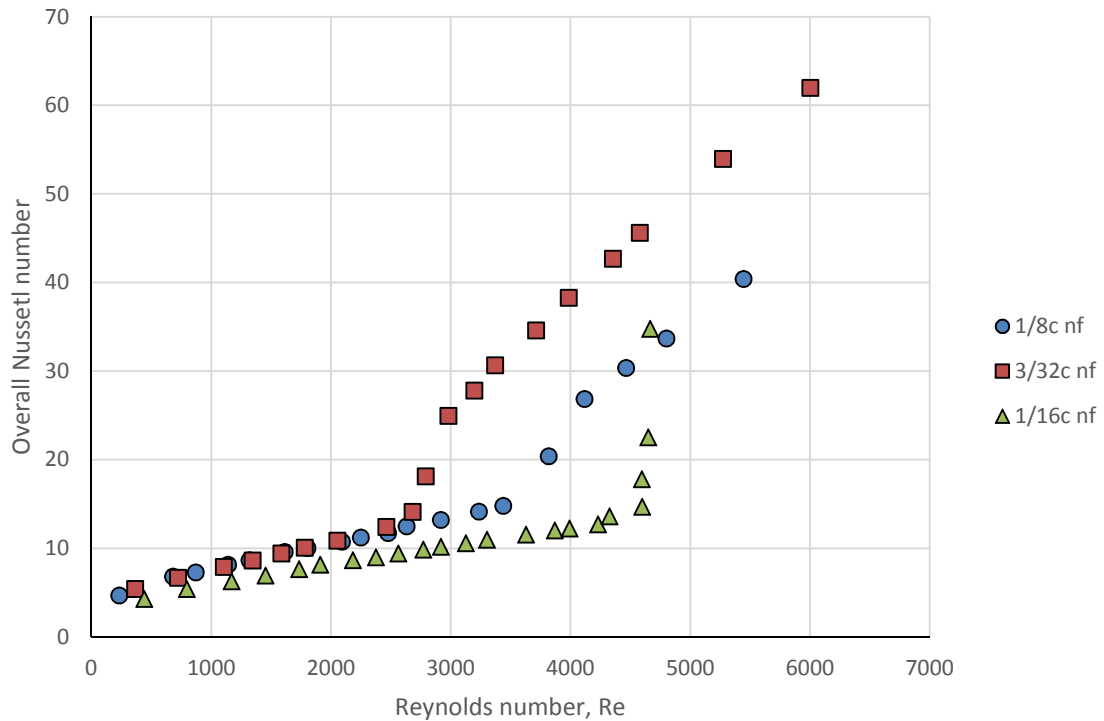
Figure 85. Overall Nusselt number versus Reynolds number for nf in circular tubes of different hydraulic diameters

4.5.2.2 Square tubes

In Figure 86 local Nusselt numbers are plotted against the dimensionless locations along the tube length for three sizes for square tubes. For each tube size the local Nusselt number is plotted for three Reynolds numbers. For the three different sizes of tube local Nusselt number at exact Reynolds number were not available, so Nu at comparable Reynolds numbers are presented in the plot. On this plot no discernable effect of hydraulic diameter on heat transfer behavior is observed. The local Nusselt number for 3/32sq and 1/16sq at

Reynolds number of 2626 and 2664 are seen to be noticeably higher than others. This can be explained by the flow regime which is turbulent at these Reynolds number.
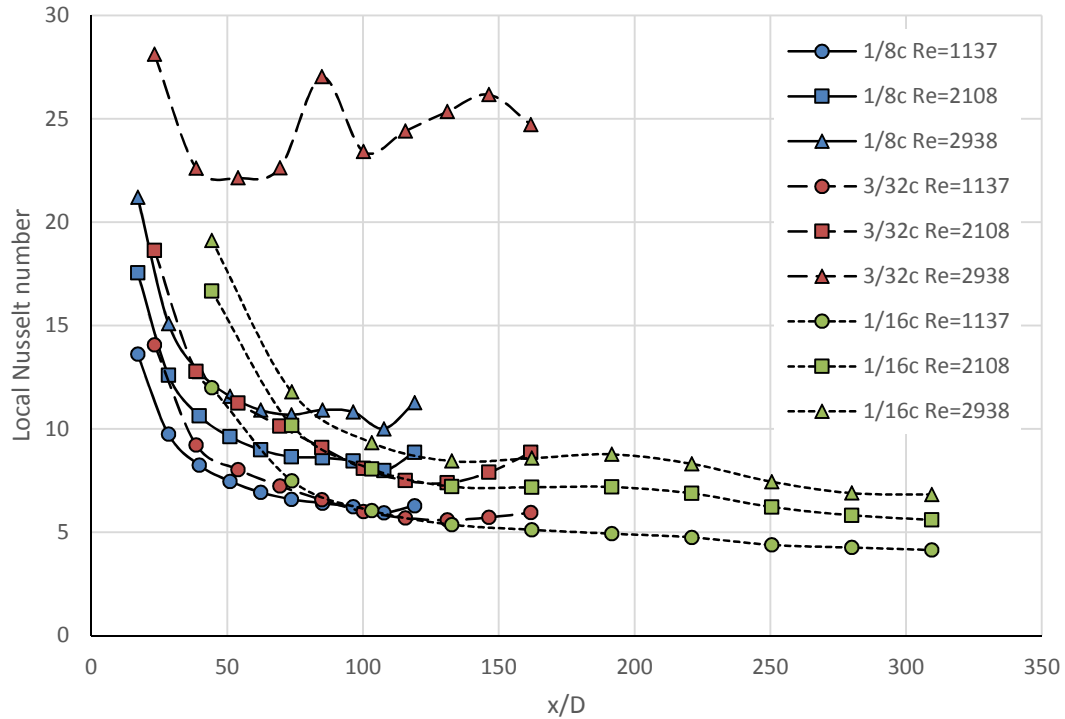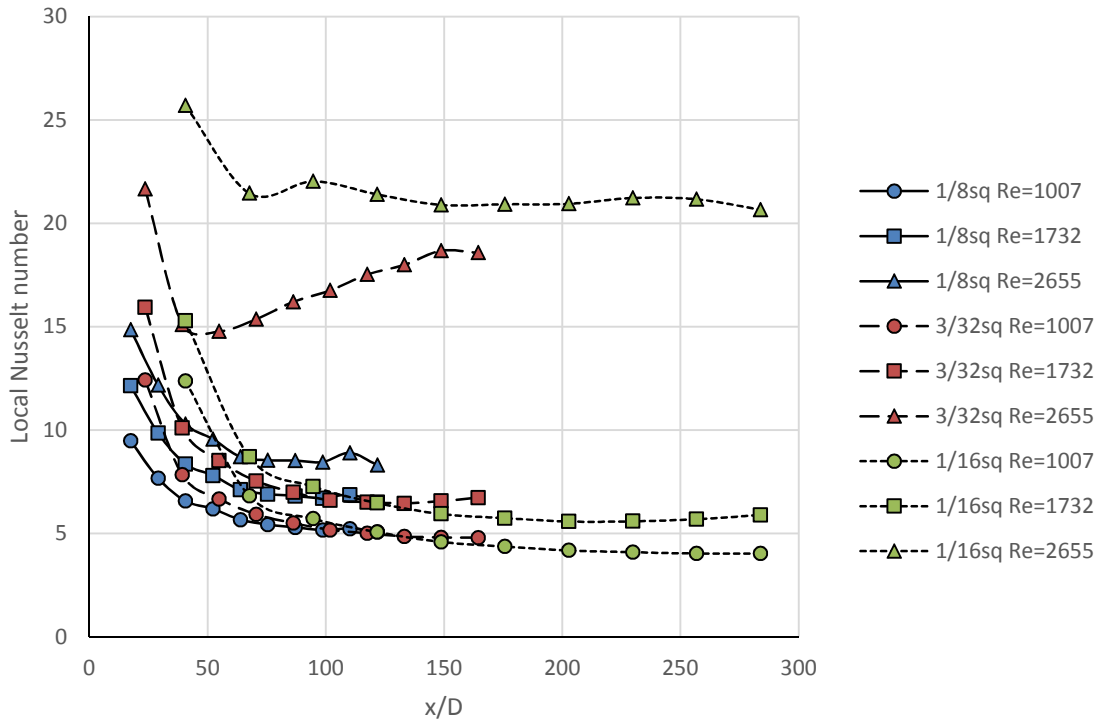

Figure 86. Local Nusselt number versus x/D for SiO_2 nf in square tubes of different hydraulic diameters

Overall Nusselt number of SiO_2 nanofluid flowing in different hydraulic diameter square tubes (1/8c, 3/32 c and 1/16c) is presented in Figure 87. Here the overall Nusselt number is plotted against their respective Reynolds number. In the laminar regime the overall Nusselt number for all the three tube tend to overlap on each other. However in post laminar regime, notable difference can be observed between the overall Nusselt numbers for different tube sizes. Test-section 1/8sq has the lowest overall Nusselt number in post laminar regime followed by 3/32sq. Only few data points are available for 1/16sq in post laminar regime and for these points overall Nusselt number for 1/16sq is slightly higher than that of 3/32sq. This suggest that the overall Nusselt number is not affected by

hydraulic diameter in laminar regime but when the flow is turbulent the overall Nusselt number seems to increase with decrease in Reynolds number.
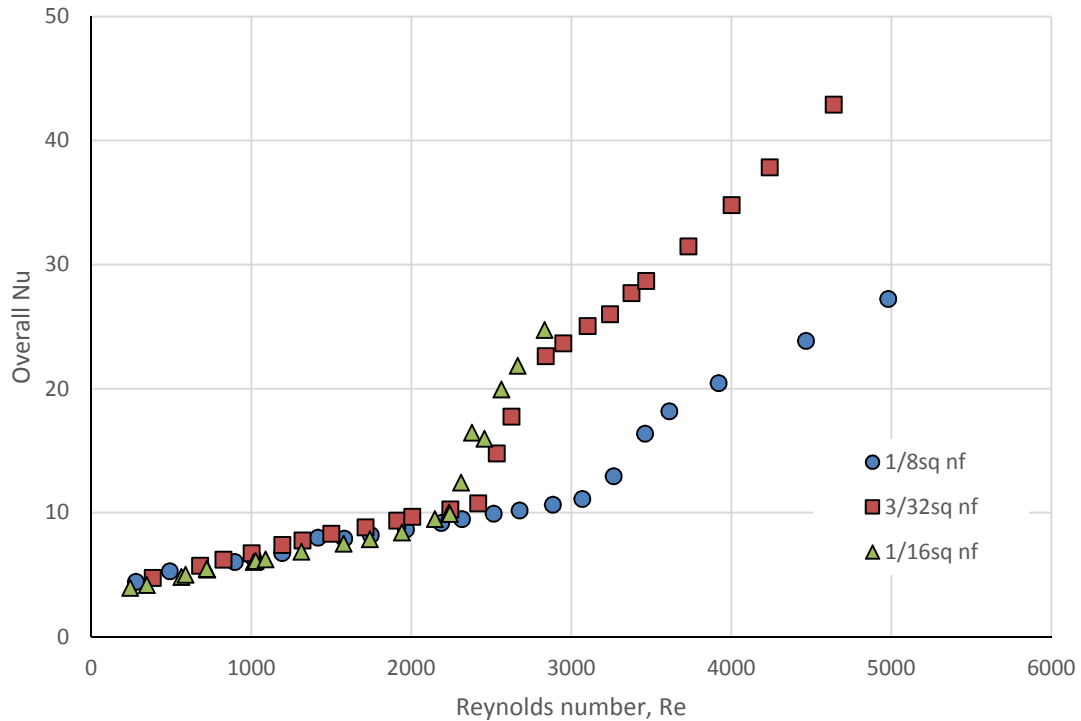
Figure 87. Overall Nusselt number versus Reynolds number for nf in square tubes of different hydraulic diameters

4.5.3 Effect of shape of cross-section on heat transfer

The effect of cross-section on heat transfer behavior is studied by comparing local and overall Nusselt number for circular and square test sections of three different hydraulic diameters.

In Figure 88 local Nusselt number for 1/8c and 1/8sq are compared at three different levels of Reynolds number. As in earlier comparisons, the comparison is again made among similar Reynolds numbers for the same reasons. The plot in this figure illustrates that the local Nusselt number for square test sections is lower than that of circular test-sections. At lower two levels of Reynolds number the local Nusselt number for circular tube is 8 to 18%

higher than the local Nusselt number for square tubes. At these Reynolds number, the flow is laminar. For the higher level of Reynolds number the local Nusselt number for 1/8c is up to 19% higher than the local Nusselt number for 1/8sq. In addition to this overall Nusselt number for 1/8c at respective Reynolds number is compared to overall Nusselt number for 1/8sq in Figure 89. The markers on the plot representing the overall Nusselt number for 1/8sq is lined up below the markers representing overall Nusselt number for 1/8c. To repeat that, for the given range of Reynolds number the overall Nusselt number for circular 1/8c is higher than that for 1/8sq. At low range of Reynolds number the markers are almost overlapping each other and as the Reynolds number increases the difference between them is observed to be increasing. At a Reynolds number of 4800 the overall Nusselt number for 1/8c is about 23% higher than that of 1/8sq. For other two sizes test section similar trend is observed and the plots are presented in following figures. From these results it can be concluded that heat transfer is higher in circular tubes than in square tubes. This is consistent with the Nusselt number behavior for different shapes discussed in literature [50]. Furthermore, the difference between the Nusselt numbers in these shapes increased with the Reynolds number.

Figure 88. Local Nusselt number versus x/D for nf in 1/8c and 1/8sq

Figure 89. Overall Nusselt number versus Reynolds number for nf in 1/8c and 1/8sq

Figure 90. Local Nusselt number versus x/D for nf in 3/32c and 3/32sq

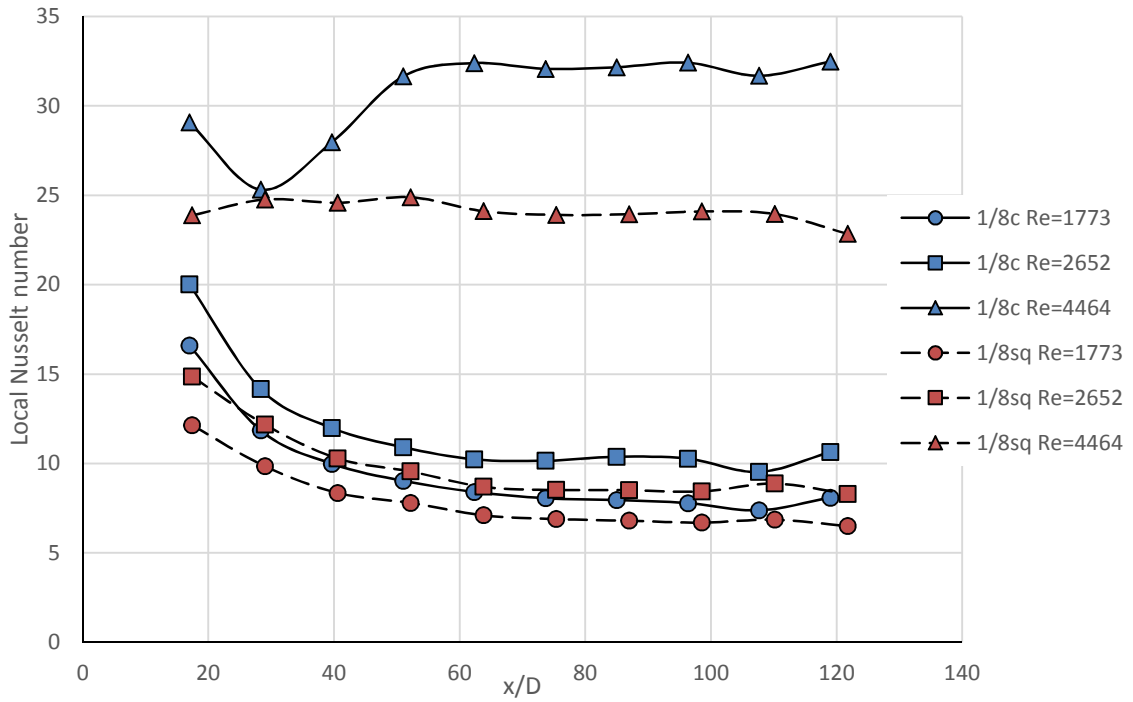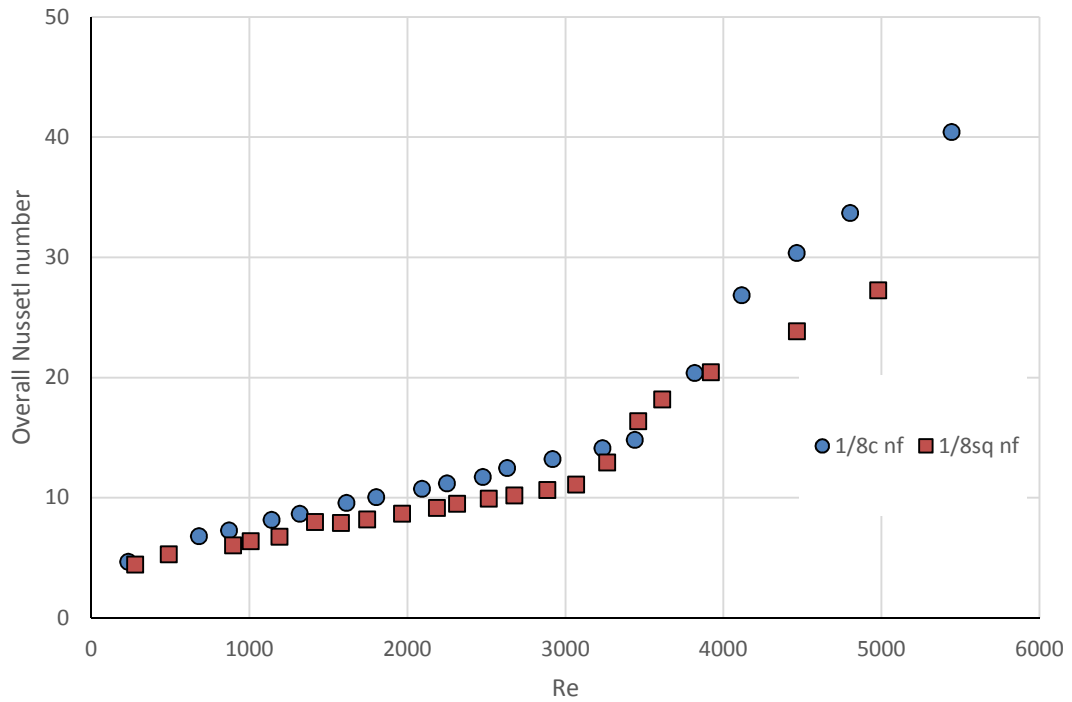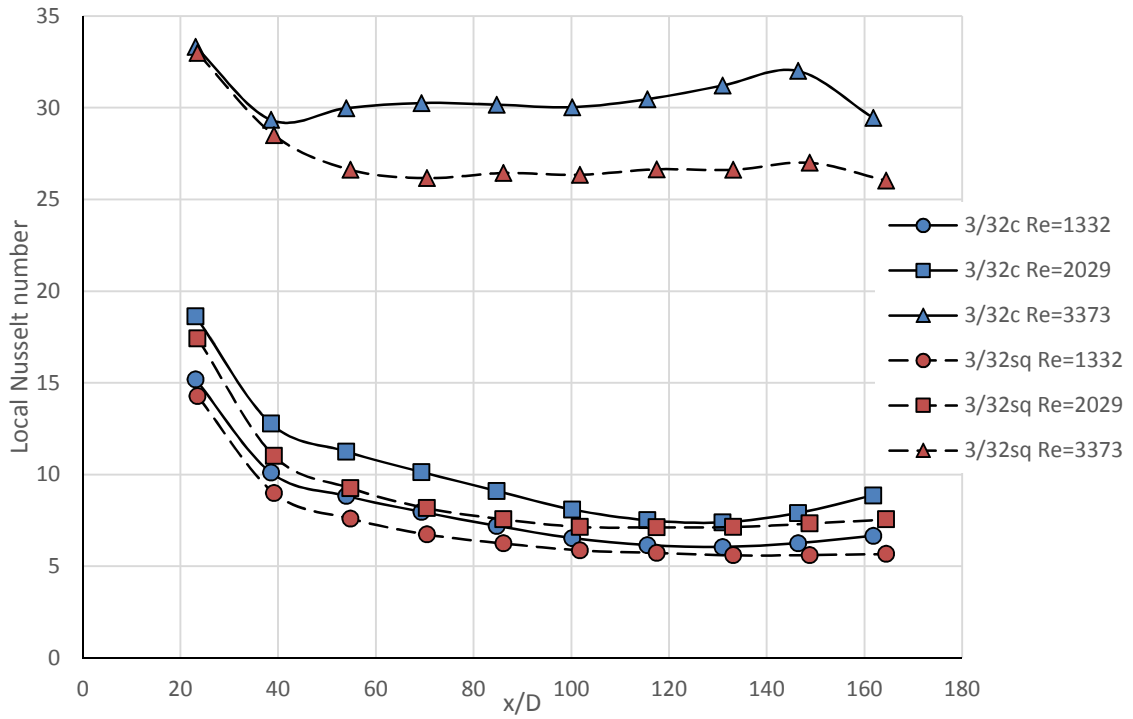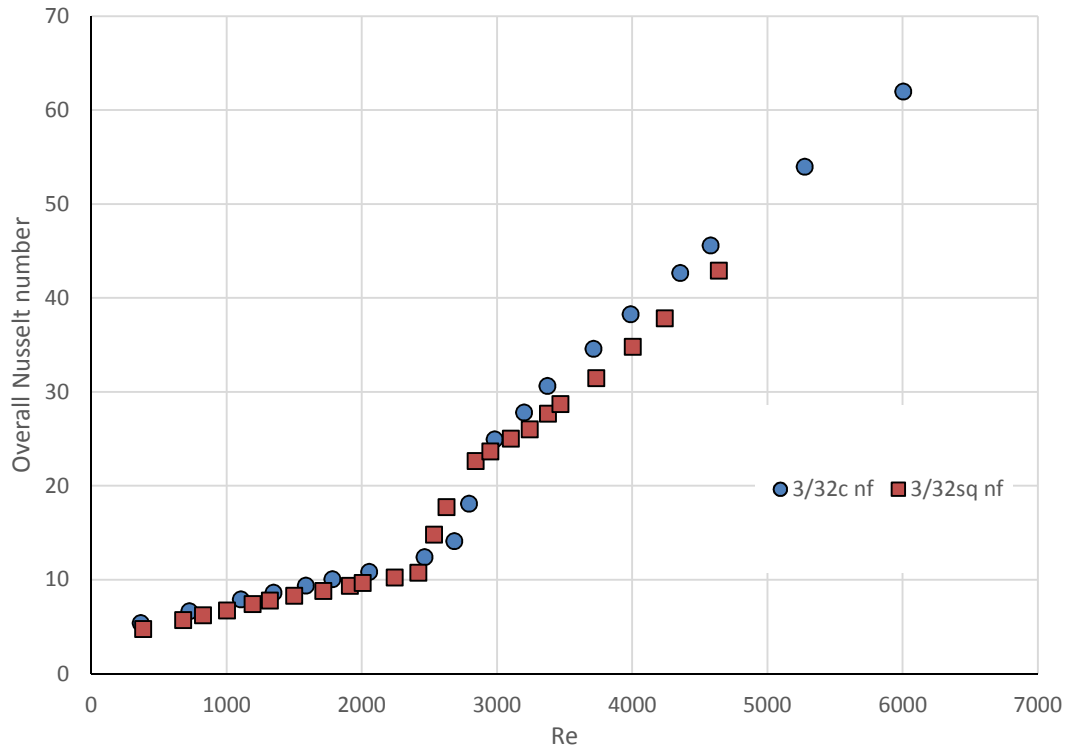Figure 91. Overall Nusselt number versus Reynolds number for nf in 3/32c and 3/32sq
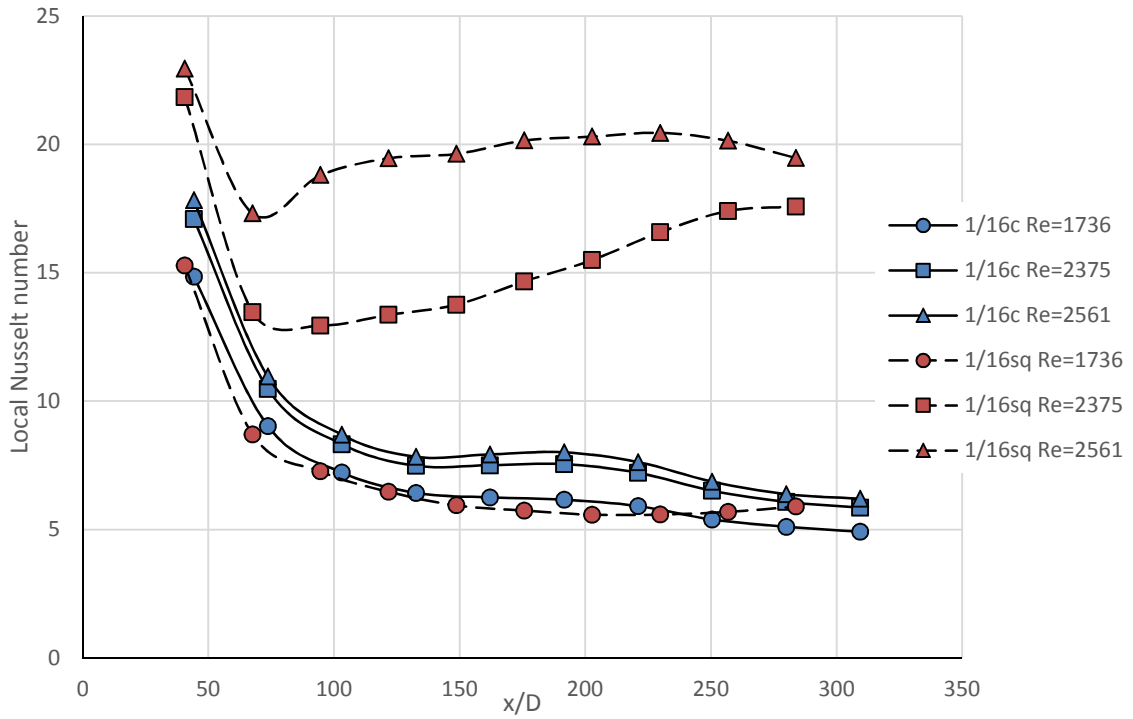
Figure 92. Local Nusselt number versus x/D for nf in 1/16c and 1/8sq
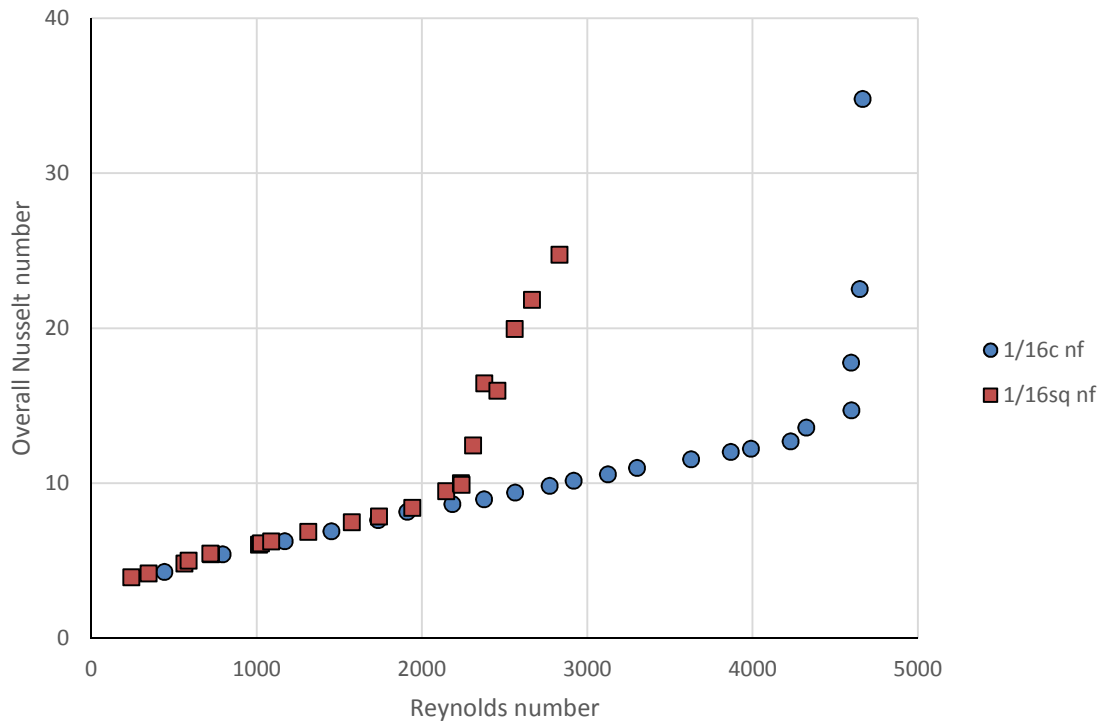
Figure 93. Overall Nusselt number versus Reynolds number for nf in 1/16c and 1/16sq

CHAPTER 5

CONCLUSION AND RECOMMENDATIONS

5.1   Conclusion

Flow and heat transfer behavior for water and silicon dioxide (SiO_2) nanofluid (9.58% by volume) was studied in six different test sections. These test sections had three different levels of hydraulic diameter and two different shapes (circular and square). Each of the test sections were 12 inches long, with wall thickness 0.014", and were made of brass. The three different outside dimensions of the cross-sections were 1/8", 3/32" and 1/16" with respective inner diameters of 0.097", 0.066", and 0.035" (2.46 mm, 1.67 mm and 0.88 mm). First the thermal conductivity and viscosity of SiO_2 nanofluid were studied. Thermal conductivity of silicon dioxide nanofluid was measured at several points between 0 and 50℃. Based on these data an empirical relation between thermal conductivity and temperature was established. At theses temperature conditions thermal conductivity of the nanofluid was 1.5 to 4.25% higher than that of water. Next the nanofluid was subjected to a range of shear rate (24 to 244 s^{-1}) at temperatures between 7 and 50℃. At these conditions it behaved as a shear thickening non-Newtonian fluid or a dilatant non-Newtonian fluid. Then the experimental flow loop was set up to measure the pressure drop across the test sections and the local heat transfer at 10 locations along the length of the test section. Pressure and temperature readings from this flow loop were first validated with water. The theoretical relations for the water friction factor and Nusselt number available in the literature could predict the experimental data within ±15%. Also the data for water was

117

later used for comparisons of flow and heat transfer behavior with SiO_2 nanofluid. Next silicon dioxide nanofluid was pumped through the test section and pressure and temperature data from the experiment was used to analyze the flow and the heat transfer behavior. From this analysis following conclusions were made:

- In the post laminar regime, SiO_2 nanofluid has lower fluid friction than that of water at the same Reynolds number.

- There was no observed effect of hydraulic diameter on friction factor.

- Square tubes have lower fluid friction than circular tubes of the same hydraulic diameter at the same Reynolds number. Also the pressure drop at equal mass flow rate is lower for square tubes and the difference in pressure drop at equal mass flow rate increases with an increase in mass flow rate. At the same hydraulic diameter square sections have larger area, so a better comparison could be made if the different cross sections with the same perimeter were also included in the study.

- The results of the heat transfer experiments suggest that adding nanoparticles improves the local convective heat transfer behavior of the fluid. Such improvement can be observed in plots of local Nusselt number for the similar Reynolds number of water and the nanofluid. However, the pumping power required for nanofluid to deliver the same amount of heat transfer as that of water is significantly higher than the pumping power required for water.

- The improvement in heat transfer by adding nanoparticles is higher at the earlier parts of the thermal entrance region (locations nearer to the inlet). At the later part of the test section (locations nearer to the outlet), the heat transfer behavior was inconclusive due to instability of the flow at those locations. Also the change in

Nusselt number, along the length, is more rapid for the nanofluid at locations near the inlet, which indicates that the dispersion of nanoparticles affect the development of thermal boundary layer. Thus to get most out of a colloid system when used as a heat transfer fluid the flow domain should be shorter than the thermal entry length. This is true for any kind of fluid. But the observation here is that colloid out performs its constituent basefluid (water) in this domain.

- The increase in the Nusselt number at same Reynolds number is more profound in turbulent flow regime.

- The heat transfer is higher in the circular tubes than in the square tubes, and the difference between the heat transfer in these shapes increased with the Reynolds number or increased with the mass flow rate.

5.2 Recommendations

Suspending nanoparticles in a heat transfer fluid improves its heat transfer characteristics at the expense of higher pumping power. There might be some potential for nanofluid in heat transfer application if the thermal conductivity and the specific heat capacity of the resulting fluid (nanofluid) is notable higher than that of the base fluid.

The Nusselt number for water and nanofluid was compared along the dimensionless distance from the entrance (x/D) of the control volume under study. It was observed that Nusselt number for the nanofluid was slightly higher than that of water and the difference between the Nusselt numbers of these working fluids were more notable in the earlier part of the control volume where the flow is still thermally developing. Thus the heat transfer application of nanofluid is recommend for thermally developing or interrupted flow domain. Also the difference in Nusselt number was higher at Reynolds number in post

119

laminar regime. The study does not include the comparison of Nusselt number in turbulent regime with higher Reynolds number (Re>8000), however from the plots it can be observed that the trend of nanofluid Nusselt number departing away from the water Nusselt number trend. Thus the heat transfer experiments of nanofluid in turbulent flow with higher Reynolds number is required to verify this claim.

There is a possibility that in the turbulent regime the Nusselt number for SiO_2 nanofluid is inversely proportional to the hydraulic diameter. This behavior could be related to non-Newtonian properties of the fluid. An in-depth study of heat transfer behavior of the non-Newtonian fluid is recommended in this area.

An extensive literature review shows that the studies related to the flow and the heat transfer of nanofluid with low volume concentrations (less than 2 % by volume). At these concentrations the fluids under study had Newtonian behavior. In the current study experiments were carried out with silicon dioxide nanofluid with comparatively higher concentration ($\sim$ 10% by volume). At this concentration the colloid behaved as a non-Newtonian fluid. A comprehensive study of relationship between concentration and rheological behavior of silicon dioxide is required to find out the concentration at which the silicon dioxide nanofluid starts to behave as a non-Newtonian fluid.

The experimental results of heat transfer behavior from these study can be implied to mass transfer behavior as there exist a close analogy between mass transfer and heat transfer.

REFERENCES

[1] R. F. Brooks, A. T. Dinsdale and P. N. Quested, "The measurement of viscosity of alloys—a review of methods, data and models," *Measurement science and technology,* vol. 16, pp. 354-362, 2004.

[2] F. W.White, Fluid Mechanics, New York: McGraw-Hill, 2008.

[3] S. Tiwari, "Evaluation of thermophysical properties, fricition factor, and heat transfer of alumina nanofluid flow in tubes," University of North Dakota, Grand Forks, 2012.

[4] D. Brkić, "Review of explicit approximations to the Colebrook relation for flow friction," *Journal of Petroleum Science and Engineering,* vol. 77, no. 1, pp. 34-48, 2011.

[5] S. K. Das, S. Choi, W. Yu and T. Pradeep, Nanofluids science and technology, Hoboken, New Jersey: John Wiley & Sons, 2008.

[6] R. K. Rajput, Heat and mass transfer, New Dehli: S. Chand, 2007.

[7] F. G. Hewitt, G. L. Shires and T. R. Bott, Process heat transfer, Boca Raton: CRC Press, 1994.

[8] C. Tang, S. Tiwari and M. C. Cox, "Experimental heat transfer study of aluminum oxide nanofluid flow in tubes for laminar thermal entry region," in *Proceedings of the ASME 2013 Summer Heat Transfer Conference*, Minneapolis, July 14-19, 2013.

[9] A. B. Metzner and D. W. Dodge, "Turbulent flow of non-Newtonian system," *A. I. Ch. E. Journal,* vol. 5, no. 2, pp. 189-204, 1959.

[10] E. V. Timofeeva, W. Yu, D. M. France, D. Singh and J. L. Routbort, "Nanofluids for heat transfer: an engineering approach," *Nanoscale research letters,* no. 6:182, 2011.

[11] S. Choi, "Special issue on nanofluids," *Nanoscale Research letters,* no. 6:99, 2011.

[12] S. Choi and J. A. Eastman, "Enhanching thermal conductivity of fluids with nanoparticles," Argonne national laboratory, Argonne, 1995.

[13] S. Lee, S. S. U. Choi, S. Li and J. A. Eastman, "Measuring Thermal Conductivity of Fluids Containing Oxide Nanoparticles," *Journal of heat transfer, ASME,* vol. 121, pp. 280-289, 1999.

[14] J. A. Eastman, S. Choi, W. Yu and L. Thompson, "Anomalously increased effective thermal conductivity of ethylene glycol based nanofluids containing copper nanoparticles.," *Applied Physics Letter,* vol. 78, pp. 718-720, 2001.

[15] S. Choi, Z. Zhang, W. Yu, F. Lockwood and E. Grulke, "Anomalous thermal conductivity enhancement in nanotube suspensions," *Applied Physics Letters,* vol. 79, 2001.

[16] H. Xie, H. Lee, W. Youn and M. Choi, "Nanofluids containing multiwalled carbon nanotubes and their enhanced thermal conductivities," *Journal of Applied Physics,* vol. 94, no. 8, pp. 4967-4971, 2003.

[17] T. Hong, H. Yang and C. J. Choi, "Study of the enhanced thermal conductivity of Fe nanofluids," *Journal of Applied Physics,* vol. 97, 2005.

[18] S. Murshed, K. Leong and C. Yang, "Enhanced thermal conductivity of TiO2—water based nanofluids," *International Journal of Thermal Sciences,* vol. 44, no. 4, p. 367–373, 2005.

[19] S. K. Das, N. Putra, P. Thiesen and W. Roetzel, "Temperature dependence of thermal conductivity enhancement for nanofluids," *Journal of Heat Transfer ,* vol. 125, no. 4, pp. 567-574 , 2003.

[20] C. Chon, K. Kihm, S. Lee and S. Choi, "Empirical correlation finding the role of temperature and particle size for nanofluid (Al2O3) thermal conductivity enhancement," *Applied Physics Letters,* vol. 87, no. 15, 2005.

[21] M. Chopkara, P. Das and I. Manna, "Synthesis and characterization of nanofluid for advanced heat transfer applications," *Scripta Materialia,* vol. 55, no. 6, p. 549–552, 2006.

[22] C. Kleinstreuer and Y. Feng, "Experimental and theoretical studies of nanofluid thermal conductivity enhancement: a review," *Nanoscale Research Letters ,* no. 6:229, 2011.

[23] Y. Ding, H. Chen, L. Wang, C. Yang, Y. He, W. Yang, W. Lee1, L. Zhang1 and R. Huo, "Heat Transfer Intensification Using Nanofluids," *KONA Powder and Particle Journal,* vol. 25, pp. 23-38, 2007.

[24] S. Murshed, K. Leong and C. Yang, "A model for predicting the effective thermal conductivity of nanoparticle-fluid suspensions," *International Journal of Nanoscience ,* vol. 5, no. 1, 2006.

[25] J. Avsec and M. Oblak, "The calculation of thermal conductivity, viscosity and thermodynamic properties for nanofluids on the basis of statistical nanomechanics," *International Journal of Heat and Mass Transfer,* vol. 50, no. 21-22, p. 4331–4341, 2007.

[26] V. Y. Rudyak, "Viscosity of nanofluids—Why it is not described by the classical theories," *Advances in Nanoparticles,* vol. 2, pp. 266-279, 2013.

[27] R. Prasher, D. Song, J. Wang and P. Phelan, "Measurements of nanofluid viscosity and its implications for thermal applications," 2006. [Online]. Available: http://dx.doi.org/10.1063/1.2356113. [Accessed 05 December 2013].

[28] S. W. Lee, S. D. Park, S. Kang, I. C. Bang and J. H. Kim, "Investigation of viscosity and thermal conductivity of SiC nanofluids Investigation of viscosity and thermal conductivity of SiC nanofluids," *International Journal of Heat and Mass Transfer,* vol. 54, p. 433–438, 2011.

[29] D. Nield and A. Kuznetsov, "A note on the variation of nanofl uid viscosity with temperature," *International Communications in Heat and Mass Transfer,* vol. 41, p. 17–18, 2013.

[30] C. J. Seeton, "Viscosity–temperature correlation for liquids," *Tribology Letters,* vol. 22, no. 1, pp. 67-78, 2006.

[31] M. Kole and T. Dey, "Viscosity of alumina nanoparticles dispersed in car engine coolant," *Experimental Thermal and Fluid Science ,* vol. 34, pp. 677-683, 2010.

[32] S. W. Lee, S. D. Park, S. Kang, I. C. Bang and J. H. Kim, "Investigation of viscosity and thermal conductivity of SiC nanofluids for heat transfer applications," *International Journal of Heat and Mass Transfer,* vol. 54, pp. 433-483, 2011.

[33] I. Mahbubul, R. Saidur and M. Amalina, "Latest developments on the viscosity of nanofluids," *International Journal of Heat and Mass Transfer,* vol. 55, pp. 874-885, 2012.

[34] E. V. Timofeeva, J. L. Routbort and D. Singh, "Particle shape effects on thermophysical properties of alumina nanofluids," *Journal of appleid Physics,* vol. 106, no. 1, 2009.

[35] P. Kumar, J. Kumar and S. Suresh, "Review on Nanofluid Theoretical Viscosity Models," *International Journal of Engineering Innovation & Research,* vol. 1, no. 2, pp. 182-188, 2012.

[36] S. Kakac and A. Pramuanjaroenkij, "Review of convective heat transfer enhancment with nanofluid," *International Journal of Heat and Mass Transfer,* vol. 52, pp. 3187-3196, 2009.

[37] Y. Ding, et al., "Heat transfer intensification using nanofluids," *KONA,* vol. 25, pp. 23-36, 2007.

[38] D. Kim, Y. Kwon, Y. Cho, C. Li, S. Cheong, Y. Hwang, J. Lee, D. Hong and S. Moon, "Convective heat transfer characteristics of nanofluids under laminar and turbulent flow conditions," *Current Applied Physics,* vol. 9, p. e119–e123, 2009.

[39] W. Duangthongsuk and S. Wongwises, "An experimental study on the heat transfer performance and pressure drop of TiO2-water nanofluids flowing under a turbulent flow regime," *International Journal of Heat and Mass Transfer,* vol. 53, pp. 334-344, 2010.

[40] J. Lee and I. Mudawar, "Assessment of the effectiveness of nanofluids for single-phase and two-phase heat transfer in micro-channels," *International Journal of Heat and Mass Transfer,* p. 452–463, 2007.

[41] B. Sahin, G. G. Gültekin, G. G. Gültekin and S. Karagoz, "Experimental investigation of heat transfer and pressure drop characteristics of Al2O3–water nanofluid," *Experimental Thermal and Fluid Science,* 2013.

[42] P. Selvakumar and S. Suresh, "Convective performance of CuO/water nanofluid in an electronic heat sink," *Experimental Thermal and Fluid Science,* vol. 57–63, p. 40, 2012.

[43] Jacopo Buongiorno, et al., "A benchmark study on the thermal conductivity of nanofluids," *Journal of Applied Physics,* vol. 106, 2009.

[44] D. C. Venerus, et al., "Viscosity of collidial dispersion (nanofluids) for heat transfer application," *Applied Rheology,* vol. 20, no. 4, 2010.

[45] J. E. Julia, L. Hernández, R. Martínez-Cuenca, T. Hibiki, R. Mondragón and J. C. J. C. Segarra, "Measurement and modelling of forced convective heat ransfer coefficient and pressure drop of Al2O3- and SiO2- water nanofluids," *6th European Thermal Sciences Conference (Eurotherm 2012),* vol. 395, no. 012038.

[46] W. Azmi, K. Sharma, P. Sarma, R. Mamat and G. Najafi, "Heat transfer and friction factor of water based TiO2 and SiO2 nanofluids under turbulent flow in a tube," *International Communications in Heat and Mass Transfer,* vol. 59, pp. 30-38, 2014.

[47] A. M. Hussein, K. V. Sharma, R. A. Bakar and K. Kadirgama, "The effect of nanofluid volume concentration on heat transfer and friction factor inside a horizontal tube," *Journal of Nanomaterials,* vol. Article ID 859563, 2013.

[48] C. Tang, S. Tiwari and M. W. Cox, "Experimental characterization of viscosity and thermal conductivity of aluminum oxide nanofluid," in *Proceedings of the ASME 2013 Summer Heat Transfer Conference*, Minneapolis, July 14-19, 2013.

[49] J. P. Holman, Experimental Methods for Engineers, The McGraw-Hill Companies, 2011.

[50] W. Kays, M. Crawford and B. Weigand, Convective Heat and Mass Transfer, New York: The McGraw-Hill Companies, Inc., 2012.

[51] V. Gnielinski, "New equation for heat and mass transfer in trubulent pipe and channel flow," *International Chemical Engneering* , vol. 16, pp. 359-368, 1979.

[52] S. K. Das, S. Choi and H. E. Patel, "Heat Transfer in Nanofluids—A Review," *Heat Transfer Engineering,* vol. 27, no. 10, 23 February 2007.